DIFFUSION COEFFICIENTS IN CARBON DIOXIDE-[bmim][PF_6] MIXTURE AT HIGH PRESSURE: TRANSPORT AND THERMODYNAMIC MODELING OF EXPERIMENTAL SOLUBILITY

by
Melek Çetin

Submitted to Graduate School of Natural and Applied Sciences
in Partial Fulfillment of the Requirements
for the Degree of Doctor of Philosophy in
Chemical Engineering

Yeditepe University
2023

DIFFUSION COEFFICIENTS IN CARBON DIOXIDE-[bmim][PF_6] MIXTURE AT HIGH PRESSURE: TRANSPORT AND THERMODYNAMIC MODELING OF EXPERIMENTAL SOLUBILITY

APPROVED BY:

Assoc. Prof. Dr. Betül Ünlüsü ……
(Thesis Supervisor)
(Yeditepe University)

Prof. Dr. Sermin Örnektekin ……
(Yeditepe University)

Prof. Dr. Mustafa Özilgen ……
(Yeditepe University)

Assoc. Prof. Dr. Nilay Baylan Gülsoy ……
(İstanbul University)

Assoc. Prof. Dr. Yaşar Andelib Aydın ……
(Marmara University)

DATE OF APPROVAL: ..../..../20..

I hereby declare that this thesis is my own work and that all information in this thesis has been obtained and presented in accordance with academic rules and ethical conduct. I have fully cited and referenced all material and results as required by these rules and conduct, and this thesis study does not contain any plagiarism. If any material used in the thesis requires copyright, the necessary permissions have been obtained. No material from this thesis has been used for the award of another degree.

I accept all kinds of legal liability that may arise in case contrary to these situations.

Name, Last name Melek Çetin

Signature …..…….……

ACKNOWLEDGMENTS

I am very thankful to my thesis advisor Assoc. Prof. Betül Ünlüsü for her help and patience. Also I want to thank, Prof. Dr. Süheyla Uzman and Prof. Dr. Mustafa Özilgen for their help. I am thankful to Prof. Dr. Sermin Örnektekin, Assoc. Prof. Nilay Baylan Gülsoy and Assoc. Prof. Yaşar Andelib Aydın for their contribution to my thesis.

I would like to thank to my dearest friends Dr. Gülçin Cem Özeral, Dr. Hatice Semizer Aksoy, Dr. Binnaz Coşkunkan, Emine Elif Yıldız and Nermin Şen.

Especially , I'm thankful to Ömer Barış Emek for always helping, encouraging me during sleepless nights at the laboratory. He is the best team mate I have ever worked with. There is so much to be said for him.

I would like to thank my besties Işıl Ural, Perihan Şahin, Kübra Enis, Çiğdem Ürkmez and Çisem Efe for always helping and encouraging me whenever I feel hopeless. I would like to thank Ömür Dinek, Önder Özkan, Ömer Alma and Gökhan Yıldırım for their help to me.

I'm thankful to my precious mum Hilkat Şekerci and my brother Ali Fuat Şekerci, for their patience and encouragement. I really appreciate Somalı family for their help to me all throughout of my life. In this long journey I want to thank my husband, Bora Çetin; without him this thesis could not be finished. My special thank goes to my little daughter Elif Çetin for her endless patience at this age. I am lucky to have you. Thank you my whole family! Lastly, I dedicated my dissertation to my dad Assoc. Prof. Osman Şekerci who always wanted to see me in a good place.

ABSTRACT

DIFFUSION COEFFICIENTS IN CARBON DIOXIDE-[bmim][PF_6] MIXTURE AT HIGH PRESSURE: TRANSPORT AND THERMODYNAMIC MODELING OF EXPERIMENTAL SOLUBILITY

Ionic liquids are defined as molten salts which have melting point below 100°C. They have unique properties such as low vapor pressure, non-flammability and good thermal stability, that make them attractive as solvents. On the other hand, carbon dioxide, has been used as a solvent in both supercritical and liquid phases for decades. It can form a solvent system with ionic liquids to be used in different applications. A mass transfer process in one-direction starts with the introduction of carbon dioxide at high pressure to an ionic liquid containing system. Carbon dioxide dissolves in the liquid phase. However, the transport of the ionic liquid into the gas phase does not occur in measurable quantities. In this study, the objective is to determine the mutual diffusion coefficients of the carbon dioxide-ionic liquid, [bmim][PF_6], system at temperatures of 313.15 K and 323.15 K and pressures of 5 MPa and 8 MPa. Experiments have been run to find time-dependent carbon dioxide solubilities in the ionic liquid and then, a transport model is fit to the experimental data in order to estimate the diffusion coefficients. The system is modeled as one-directional mass transfer from gas phase to liquid phase with a moving interface. The volume-of-fluid method is used to model the change in the position of the interface. To account for the variation in liquid density, an equation fit to the experimental density data is included in the transport model. The diffusivities at dilute concentration and at thermodynamic phase equilibrium are determined and compared with the literature values and those obtained from correlations.

ÖZET

YÜKSEK BASINÇTA KARBONDİOKSİT-[bmim][PF_6] KARIŞIMINDA YAYINIM KATSAYILARI: DENEYSEL ÇÖZÜNÜRLÜĞÜN TAŞINIM VE TERMODİNAMİK MODELLEMESİ

İyonik sıvılar, erime noktası 100°C'nin altında olan erimiş tuzlar olarak tanımlanır. Düşük buhar basıncı, alev almazlık ve iyi ısıl kararlılık gibi, çözücüler olarak çekici olmalarını sağlayan benzersiz özelliklere sahiptirler. Öte yandan karbondioksit hem kritik ötesi hem de sıvı fazda çözücü olarak onlarca yıldır kullanılmaktadır. Farklı uygulamalarda kullanılmak üzere iyonik sıvılar ile çözücü sistemi oluşturulabilir. Tek yönlü bir kütle aktarımı süreci, yüksek basınçta karbondioksitin iyonik sıvı olan bir sisteme eklenmesiyle başlar. Karbondioksit sıvı fazında çözünür. Ancak, iyonik sıvının gaz fazına taşınımı ölçülebilir miktarlarda gerçekleşmez. Bu çalışmada amaç, karbondioksit-iyonik sıvı, [bmim][PF_6], sisteminin yayınım katsayılarının 313.15 K ve 323.15 K sıcaklıklarında ve 5 MPa ve 8 MPa basınçlarında belirlenmesidir. Karbondioksitin zamana bağlı olarak iyonik sıvı içerisindeki çözünürlüğünü bulmak için deneyler yapılmıştır. Sonra, difüzyon katsayılarını hesaplamak üzere, deneysel veriye bir taşınım modeli uygulanmıştır. Sistem, hareketli bir ara-yüzeyle gaz fazından sıvı fazına doğru tek yönlü bir kütle transferi olarak modellenmiştir. Fazlar arasındaki ara-yüzeyin konumunda oluşan değişim için Akışkan-Hacmi yöntemi kullanılmıştır. Sıvı yoğunluğundaki değişimi hesaba katmak için, taşınım modeline deneysel yoğunluk verilerine uyan bir denklem dahil edilmiştir. Seyreltik konsantrasyon ve termodinamik faz dengesindeki yayınım katsayıları belirlenmiş ve literatürdeki değerler ve korelasyonlarla elde edilen sonuçlarla karşılaştırılmıştır.

TABLE OF CONTENTS

LIST OF FIGURES

LIST OF TABLES

LIST OF SYMBOLS/ABBREVIATIONS

g	Gravitational acceleration
k_{ij}	Binary interaction parameter
m	Mass
t	Time
u	Velocity
w	Mass fraction
x	Mole fraction
D	Diffusion coefficient
D^0	Initial diffusion coefficient
D	Diffusion coefficient
J	Diffusion flux
Mw	Molar mass
P	Pressure
T	Temperature
V	Volume
V'_{IL}	Volume of the ionic liquid sample
Vm	Molar volume
w_{CO2}	Mass fraction of CO_2

α	Volume fraction
ɣ	Activity coefficient
Γ	Thermodynamic correction factor
μ	Viscosity
ρ	Density
τ_{ij}	Binary interaction parameter in liquid activity coefficient
Φ	Fugacity coefficient
ω	Acentric factor

c	Critical

r	Reduced
A	Solute
B	Solvent
IL	Ionic liquid

1. INTRODUCTION

Ionic liquids (ILs) are salts which remain in the liquid state at room temperature. Their properties such as non-flammability, very low or non-volatility and being recyclable, increase their potential as green solvents [1,2]. They have high polarity and can dissolve organic, inorganic and organometallic materials. Also, they are thermally stable. It is possible to develop the best IL solvent for green processes by choosing the right anion and cation [1,2]. ILs are generally categorized by their cation [2].

Above its critical point (304.2 K, 7.38 MPa), carbon dioxide is used as a supercritical fluid ($scCO_2$) [3]. The inexpensive, relatively inert, non-flammable, non-toxic, and non-viscous characteristics make $scCO_2$ the supercritical fluid of choice [4]. $scCO_2$ can be used as a solvent in petroleum refining and petrochemistry. It is also an ideal solvent for food industry in extraction processes such as coffee and tea decaffeination, chlorestol or lipid extraction from meat [3]. It is also used in fluid extraction in biotechnology, and extrusion processes in food processing [5].

The addition of high-pressure CO_2 to an IL initiates one-way mass transfer. While CO_2 readily dissolves in the IL, the IL itself does not significantly diffuse into the vapor phase. A gas-expanded liquid (GXL) system forms when dissolution takes place. A GXL, referred to as a liquid, undergoes an expansion in volume when subjected to pressure by a condensable gas like carbon dioxide [6].

GXLs are environmentally benign solvents applied to separations, extractions and reactions [6,7]. There are three classes of carbon dioxide-expanded liquids (CXLs) [6,8]. The solubility of CO_2 is limited in Class I CXL, as in the case of water-carbon dioxide systems, and the liquid volume undergoes only slight expansion. Class II CXLs dissolve large amounts of CO_2, and expansion is high, such as CO_2 and methanol. In Class III, the gas is moderately soluble and liquid expands more than Class I systems, such as, CO_2 and ILs [9].

[bmim][PF_6] is one of the most widely investigated ionic liquids [2,10]. It has applications in catalysis, separation and synthesis [10]. CO_2-[bmim][PF_6] solvent system is recently applied in the oxidation reaction of cyclohexane using different catalysts. The mixed solvent has provided some favorable results regarding reaction times, dissolution and recycle of catalysts, and yield [11,12]. In recent studies, [bmim][PF_6] has been employed in the

synthesis of ionogels under CO_2 pressure [13] and another example is the separation of CO_2 from biogas (ie. biogas upgrading) by using [bmim][PF_6] as solvent [14,15]. Also, during the formation of the carbon dioxide-1-butyl-3-methylimidazolium hexafluorophosphate system, mass transfer is one-way, from the gas phase to the liquid phase.Through the dissolution of carbon dioxide, the transport properties of the liquid phase can be changed [16].

High pressure diffusion coefficients are determined for 1-butyl-3-methylimidazolium hexafluorophosphate-carbon dioxide system and the change in the binary diffusivities with the liquid mole fraction of carbon dioxide is examined at different pressures and temperatures. The experimental set-up is designed for this system. The mainly used equipments in this system are: a syringe pump, a cathetometer and a high pressure view cell. Carbon dioxide can be loaded to the system by using syringe pump at a constant pressure. During the experiments, a cathetometer is utilized to track the rise in the liquid level. This enables the determination of the solubility values of CO_2.

The system is modeled with computational fluid dynamics (CFD) where the flow field is divided into cells. The equations governing momentum, energy, and mass balances are discretized and expressed in terms of variables located at the cell centers or at specified positions within the cells. Subsequently, these equations are solved [17]. The CFD model we have developed accounts for the changes in the position of the phase interface using the volume-of-fluid method (VOF) and the density of the liquid phase during the process. This model is fit to the experimental solubilities to find diffusion coefficients.

The thesis starts with literature survey on ionic liquids, supercritical fluids, gas-expanded liquids, [bmim][PF_6]-CO_2 system and computational fluid dynamics. In the next part, details of experiments and transport model are explained. The experimental solubility and calculated diffusivity values of carbon dioxide in the ionic liquid at various temperatures and pressures are presented in the results and discussion sections. Finally, the conclusions and some suggestions for future work are stated.

2. LITERATURE SURVEY

The toxic organic solvents can escape into the atmosphere and make a contamination to the environment after a reaction. Therefore, alternative solvents, such as ionic liquids, are preferred to be used in application areas of science and industry. They prevent the negative impacts to the environment that organic solvents cause because; they are non-volatile. Therefore they are stated as environmentally benign solvents [2]. This section gives brief description about ionic liquids, their properties and application areas; supercritical fluids and their applications; gas-expanded liquids, high pressure carbon dioxide and ionic liquid systems; and also computational fluid dynamics.

2.1. IONIC LIQUIDS

Scientists agree that, ionic liquids can be ideal examples in the near future for catalyst and separation applications in the industry due to having such properties of non-volatility, thermal stability and wide liquid range [9,18,19].

Solvents made solely of ions are known as ionic liquids. ILs can be distinguished by this definition from salt solutions (salt+ions) and molecular solvents (only neutral molecules) [9]. Ionic liquids can be described as organic salts that are created through the combination of cations and anions. As cations show high degree of asymmetry, ILs remain liquid at ambient conditions as the ions do not pack well [2,7,9,20]. To put it another way, salts that their melting point (T_m) is low, called as ionic liquids [5]. Even at elevated temperatures, their vapor pressure can be disregarded. These non-flammable organic fluids possess qualities that make them appealing for industrial applications [20]. Ionic liquids are typically named as [cation][anion] [7]. Figure 2.1 displays the cations and anions commonly utilized for ILs as reported in the literature [21]. The structures and abbreviations of generally used ILs are given in Table 2.1 [22].

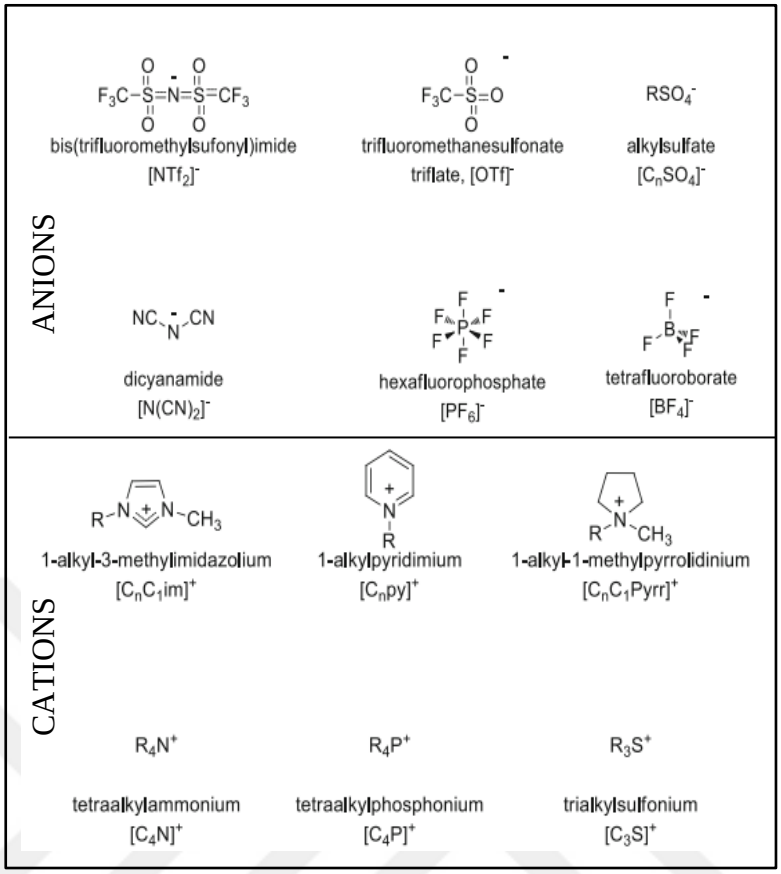

Figure 2.1. Frequently used cations and anions for ionic liquids in the literature [21]

Table 2.1.Names and structures of common ILs [22]

Ionic Liquid	Structure	Short Name
1-butyl-3-methylimidazolium tetrafluoroborate	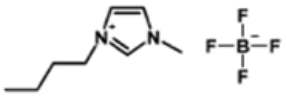	[bmim][BF_4]
1-butyl-3-methylimidazolium hexafluorophosphate	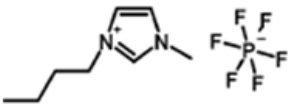	[bmim][PF_6]
1-hexyl-3-methylimidazolium bis(trifluoromethylsulfonyl) imide R=C_6H_{13}	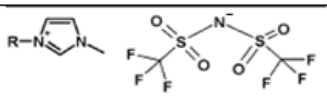	[hmim][TF_2N]

2.1.1. History of Ionic Liquids

Investigations about ILs' physical and chemical properties, their synthesis and applications as solvents and catalysts have increased over the last decade [21]. According to the literature nearly 3500 papers about these topics are published every year [21].

Paul Walden (1914) first synthesized an IL, ethylammonium nitrate ($[EtNH_3][NO_3]$). This IL has the melting point as 12 ºC [23].

Due to the fact that ethylammonium nitrate (Figure 2.2) was highly reactive, studies related with that IL were limited [24].

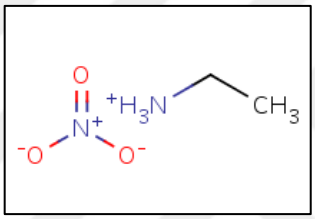

Figure 2.2. Ethylammonium nitrate ($[EtNH_3][NO_3]$) [24]

In 1982, Wilkes and colleagues conducted research on the formation of 1-alkyl-3-methylimidazolium chloride aluminum chloride ionic liquids using 1,3-dialkylimidazolium cations. [25]. For the first ILs, such as organo-aluminates were not stable to air and water, therefore they had a limited range of applications [26]. Hussey and Seddon used chloroaluminate species for the synthesis of ILs in 1983 (first generation of ILs) [26,27]. But due to their sensitivity to water it was difficult to handle these chloroaluminate systems [26,27]. This work made ionic liquids much more popular [26]. Later on in 1992, Wilkes and coworkers studied ionic liquids with tetrafluoroborate ions (second generation of ILs). As a result of their study, they proved that ionic liquids are not limited only by chloroaluminate melts, they can combine a whole range of cation/anion combination [28]. In Figure 2.3 three generations of ILs are presented [29]. Task-specific ILs (TSILs) are presented by Davis as a third generation at the beginning of 2000s. Also he reported that TSILs can easily be tuned to the reaction conditions (see Figure 2.3) [29].

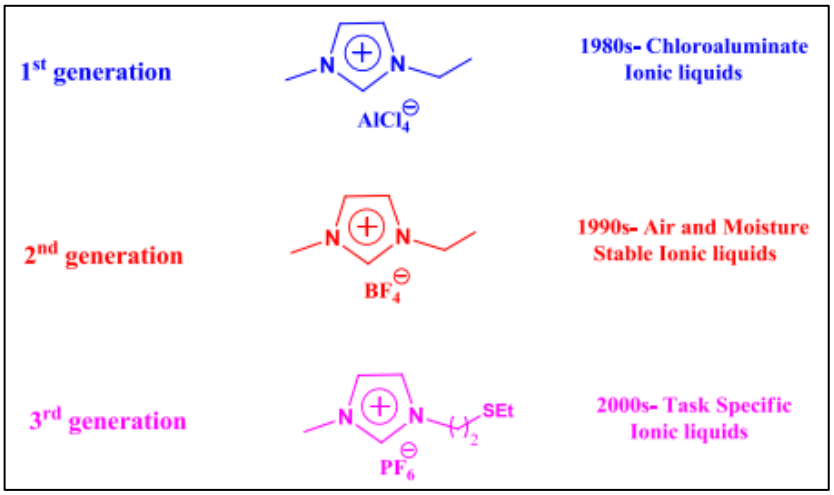

Figure 2.3. The three IL generations [29]

2.1.2. Physical Properties of Ionic Liquids

ILs possess significant characteristics, including a broad spectrum of advantageous attributes such as: a decreased melting point, non-flammability, elevated ionic conductivities [2]. Needless to say that there is no ideal ionic liquid that has all the unique properties mentioned above [20].

The inherent flexibility of ionic liquids (ILs) allows for the introduction of modifications by altering the cationic and anionic components, thereby enabling the creation of a broad range of IL variations. This capability allows for precise fine-tuning of the physical properties of ILs. That versatility indicates significant potential for ILs in various applications leading them to be referred to as "designer solvents" in multiple publications [2,30]. This term highlights their capacity to be customized and tailored to specific needs, further emphasizing their suitability for a diverse range of uses [2].

In the following section physical properties of ionic liquids are explained briefly with some examples.

2.1.2.1. Liquid range and thermal stability

In the case of amorphous ionic liquids, the liquid range is constrained by the Tg while for crystalline ionic liquids, the liquid range is limited by the melting point. Using differential scanning calorimetry (DSC), the phase transition can be measured [31]. Ionic liquids exhibit

significant liquid ranges, reaching as wide as 200-300 ºC when compared to common organic liquids (such as, benzene, hexane and ethanol) that have ranges up to 100 ºC [32,33].

As mentioned previously, ionic liquids exhibit an absence of detectable vapor pressure. Consequently, the first thing that happens when heating of the ILs is thermal decomposition. Huddleston et al. determined that the majority of ionic liquids (ILs) exhibit thermal decomposition around 400°C, indicating a notable level of thermal stability [34]. Additionally, Ngo and Villanueva observed that the thermal stability of ILs is heavily influenced by the anion present; $[Tf_2N]$- being identified as one of the most stable anions. [35,36]. Table 2.2 provides thermal decomposition temperatures for various ionic liquids (ILs) [8]. We can conclude that, alkyl chain of ILs does not exert a substantial influence on the T_d. However the selection of the anion component has an effect in this regard.

Table 2.2. T_d values of various ionic liquids (ILs)

Ionic Liquid	**T_d [°C]**
[bmim][I] [34]	265
[bmim][Cl] [34]	254
[bmim][BF_4] [34]	403
[bmim][PF_6] [34]	349
[emim][Tf_2N] [35]	455
[bmim][Tf_2N] [34]	439
[hmim][PF_6] [34]	417
[omim][PF_6] [34]	376
[emim][BF_4] [35]	412

2.1.2.2. Melting point

Du to the change in the size of cation and anion, ionic liquids' melting points change inversely. Conversely, when the cation in the IL exhibits heightened symmetry, this corresponds to a higher melting point. This phenomenon can be attributed to the improved packing efficiency of ions, which subsequently leads to higher melting points [2,37].

In Table 2.3, it is evident that the melting points follow a decreasing trend, with [emim] having a higher melting point compared to [bmim], consequently, [hmim] exhibits a lower

melting point compared to the aforementioned substances. This pattern is consistent among ionic liquids with the [PF_6] anion.

Ngo et al. stated that the introduction of larger and more asymmetrical substituted cations in imidazolium ionic liquids (ILs) leads to a decrease in their melting points [35]. According to Scurto et al., [38] the addition of carbon dioxide in an ionic liquid leads to notable reduction in the melting points, resulting in a phenomenon known as melting point depression. The researchers identified very pronounced interactions between CO_2 and the anion as the underlying cause of this effect, particularly in ionic liquids that contain fluorinated anions [2].

Table 2.3. The melting points of selected ionic liquids

Ionic Liquid	Melting Point (°C)
[bmim][Cl] [34]	41
[bmim][I] [34]	-72
[bmim][PF_6] [34]	10
[bmim][BF_4] [39]	-81
[bmim][$AlCl_4$] [40]	65
[emim][$AlCl_4$] [40]	84
[emim][PF_6] [28]	58-60
[emim][TFO] [41]	9
[emim][TF_2N] [41]	4
[hmim][PF_6] [39]	-61

2.1.2.3. Vapor Pressure

Ionic liquids have low volatility over normal operating temperatures hence; they have no measurable vapor pressure [26]. The process of separating a reaction mixture through distillation can be facilitated by utilizing of ionic liquids, as they effectively have no practical vapor pressure [26]. Rebelo et al. made an attempt to determine the critical points and normal boiling point temperatures of various ionic liquids [42]. The vapor pressures of ionic liquids are determined by Thermogravimetric analysis (TGA) [8]. Aschenbrenner et al. concluded that ionic liquids exhibit exceedingly low vapor pressures, even when compared to glycerol [43].

2.1.2.4. Density

Generally, ILs possess higher density than water, with values typically falling within the range of 1 to 1.6 g/cm^3 [8]. Elongating the alkyl chain length of the cation leads to a reduction in the density of the IL. Conversely, if the molecular weight of the anion increases, the density of the ionic liquid increases, too. In particular, among [bmim] ionic liquids, the [methide] anion exhibits the highest density in comparison to the [dicyanamide (Dca)] anion [8] Based on the discoveries made by Wasserscheid et al., there is a tendency for the density of ionic liquids to decrease as the size of the organic cation increases [26]. They suggested that even minor alterations in the structure of the IL can be utilized to finely adjust its density [26]. In order to measure the ionic liquid density, vibrating-tube densitometer is widely used. Using suitable reference fluids, a calibration is done as functions of temperature and pressure. Technically complex methods such as piezometric methods are used. However, they also provide additional thermodynamic property data [44]. Figures 2.4 and 2.5 illustrate the recorded densities of dehydrated ionic liquids plotted against temperature at a pressure of 1 bar [44].

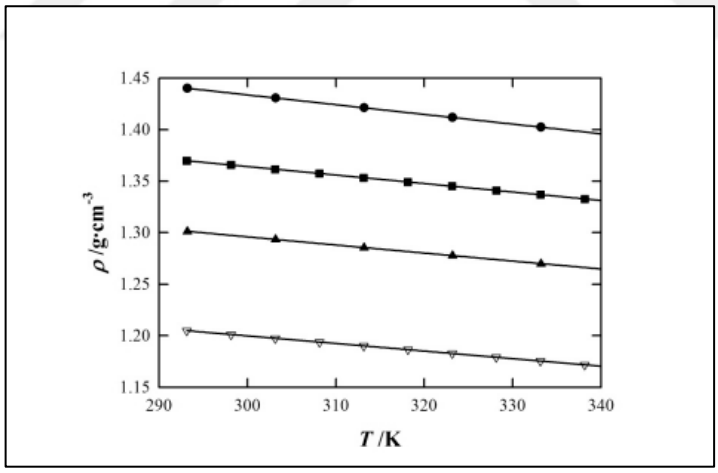

Figure 2.4. The impact of the anion on the densities of [bmim]$^-$based ionic liquids:●, [NTf_2]; ■, [PF_6]; ▲, [OTf]; ▼, [BF_4] [44]

The type of the anion strongly influences the density of ionic liquids [44]. Table 2.4 presents the densities of various anions in [bmim] ionic liquids. The presence of impurities in ionic liquids has a notable impact on their density [44]. Valkenburg et al. demonstrated that the

presence of water in ionic liquids acts as a diluent, resulting in a reduction in the density of the IL [45].

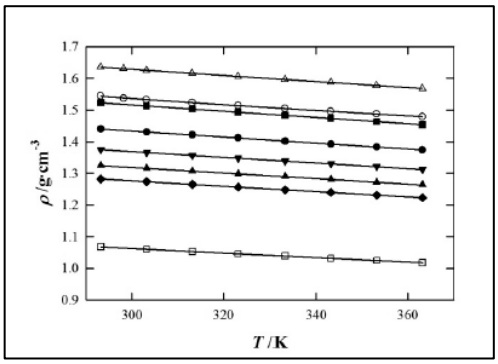

Figure 2.5. The influence of the cation on the densities of $[NTf_2]^-$based ionic liquids :■, $[C_2mim]^+$; ●, $[C_4mim]^+$; ▼, $[C_6mim]^+$, ▲, $[C_8mim]^+$; ◊, $[C_{10}mim]^+$; Δ, $[(NCCH_2)py]^+$; ○,$[(NCCH_2)mpyr]^+$; □, $[P_{6614}]^+$ [44]

Table 2.4. The densities of various anions in [bmim] ionic liquids

Anion	Density (g/cm^3)
$[BF_4]$ [46]	1.17 (30°C)
$[PF_6]$ [46]	1.37 (30°C)
$[CF_3SO_3]$ [46]	1.29 (20°C)
$[CF_3CO_2]$ [46]	1.209 (21°C)
$[Tf_2N]$ [46]	1.429 (19°C)
[Triflate] [47]	1.301 (22.6°C)
[Dca] [47]	1.058 (24°C)
[Methide] [47]	1.563 (22.5°C)

2.1.3. Transport Properties

The next section gives explanation about transport properties of ILs.

2.1.3.1. Viscosity

Viscosity is a crucial property in industrial processes as it is essential for designing processing units, and studying heat and mass transfer phenomena [32]. In the chemical

industry, ionic liquids exhibit higher viscosities compared to organic fluids that are commonly utilized. At room temperature, their viscosity values typically range from 10 cP to approximately 500 cP [37]. High viscosity can offer both benefits and drawbacks for combined heat and mass transfer operations [32].

In general, viscosity tends to decrease with increasing temperature. For example, both [hmim][PF_6] and [hmim][BF_4] experience a viscosity reduction of over 50 percent increasing the temperature from 20 °C to 30 °C [37]. Table 2.5 illustrates viscosity values of several ILs.

Table 2.5. Viscosity information for several ILs

Ionic Liquids	Temperature (°C)	Viscosity (cP)
[hmim][PF_6] [34]	20	680
[hmim][PF_6] [34]	30	363
[hmim][BF_4] [41]	20	314
[hmim][BF_4][48]	30	177
[bmim][BF_4] [48]	20	154
[emim][BF_4] [48]	20	66.5

2.1.3.2. Self-diffusion coefficients

ILs have found applications across various industries such as extraction and separation, catalysts, materials production and energy. In these processes determining the self-diffusion coefficients are crucial [49,50]. Wang et al., [50] stated that the self-diffusion coefficients of the cation exhibit higher values compared to the anion.

In their study, Umecky et al., mentioned that impurities in [bmim][PF_6] samples effect the results of self-diffusion coefficients [51].

2.1.3.3. Electrical conductivity

Ionic liquids exhibit high electrical conductivity due to the presence of both cations and anions [32]. However, their conductivities are lower comparing to concentrated aqueous electrolytes at room temperature. According to Endres et al., electrical conductivity values depend on mobility [37]. The ion mobility reduces with the large ionic buildings in ionic

liquids. For this reason, the electrical conductivity reduces. Also, they propose that ion pair formation reduces the conductivity [37].

2.1.3.4. Thermal conductivity

Valkenburg and his colleagues investigated the measurement of the thermal conductivities for ILs. Various data from research studies point to an interval of 0.106-0.238 W/mK at 298.15 K. The majority of reported values for ILs is approximately 0.15 W/mK, which is similar to the thermal conductivity of organic solvents such as toluene and methanol [45]. Tomida et al. conducted a study and concluded that there is no effect of the alkyl chain length on the thermal conductivity [52]. They stated that pressure dependence of thermal conductivity was small compared to toluene and benzene. They explained this phenomenon as low pressure dependence of IL density [52]. In a study conducted by Ge et al. (see Figure 2.6), thermal conductivity measurements were performed on eleven different ILs over a temperature range of 293-353 K [53].

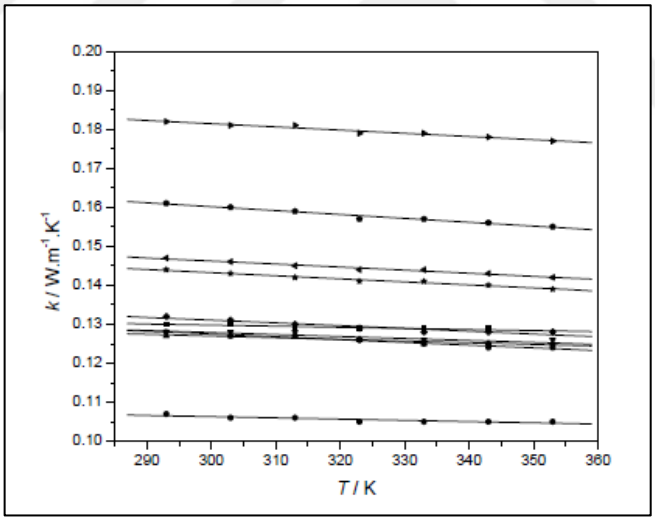

Figure 2.6. Thermal conductivities of ionic liquids at different temperatures: ■,[C_2mim][NTf_2]; ●, [C_4mim][NTf_2]; ▲, [C_6mim][NTf_2]; ▼, [C_8mim][NTf_2], ◊, [C_{10}mim][NTf_2]; ◄, [C_{10}mim][OTf]; ►, [C_2mim][$EtSO_4$]; ●, [C_4mpyrr][FAP] [53]

2.1.4. Application Areas of Ionic Liquids

Figure 2.7 [29] presents main areas of IL applications.

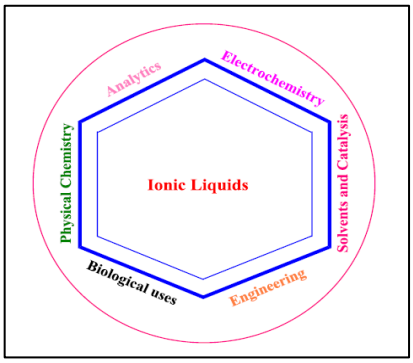

Figure 2.7. Application of ILs in various fields [29]

2.1.4.1. Solvent replacement

ILs, unlike volatile organic compounds (VOCs), possess extremely low vapor pressure, which makes them environmentally favorable. This characteristic minimizes the escape of harmful gases into the atmosphere and can effectively mitigate the emission of VOCs. [2]. ILs are regarded by the pharmaceutical and petrochemical industries as solvent alternatives that can replace the use of VOCs, leading to a paradigm shift aimed at reducing waste generation and eliminating the reliance on hazardous chemicals. This shift is driven by the industry's desire to minimize environmental impact and promote sustainable practices. [2,54,55]. Environmental factor (*E* factor) is developed by Roger Sheldon and named after him as Sheldon *E*- factor [55]. It is a metric of the waste generated during a process per unit of product produced, calculated by dividing the weight of waste (in kilograms) by the weight of product (in kilograms) [55]. A higher *E*-factor corresponds to a greater amount of waste generated, leading to a higher negative environmental impact. Table 2.6 presents the *E*-factor values, generated in the chemical industry [55]. The table illustrates that *E*-factor values for pharmaceutical industries range from 25 to 100, corresponding to production quantities of 10 to 10^3 t/year [55]. Hence, when comparing pharmaceutical industries to oil refining industries, it becomes evident that pharmaceutical industries employ less efficient and environmentally detrimental processes, albeit on a smaller scale. To mitigate the negative environmental impact, the widespread adoption of environmentally friendly ionic liquids as substitutes for hazardous VOCs can significantly reduce the *E*-factors and promote sustainable practices [55].

Table 2.6. *E*- Factors observed in the chemical industry [55]

Industry Segment	Tonnes per annum	*E*- Factor (Kg (waste)/ Kg (product)
Oil refining	10^6-10^8	<0.1
Bulk chemicals	10^4-10^6	<1-5
Fine chemicals	10^2-10^4	5-50
Pharmaceuticals	10-10^3	25->100

Huddleston conducted experiments showing the effectiveness of [bmim][PF_6] in extracting aromatic compounds from water [56]. Recently, several research groups have extensively studied the solvent properties of ILs to gain a comprehensive understanding. Additionally, solubilities of various organic compounds and water in ILs have been examined, providing valuable insights into their solvent behavior [2,54].

Chapeaux and Wishart et al. [57,58] have examined the application of IL pre-treatment of biomass for ethanol and butanol production. Furthermore, ILs have shown promising effectiveness in extracting sulfur from fossil fuels [59].

Ionic liquids offer an alternative as solvents or stabilizers to prevent the aggregation of nanoparticles. By incorporating ionic liquids into the nanoparticle synthesis process, they can influence the particle size by impeding crystal growth, leading to the formation of smaller nanoparticles [59].

2.1.4.2. Purification of Gases

Through experimental investigations, researchers have provided valuable insights into the solubility of various gases in ILs, leading to the development of gas purification processes that employ ILs [2].

All researchers concur that carbon dioxide (CO_2) exhibits exceptional solubility in ILs compared to other gases [2, 31]. Moganty and colleagues conducted an investigation on the solubility of CO_2 in eight distinct ILs, employing a quartz crystal microbalance technique [65]. They determined the Henry's constants for carbon dioxide in nine different ionic liquids with all measurements occured at a temperature of 298 K and pressures below 1 bar. Based on their discoveries, they reached the conclusion that the high solubility of gases in ionic liquids can be attributed to the characteristics of the anion present in the structure of the IL [60]. Anthony et al. conducted a study to investigate the solubility of nine different gases, in

[bmim][PF_6] at pressures up to 13 bar at a temperature of 25 °C (see Figure 2.8) [61]. Additionally, Figure 2.9 demonstrates the solubility curve of CO_2 in [bmim][PF_6] at different temperatures [61]. Moreover, the study has shown that as the temperature increased, the solubility of CO_2 in [bmim][PF_6] decreased at a constant pressure [61].

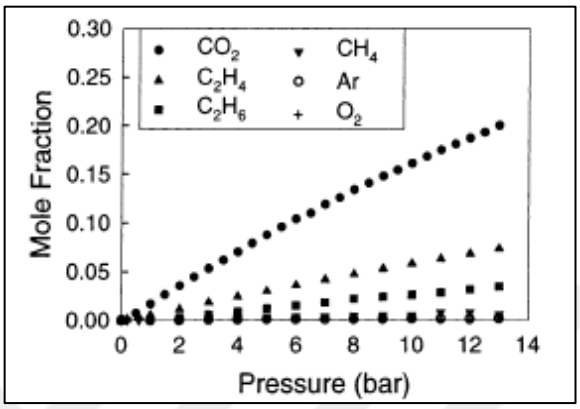

Figure 2.8. The solubility of several gases in [bmim]-[PF_6] at a temperature of 25 °C [61]

Camper et al. conducted a study on the solubility of CO_2 and C_2H_4 in various ionic liquids. Additionally, they investigated the impact of pressure and temperature on gas solubility in RTILs. However, it was observed that at higher pressures, the regular solution theory became ineffective as entropic effects became more prominent [62].

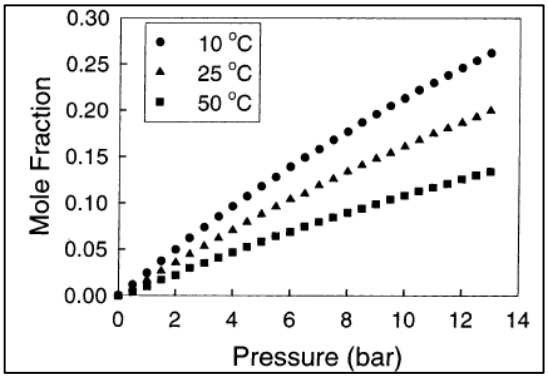

Figure 2.9. Solubility of CO_2 in 1-butyl-3-methylimidazolium hexafluorophosphate at temperatures of 10, 25, and 50 °C [61]

2.1.4.3. Homogenous and Heterogeneous Catalysis

A catalyst makes the reaction faster without being consumed. There are three types of catalysis: homogeneous, heterogeneous and bio-catalysis. By the help of catalysis, industrial processes become more efficient and economic. Catalysts are required in small quantities. They are preferable for green chemistry as they go back to their initial state after the reaction takes place [29]. Although there are some controversies about types of catalysts, homogeneous catalyst is generally associated with molecular organometallic chemistry. On the other hand, heterogeneous catalysts are associated with surface science and solid-state chemistry [29]. Homogeneous catalysis finds extensive applications in the chemical industry, offering several advantages over traditional heterogeneous catalysis systems. These catalysts exhibit high activity and selectivity while operating under relatively mild conditions. Table 2.7 presents the comparison of both types [29]. Because of their unique properties, they can offer advantages for both homogeneous and heterogeneous catalysis [72].

Table 2.7. Comparison between Homogeneous vs. Heterogeneous Catalysis [29]

	Homogeneous Catalysis	Heterogeneous Catalysis
Activity (relative to metal content)	High	Variable
Selectivity	High	Variable
Reaction conditions	Mild	Harsh
Service life of catalysts	Variable	Long
Sensitivity towards catalyst poisons	Low	High
Diffusion problems	None	May be important
Catalyst recycling	Expensive	Not necessary

Here is few instances of chemical reactions and catalysis involving ionic liquids (ILs). They can be used both in homogeneous and heterogeneous catalysis. The choice of catalyst depends on factors such as the nature of the reactants, the reaction conditions, and the desired selectivity and stability of the catalyst [2].

- Aromatic ring reactions and polymerization processes, ensuring cleaner and more efficient polymerization reaction.

- Friedel-Crafts alkylation reactions and reduction of aromatic rings, allowing for selective and controlled transformations.
- Carbonylation reactions, facilitating the introduction of carbonyl groups into organic compounds.
- Halogenation reactions, providing a suitable medium for the halogenation of various substrates.
- Oxidation reactions, enabling the oxidation of organic compounds with improved efficiency and selectivity.
- Nitration reactions, allowing for the introduction of nitro groups into organic molecules.
- Sulfonation reactions, facilitating the addition of sulfonic acid groups to organic compounds [2].

2.1.4.4. Biological Reactions Media

Lignocellulosic materials, which are renewable biomass, hold promise as sustainable feedstock for future biofuels and chemicals production. Figure 2.10 shows representative reaction for lignocellulose processing [29]. In order to produce energy lignocellulose should be broken down. Ionic liquids containing anions with hydrogen bonding capability have the ability to dissolve cellulose by disrupting the bonds within biomass [59].

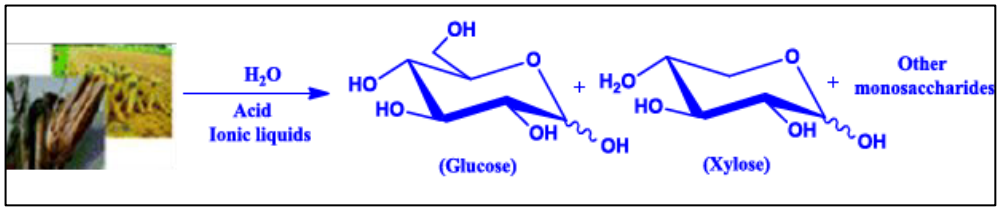

Figure 2.10. Exemplary reaction for the processing of lignocellulose [29]

Zhao and colleagues conducted a study to explore an effective system for the hydrolysis of lignocellulosic materials, employing various combinations of ILs. They discovered that the solubility of cellulose was enhanced as the ILs' anions exhibited stronger hydrogen bonding. The IL system they utilized as a solvent was based on 1-butyl-3-methylimidazolium [64].

2.1.5. 1-Butyl-3-Methylimidazolium Hexafluorophospate ([bmim][PF_6])

This ionic liquid is widely used in separation, catalysis and synthesis applications [22]. Figure 2.11 illustrates the structure of [bmim][PF_6] [65]. Table 2.8 presents most important parameters of [bmim][PF_6] [66].

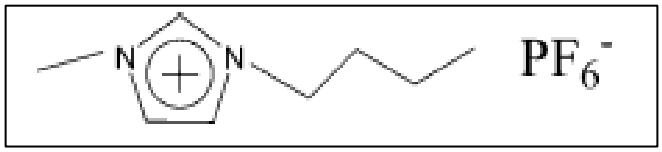

Figure 2.11. The molecular structure of [bmim][PF_6] [65]

Table 2.8. Some important properties of [bmim][PF_6] [66]

Ionic Liquid	**[bmim][PF_6]**
Cation	$C_8H_{15}N_2^+$
Anion	PF_6^-
Molecular weight (g/mol)	284
Tmelting (°C)	10
T_d (°C)	300
Density (g/cm^3)	1.37
Kinematic viscosity (mm^2/s)	281 (20°C)
Specific heat (J/g K)	78.7 (40°C)
Thermal conductivity at 25 °C (W/ mK)	0.15

2.2. SUPERCRITICAL FLUIDS (SCFS)

The origins of supercritical fluids can be traced back to the 1800s. It refers to a state of matter where the temperature has been raised beyond its critical temperature (Tc) and the pressure has been increased above its critical pressure (Pc), causing the distinction between liquid and gas phases to disappear. In this state, a supercritical fluid can permeate solids similar to a gas while also dissolving materials like a liquid [67]. A typical phase diagram of SCF is illustrated in Figure below 2.12 [68].

As we ascend along the boiling curve in Figure 2.12, the temperature and pressure experience a simultaneous rise. This causes the liquid to undergo thermal expansion, resulting in

reduced density, while the gas becomes denser due to increased pressure. Ultimately, at the critical point, the densities of the two phases converge and become indistinguishable, causing the disappearance of the clear boundary between gas and liquid [68]. Table 2.9 provides data on physical properties of supercritical fluids in comparison to liquids and gases. In Table 2.10 critical point and density values for some compounds are given. The advantages of using supercritical fluids in chemical reactions are given in Table 2.11. Supercritical fluids exhibit advantageous mass transfer characteristics, including diffusivities that are at least ten times higher and viscosities that are at least ten times lower compared to those of a liquid solvent [69,70].

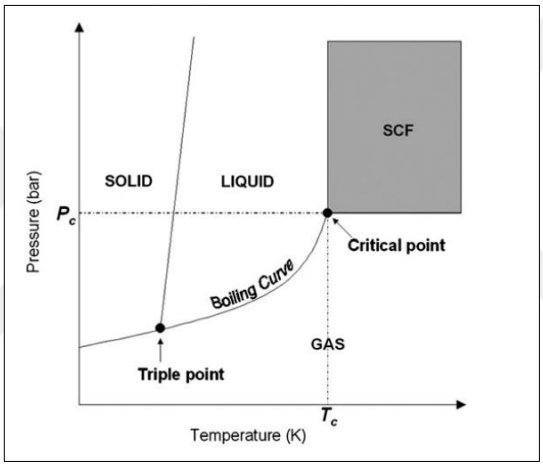

Figure 2.12. Single-component phase diagram [68]

Table 2.9. Physical properties of supercritical fluids in comparison to liquids and gases [68]

State	Density (kg/m^3)	Viscosity (Pa.s)	Diffusivity (m^2/s)
Liquid	$<10^{-5}0$	1	1000
SCF	10^{-2}-10^{-3}	10^{-2}	300
Gas	0.1	10^{-2}	1

Table 2.10. Critical point and density values for some compounds [71]

Substance	T_c/K	P*c*/atm	ρ/gml^{-1}
CHF_3	299.3	46.9	0.528
CH_4	190.5	41.4	0.162
C_2H_4	282.3	50.5	0.215
C_2H_6	305.2	48.2	0.203
CO_2	304.1	72.8	0.469
H_2O	647.1	218.3	0.348
CH_3CH_2OH	513.9	60.6	0.276

Table 2.11. Advantages of using SCFs rather than liquids as reaction media [71]

Category	Advantage	Which SCFs
ENVIRONMENT	Do not damage ozone layer	Most
	Do not contribute to smoke	Most
	No acute ecotoxicity	CO_2, H_2O
	No liquid wastes	CO_2, and other volatile SCFs
HEALTH & SAFETY	Noncarcinogenic	Most
	Nontoxic	Most
	Nonflammable	CO_2, N_2O, H_2O,Xe, Kr
PROCESS	No solvent residues	CO_2 and other volatile SCFs
	High diffusion rates	All
	Low viscosity	All
	Adjustable density	All
	Inexpensive	CO_2, H_2O
CHEMICAL	High miscibility with gases	All
	High compressibility	All

2.2.1. Supercritical CO_2

The majority of chemical reactions conducted in industrial settings take place within organic solvents, which encompass substances such as benzene, chlorofluorocarbons (CFCs), and carbon tetrachloride. However, it is important to note that CFCs and CCl_4 pose a threat to the ozone layer and are recognized as some of the most frequently released chemicals into the environment. There is a wide range of compounds suitable for use as fluids in supercritical techniques, but carbon dioxide stands out due to its non-toxic, non-flammable,

inexpensive, and chemically stable nature. Consequently, $scCO_2$ is the most favored choice in various industries [69,72]. The state of CO_2 can be either liquid or supercritical fluid depending on the pressure and temperature conditions. Carbon dioxide phase behavior is illustrated in the Figure 2.13 [73]. The liquid phase exists at pressures and temperatures above the triple point (0.52 MPa, 216.75 K). Similarly, above the critical point (7.38 MPa, 304.2 K), the supercritical phase is present [73]. Upon reaching the critical point, meniscus separating the liquid and gas phases vanishes as illustrated in Figure 2.14 [69,70].

Precautions about safety should be taken into considerations during the experiments because; they are conducted pressures between 100-200 bars [68]. Table 2.12 outlines the advantages and disadvantages of utilizing supercritical carbon dioxide as a solvent [68].

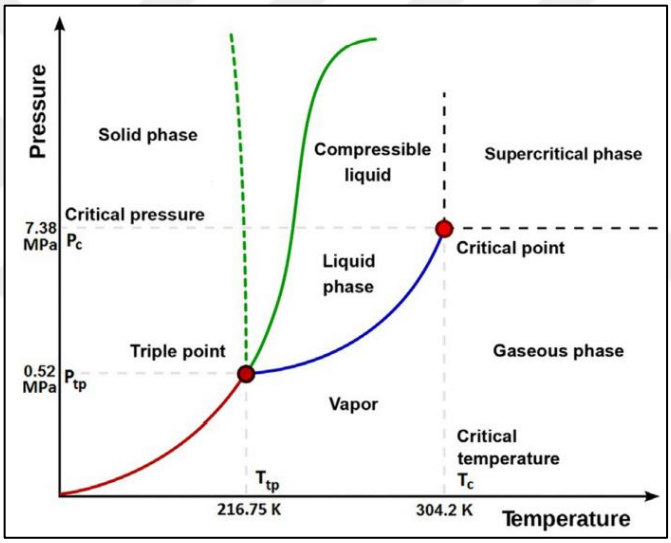

Figure 2.13. Phase behavior of CO_2 [73]

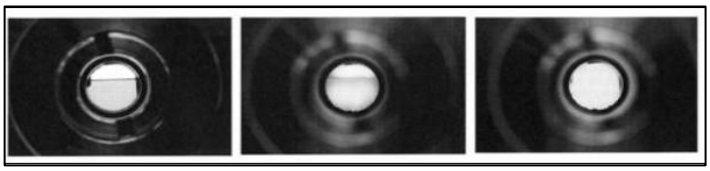

Figure 2.14. CO_2 becoming a SCF [74]

Table 2.12. The advantages and disadvantages of $scCO_2$ [68]

Advantages	Disadvantages
Nonflammable	Involves high pressures
Nontoxic to the environment	
Low viscosity	Equipment costs may be high
Gas miscibility	
Tunable solvent	Weak solvent
Relatively inert	
Nonoxidisable	

Due to the presence of strong electrostatic forces between ions, supercritical carbon dioxide ($scCO_2$) is soluble in ionic liquids. However, the reverse is not true, as ionic liquids do not dissolve in $scCO_2$. As temperature rises the solubility of CO_2 decreases. Additionally, when the moisture content of an ionic liquid increases, it causes a reduction in the solubility of CO_2 [61].

2.2.2. Applications of Supercritical Fluids

Supercritical fluids find extensive applications in various industries, including food, pharmaceutical, chemical, textile, and fuel industries. [67]. Extraction, which is one of the extensively researched methods, plays a significant role in the applications of supercritical fluids [67].

It is known that $scCO_2$ is chemically pure, nontoxic, nonflammable, nonpolar, stable, colorless, odorless, and can easily be removed, therefore it is a good extraction solvent [69,72]. Chemicals or flavors can be extracted from products like coffee, tea, herbs, and spices using extraction [5,75].

Decaffenication of coffee process by using $scCO_2$ as a solvent is given in Figure 2.15 [76]. In the process of steaming, coffee beans are subjected to elevated temperatures until their moisture content reaches 30% of their weight, resulting in a substantial expansion of the beans. The operating conditions are 90 °C and 250 bar for this system. Inside the extractor, the coffee beans are charged and pressurized with carbon dioxide. Finally, the extractor enters a downtime after extraction is finished so that it can be emptied and recharged with new beans [76].

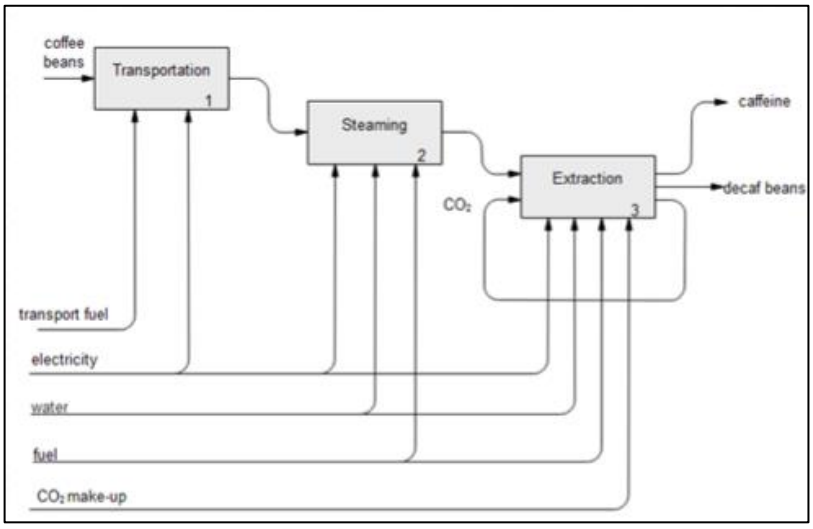

Figure 2.15. Industrial decaffeination of coffee beans [76]

Figure 2.16 illustrates a suggested method for extracting canola oil using a supercritical extraction process by using $scCO_2$ as a solvent. Furthermore, after the extraction process, the solvent can be easily depressurized, allowing for the removal or condensation of CO_2. [77].

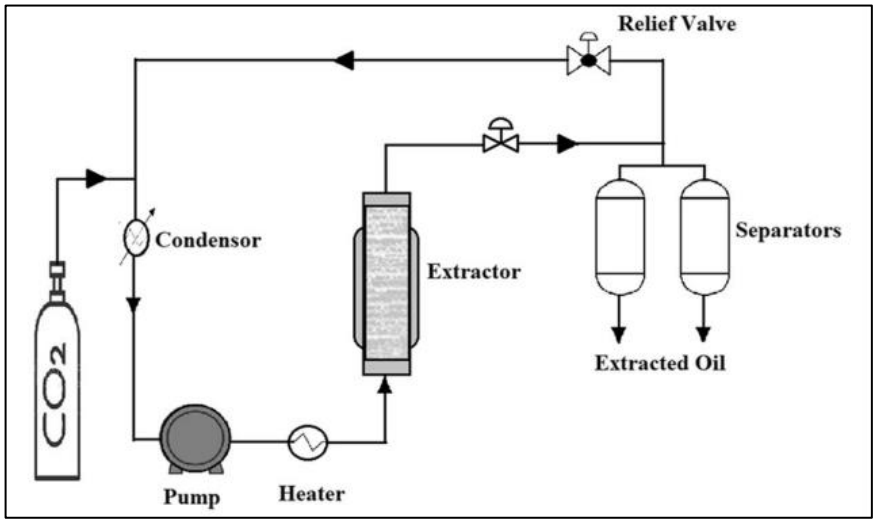

Figure 2.16. Extraction of canola oil by using sCO_2 [77]

On the other hand supercritical water (sH_2O) is also used as a solvent and reaction medium for its unique properties. The critical temperature and pressure of water are 374.3 ℃ and

22.1 MPa, respectively. The physical characteristics of supercritical water are clearly distinct from those of ordinary water. In the supercritical state, the density of water is reduced compared to that of regular water, approximately by a factor of one-third [78]. Treating wastewater and sewage has been a widely common application for SCWO technology [79] Figure 2.17 shows supercritical water oxidation in waste water treatment [80]. The SCWO process consists of four primary stages for the elimination of organic wastes: 1) Preparation and pressurization of the feed. 2) Reaction. 3) Separation of salts and 4) Recovery of heat and depressurization [80].

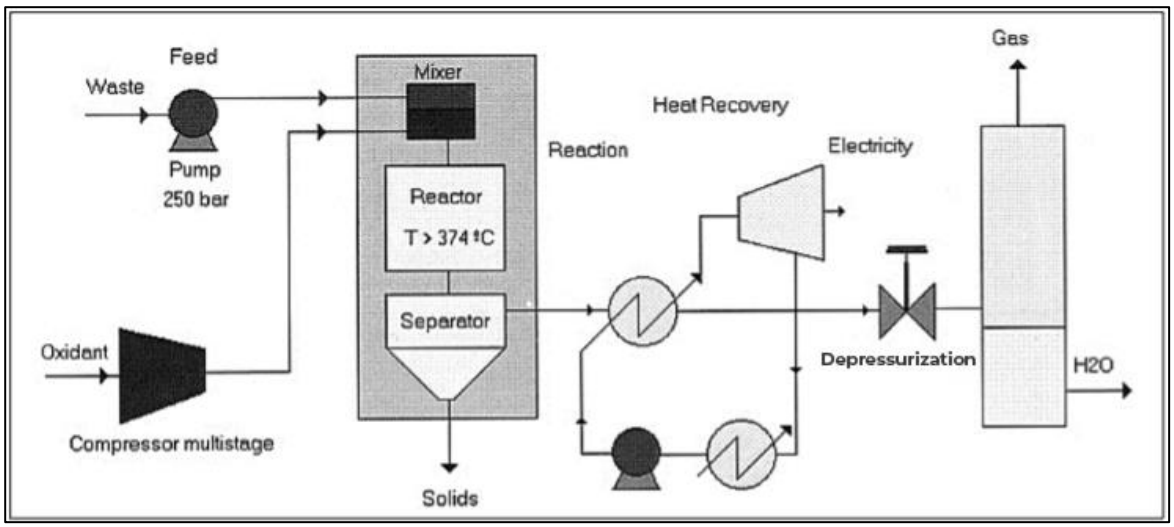

Figure 2.17. SCWO in waste water treatment [80]

2.3. THE DEFINITIONS OF GAS EXPANDED LIQUIDS (GXLS) AND CO_2 EXPANDED LIQUIDS (CXLS)

As a general definition, a gas-expanded liquid (GXL) refers to a liquid that undergoes an increase in volume when pressurized with a compressed gas, like ethane or CO_2. Jessop et al. classified GXLs because they exhibit different behaviors with expanding gases. When subjected to CO_2 pressure, liquids do not exhibit uniform expansion. As a result, researchers have proposed three broad categories to classify their behavior [7].

Class 1 liquids, such as water, expand insufficiently due to the fact that they are not able to dissolve enough CO_2 [7].

Class II liquids, such as methanol, hexane, acetone, etc. are able to dissolve CO_2 in significant amounts and consequently, expand greatly [7].

Class III GXLs, for example ILs, liquid polymers, and crude oil expansion is moderate. In ILs-CO_2 systems CO_2 has high solubility in ILs, yet the volumetric expansion is moderate because the empty spaces of the network formed by anion and cation in ILs are filled with CO_2. So, the density of the liquid phase increases [6]. While viscosity changes significantly, polarity does not change as, accordingly [62].

The critical location of a mixture refers to the maximum operating point within a GXL system before transitioning into the supercritical fluid state [81]. Figure 2.18 presents the critical point of CO_2 and methanol mixture. Once the critical exceeded, the two components become infinitely miscible, or in other words, they exhibit complete miscibility [81].

When CO_2 dissolves in the liquid state, it leads to a reduction in viscosity. Sih et al.'s study indicated that at elevated pressure (77 bar) and temperature (40ºC), the viscosity of methanol reduces by 80% when transitioning from pure methanol to CXL methanol, as depicted in Figure 2.19 [82].

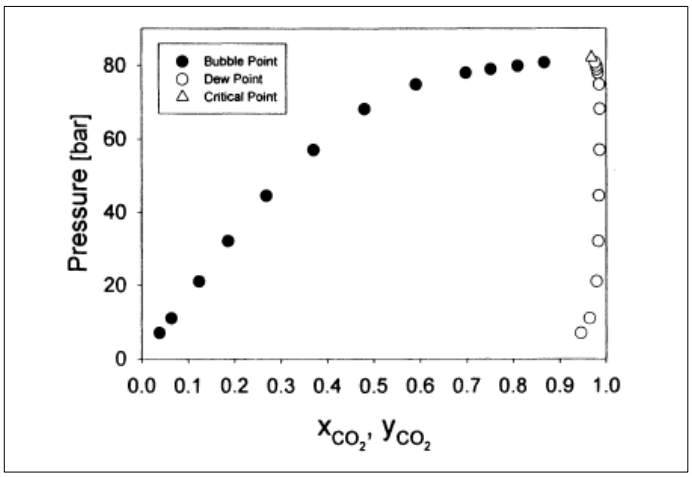

Figure 2.18. The equilibrium between vapor and liquid phases of methanol and CO_2 at a temperature of 40ºC [81]

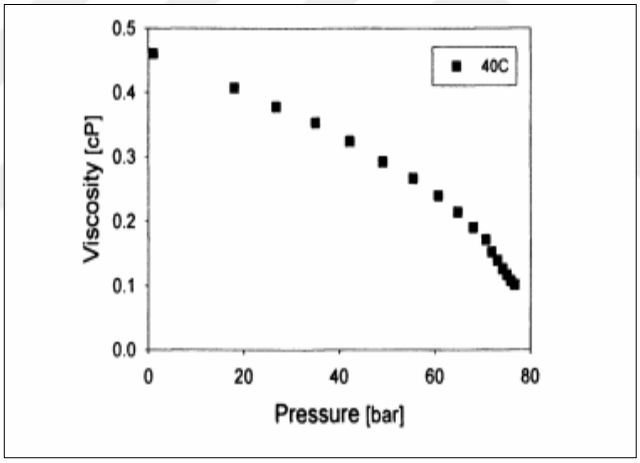

Figure 2.19. Viscosity of methanol and CO_2 at 40ºC [82]

The Stokes-Einstein relationship establishes a reciprocal connection between diffusivity and viscosity. In their research, Eckert et al. discovered that, the diffusivity of benzene in CO_2-expanded methanol increases by more than 200 percent at 40ºC and 15 MPa. Figure 2.20 provides a visual representation of this scenario [83].

Multiple research groups have acknowledged that gas expanded liquids are recognized as a promising substitute medium for conducting various processes such as separations, extractions, reactions, and other applications.As environmentally benign solvents, $scCO_2$, water, CXLs, ILs, have received much attention from scientific community [7].

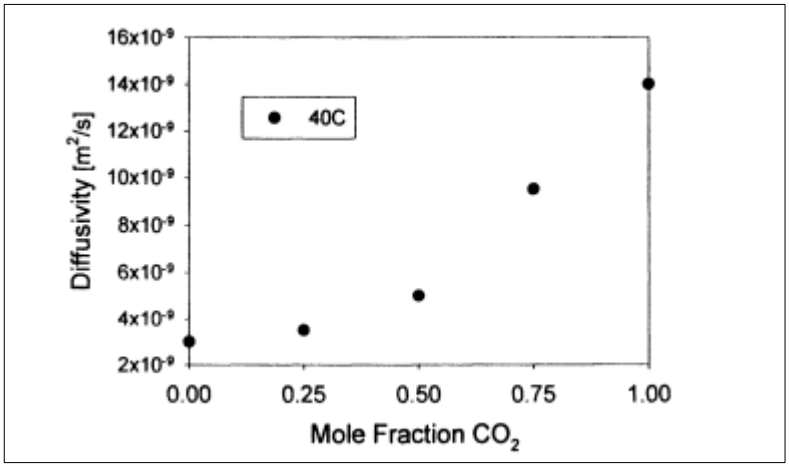

Figure 2.20. Diffusion of benzene in methanol expanded with CO_2 [83]

The application areas of CXLs include, utilizing as reaction solvents in catalytic reactions, for polymer processing, and in separations processes [7].

Moreover, GXLs and CXLs have benefits such as, CO_2 can be easily removed from the system compared to liquid solvents, they enhance the solubility of reagent gases, etc.[8].

2.4. HIGH PRESSURE PHASE BEHAVIOR OF CO_2-IL SYSTEMS

Prior research indicates that supercritical CO_2 extraction is an effective technique for extracting solute from ionic liquids (ILs). To advance such applications, it is necessary to explore the phase behavior of IL-CO_2 systems. While CO_2 dissolves in ionic liquids, the reciprocal dissolution of ionic liquids in CO_2 occurs insignificantly [2].

2.4.1. [bmim][PF_6]-CO_2 Systems

As mentioned before due to its non-volatility, non-water solubility, and having low melting point, [bmim][PF_6] is one of the most widely studied ionic liquids [2]. Ionic liquids are generally highly viscous; addition of high pressure carbon dioxide decreases the liquid phase viscosity and mass transfer properties improve [18,84].

Numerous articles in the literature have extensively explored the solubilities of CO_2 in ILs under high pressure conditions [85,86]. Blanchard et al. conducted a study focusing on the solubility of CO_2 in [bmim][PF_6] at various temperatures (313.15, 323.15, and 333.15 K) and pressures up to 93 bar. Two distinct experimental set-up for their research are used:one is a static high-pressure phase equilibrium apparatus and the other one is: dynamic flow apparatus. In Figure 2.21 a static high-pressure vapor-liquid equilibrium apparatus is presented [87]. The researchers exhibited that as the pressure rises, the solubility of CO_2 in [bmim][PF_6] increases, while it decreases with a decrease in temperature [87]. Within this specific temperature and pressure range, they observed a relatively minimal dependence of solubility on temperature [87].

Additionally, the substantial solubility of CO_2 has a noteworthy impact on the viscosity of the IL. Their findings indicate that the solution process becomes easier due to the reduction in the viscosity [2,87]. Various experimental configurations were employed by researchers in their investigations of measuring the solubility of CO_2 in [bmim][PF_6] [2]. At a temperature of 25° C and pressures reaching up to 10 bar, Kim et al. examined the solubility of CO_2 in [bmim][PF_6] [88]. The general form of the experimental set-up used by Kim et al. is illustrated in Figure 2.22 [88]. The results they obtained were in strong concurrence with the findings previously reported by Kamps et al.,is given in Figure 2.23 [88,89].

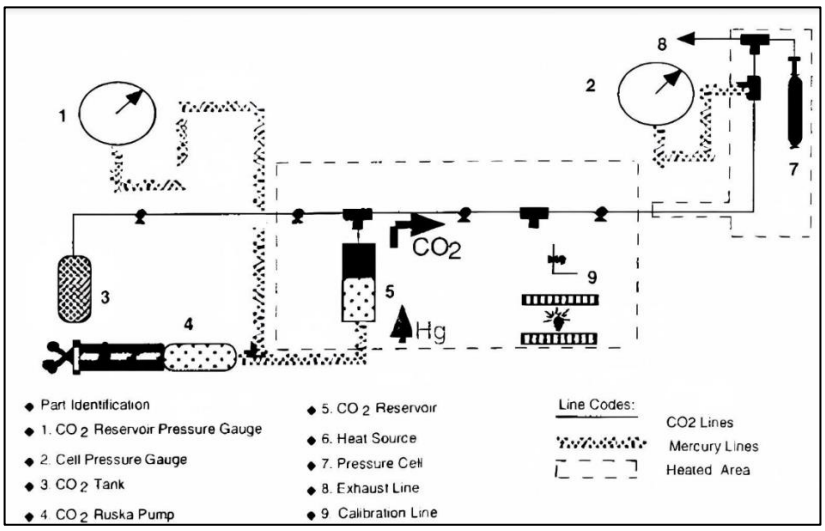

Figure 2.21. A Static high-pressure vapor-liquid equilibrium apparatus [87]

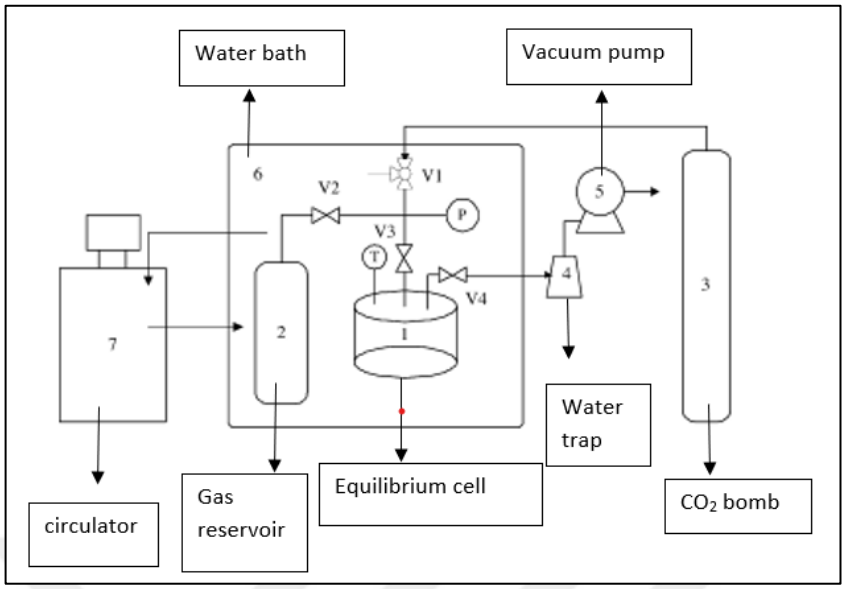

Figure 2.22. Schematic diagram of experimental apparatus [88]

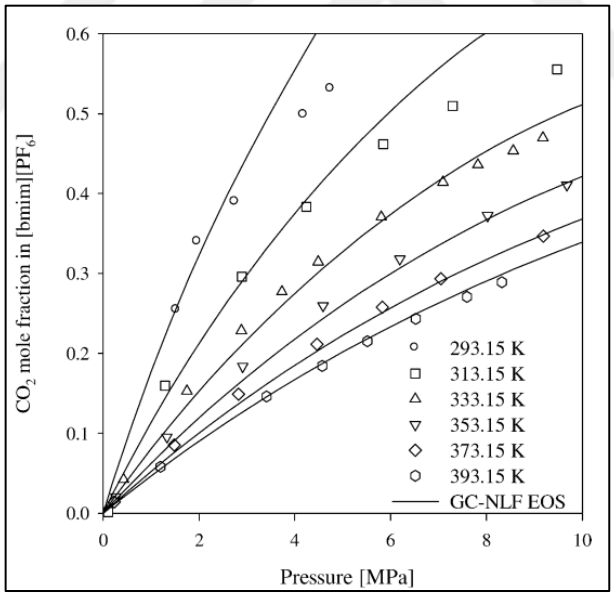

Figure 2.23. Comparisons of experimental solubility values of CO_2 in [bmim][PF_6] [88] with calculated values [89] at varying pressures

Kamps et al. conducted a study where they presented data regarding the solubility of carbon dioxide in [bmim][PF_6] over a temperature range spanning from 20° C to 120° C and pressures reaching up to 97 bar [89]. For measuring the solubility of CO_2 in [bmim][PF_6], a

thermostated high-pressure cell was employed as their experimental set-up. In Figure 2.24, their set-up is presented and the names of the equipments are labeled [90]. They employed Henry's extended law to model the solubility, and the data they presented exhibited contrasting results compared to the reported solubility data by Blanchard et al., as illustrated in Figure 2.25 [2,89,91].

Aki et al. [22] reported the solubility of CO_2 in [bmim][PF_6] at 40 °C, and their results were compared to earlier studies conducted by Kamps et al. [89], Blanchard et al. [87], and Liu et al. [92]. As expected, there is a satisfactory agreement among the data points at low pressures. However, in Figure 2.25 a noticeable disparity emerges at high pressures is presented [22].

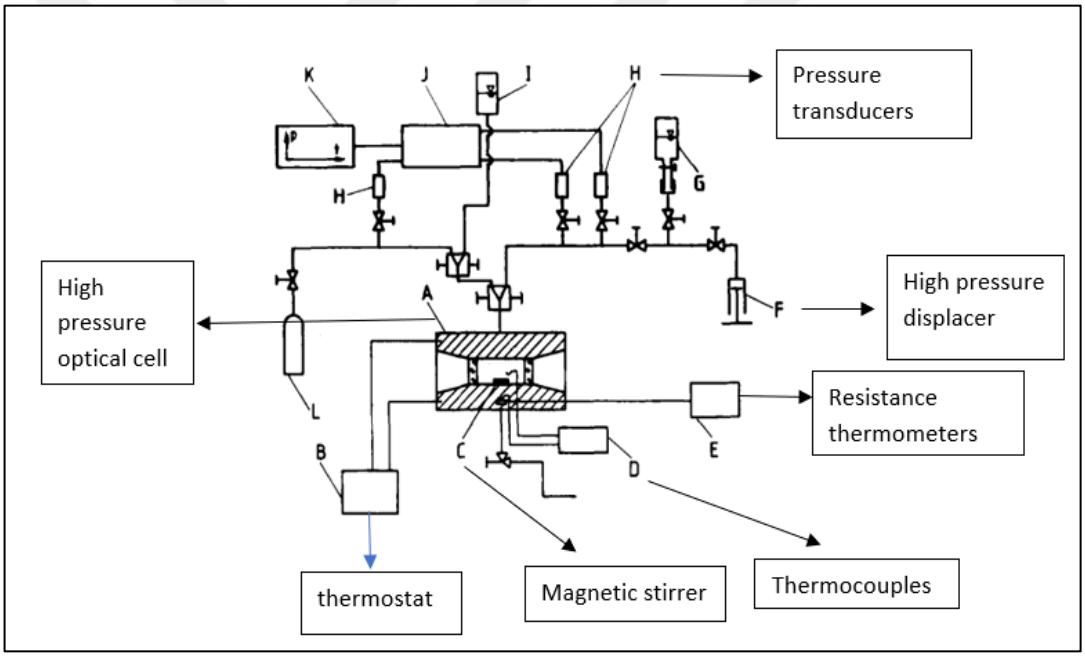

Figure 2.24. The experimental apparatus designed for measuring the solubility [90]

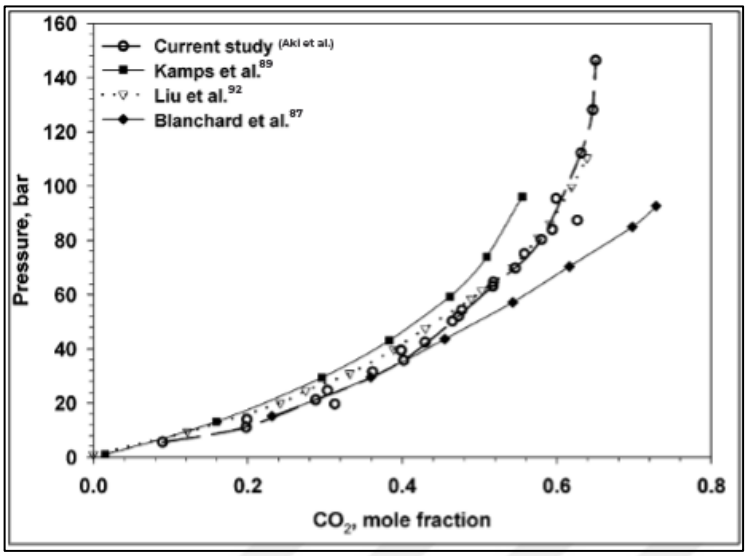

Figure 2.25. The solubility of CO_2 in [bmim][PF_6] at 40 °C, values reported in the literature [22]

According to the study of Lim et al. the solubility of carbon dioxide in [bmim][PF_6], was measured at pressures up to 320 bar and at temperatures of 40, 50, and 60 °C in a high-pressure viewcell [93]. They conducted a comparison between the solubility of carbon dioxide in [bmim][PF_6] and other ionic liquids, namely [bmim][BF_4] and [omim][BF_4].They have found that the solubility of CO_2 was higher for the ILs that have longer cationic alkyl group and lower anion polarity [93].

There is a scarcity of research on the diffusion coefficients of CO_2-IL systems, especially under high pressure conditions. However, they need to be known for the design and development of the applications of these systems [94–98].

Barghi et al. stated that, the average diffusion coefficient was measured to be 4.3×10-10 m^2/s at 5 MPa and a temperature of 323.15 K [98]. Another researcher Gong et al. [96] had also this value and at 8 MPa the average diffusion coefficient that they had found increased to 5.7 $x10^{-10}$ m^2/s . Moya et al. found a higher value for the diffusivity at 318 K and 2 MPa (about 9.0 $x10^{-10}$ m^2/s) [15,97].

2.5. COMPUTATIONAL FLUID DYNAMICS (CFD)

The utilization of applied mathematics, physics, and computational software in conjunction with Computational Fluid Dynamics (CFD) is instrumental in visually representing the flow of gases or liquids and understanding the impact of such flow on objects [99].

Partial differential equations (PDEs) serve as the governing equations for fluid flows, encompassing the conservation principles of mass, momentum, and energy. Kuzmin describes CFD as the practice of substituting these PDE systems with a set of algebraic equations that can be efficiently solved using digital computers [100].

Equation 2.1 signifies the equation of mass conservation, also known as the continuity equation [101]:

$$\frac{\partial \rho}{\partial t} + \nabla . (\rho \vec{V}) = 0¤ \tag{2.1}$$

The equations governing momentum balance, known as the Navier-Stokes equations, can be formulated as follows (Eq. 2.2) for three-dimensional, incompressible flow [101].

$$\rho \frac{DV}{Dt} = \rho g - \nabla p + \mu \nabla^2 V \tag{2.2}$$

Equations can be expressed in x,y,and z dimensions as Eq. 2.3, 2.4 and 2.5.

$$\rho \left(\frac{\partial u}{\partial t} + u \frac{\partial u}{\partial x} + v \frac{\partial u}{\partial y} + w \frac{\partial u}{\partial z} \right) = \rho g_x - \frac{\partial p}{\partial x} + \mu \left(\frac{\partial^2 u}{\partial x^2} + \frac{\partial^2 u}{\partial y^2} + \frac{\partial^2 u}{\partial z^2} \right) \tag{2.3}$$

$$\rho \left(\frac{\partial v}{\partial t} + u \frac{\partial v}{\partial x} + v \frac{\partial v}{\partial y} + w \frac{\partial v}{\partial z} \right) = \rho g_y - \frac{\partial p}{\partial y} + \mu \left(\frac{\partial^2 v}{\partial x^2} + \frac{\partial^2 v}{\partial y^2} + \frac{\partial^2 v}{\partial z^2} \right) \tag{2.4}$$

$$\rho \left(\frac{\partial w}{\partial t} + u \frac{\partial w}{\partial x} + v \frac{\partial w}{\partial y} + w \frac{\partial w}{\partial z} \right) = \rho g_z - \frac{\partial p}{\partial z} + \mu \left(\frac{\partial^2 w}{\partial x^2} + \frac{\partial^2 w}{\partial y^2} + \frac{\partial^2 w}{\partial z^2} \right) \tag{2.5}$$

With the help of CFD software, one can analyze turbulent and laminar flow problems in arbitrary complex geometries. Applications characterized by interactions between complex

flow fields and chemical reactions can be studied. As examples of the widely used software packages, FLUENT and CFX from ANSYS and STAR-CD from CD Adapco Group can be counted [102].

The limitations that experiments bring, can be overcome more easily and efficiently by using CFD [103]. For reactor design, studying bubble behavior in liquids is of significant interest [104].

FLUENT was utilized to investigate the gas-liquid mass transfer behavior within ionic liquids in the study of Wang et al. [105]. Their experimental set up is given in Figure 2.26 [105].

Meikandan et al. conducted a study utilizing CFD analysis to examine the heat transfer properties of ionic liquids within a tubular heat exchanger [106].

Ouyang and his colleagues utilized CFD to investigate the flow of CO_2 in [bmim][BF_4] within a stirred tank. To accurately describe the behavior of bubbles, they employed the population balance method [103].

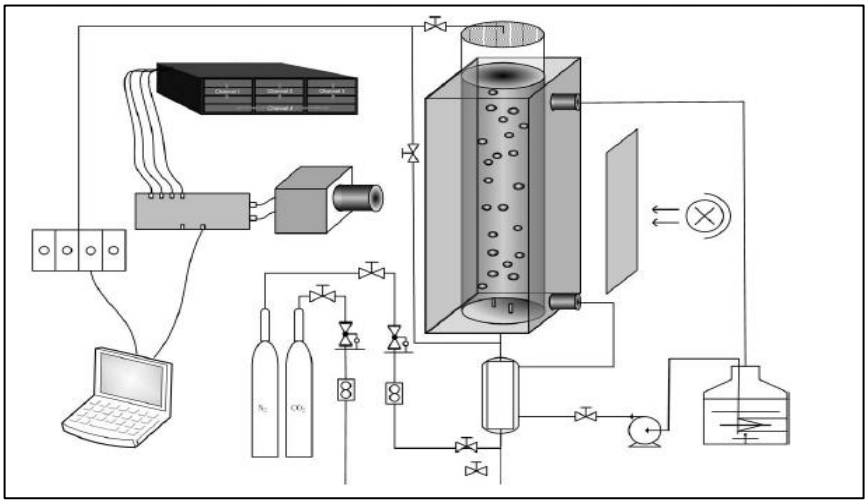

Figure 2.26. Sketch of the experimental apparatus for CFD-PBM [105]

3. METHODOLOGY

In this section, a comprehensive explanation of the experimental system, procedure, and transport model will be presented.

3.1. EXPERIMENTAL SET-UP AND PROCEDURE

Figure 3.1. shows the experimental system. The mainly used equipments in this system are: a syringe pump, a cathetometer and a high pressure view cell. Carbon dioxide can be loaded to the system by using syringe pump at a constant pressure. During the experiments, a cathetometer is used in order to follow to track the rise in the liquid level.

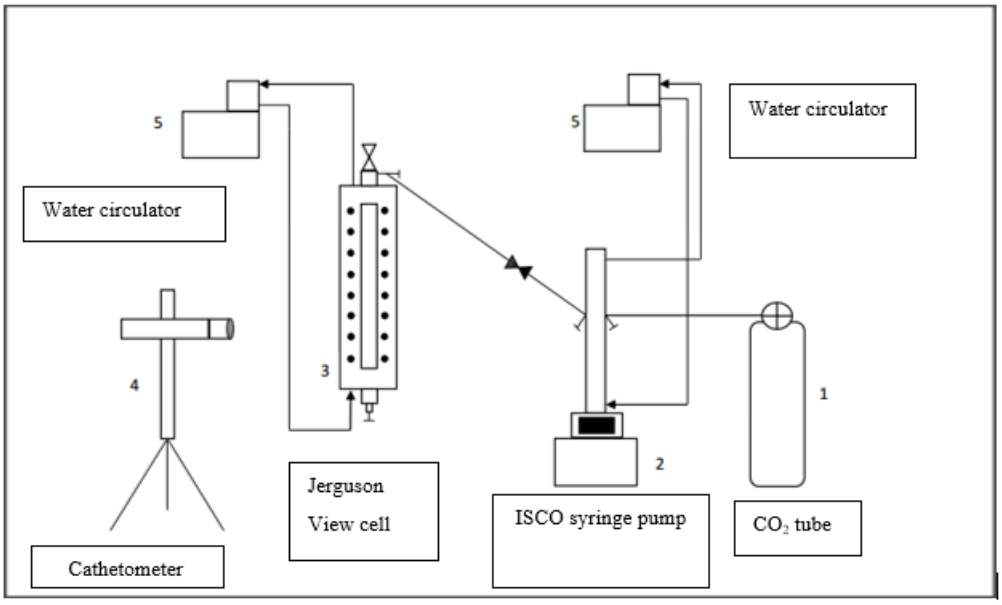

Figure 3.1. Experimental set-up of CO_2-[bmim][PF_6] system [107]

Before each experiment, leakage test is carried out in order to see if there is carbon dioxide leak in the system. The view-cell is tested for 1500-2000 psi; CO_2 is loaded to the view-cell. Until it remains stable, the pressure is carefully monitored.

Generally; experiments begin with filling syringe pump with liquid carbon dioxide at a temperature of 10° C. Following the filling of the pump, the pressure is adjusted to the desired value. Using two water circulators , the temperature is set and kept constant at the

same time. When the desired pressure is reached, the carbon dioxide is introduced into the line connecting the view-cell and syringe pump.

Carbon dioxide with a purity of 99.9 % is purchased from Habas. [bmim][PF_6] with a purity of 99% is purchased from IOLITEC. Karl-Fischer titration has resulted in a water content less than 300 ppm in all the ionic liquid samples used in the experiment which is adequately low for precise determination of mole fractions [15,93,108].

Ionic liquid is injected with a syringe from the bottom valve of the view-cell. The syringe was weighed with an analytical balance. The difference between the weights of the syringe before and after injection indicates the mass of IL. The IL is kept in the view-cell before carbon dioxide loading to ensure the thermal equilibration. The cathetometer is placed approximately one meter away faced to the view-cell. The initial liquid level is set to zero by targeting the cross hair to the meniscus line of the liquid. The initial volume of CO_2 in syringe pump is recorded. Subsequently, high-pressure carbon dioxide is loaded into the view-cell. CO_2 is supplied at a constant pressure regulated by a high pressure syringe pump, initiating the flow of it. There is a check valve between the pump and view-cell to prevent the back flow from the view-cell to the syringe pump.

A pressure transducer is used to monitor the pressure of the carbon dioxide in the view-cell. As the carbon dioxide starts to dissolve in the liquid phase, the liquid height starts to show an increment. The interface position is tracked during the dissolution process. The liquid level in the cell is monitored. The decreased volume of CO_2 in the syringe pump is also continously monitored. This situation continues until the system reaches equilibrium. After collecting the final measurements, the system undergoes depressurization. To prevent any accidents, it is crucial to release high pressure CO_2 at a very slow flow rate.

The mass fraction of carbon dioxide in the liquid can be determined by using the liquid height and CO_2 volume data as follows:

$$m_{CO_2\ in\ the\ liquid\ phase} = m_{CO_2\ delivered\ to\ the\ system} - m_{CO_2\ \text{in the gas phase}} \qquad (3.1)$$

Mass of the carbon dioxide delivered to the system and in the gas phase can be calculated from the carbon dioxide molar volume data at constant temperature and pressure reported in the literature. The total liquid volume in the view-cell at any time can be found using the

initial ionic liquid volume and cathetometer is used in order to determine the boost in the liquid volume [15].

The measurement uncertainties for liquid level, volume, temperature, and pressure are ±0.01 mm, ±0.01 mL, ±0.1 K, and ±0.0138 MPa, respectively. The estimation of the overall error in determining the equilibrium mole fractions is around ±0.002 [15].

3.2. THE TRANSPORT MODEL

One-way mass transfer is triggered by introducing high pressure carbon dioxide into IL system. The carbon dioxide dissolves in the ionic liquid, but there is negligible diffusion of the ionic liquid into the gas phase. During this process, interface of the phase moves upward and the liquid phase density changes (see Figure 3.2) [107].

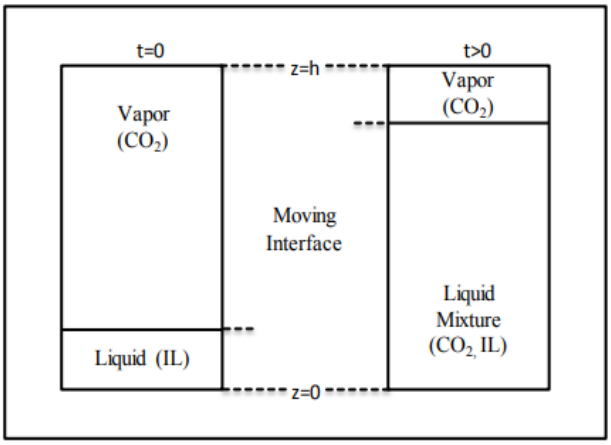

Figure 3.2. Interface position of IL-CO_2 system

The transport model of the system, two phases separated by a dynamic boundary, is developed using ANSYS FLUENT [107]. The continuity equation solved throughout the entire flow domain is represented by the following equation [109–111].

$$\frac{\partial(\rho\phi_k)}{\partial t} + \nabla.(\rho u\phi_k) = -\nabla.(J_{\phi_k}) + S_{\phi_k} \quad (3.2)$$

$$J_\phi = -\rho_L D\nabla w_{CO_2} \quad (3.3)$$

In the model, the mass fraction is represented by a user-defined function ϕ. At the phase interface, the mass fraction stays constant at the thermodynamic equilibrium value and increases from zero in the liquid phase during the diffusion process. To maintain the gradient's continuity, ϕ is also defined within the gas phase and kept constant at the equilibrium value using a source term, S [107].

$$S_{\phi_k} = A(\phi_{k,eq} - \phi_k) \quad (3.4)$$

In Equation (3.4), a suitably large value is assigned to A to prevent ϕ from decreasing in the gas phase during diffusion. In contrast, S is set to zero in the liquid phase [107].

Movement of the phase-interface is tracked by the Volume-of-fluid method [112] where a function for the liquid phase volume fraction is defined in every grid cell and advected by the velocity field as described by the following equation [107]:

$$\frac{\partial(\alpha_L\rho_L)}{\partial t} + \nabla.(\alpha_L\rho_L u) = S_{\alpha L} \quad (3.5)$$

where α_L presents the volume fraction of the liquid phase .The value of α_L is between 0 and 1 if the computational cell contains the phase interface. The source term, $S_{\alpha L}$, is nonzero due to the interphase mass transfer and calculated using equation 3.6 where ρ_L, D and w_{CO_2} denote the liquid phase density, binary diffusion coefficient and mass fraction of carbon dioxide respectively [107].

$$S_{\alpha L} = -\rho_L D\nabla w_{CO_2}.\nabla\alpha_L \quad (3.6)$$

The volume fraction of the gas phase, α_G is calculated using the constraint that the volume fractions of the phases must add up to unity. To satisfy the mass balance, in the gas phase,

the source term, $S_{\alpha G}$ must be equal to $S_{\alpha L}$ in magnitude with opposite sign (See Equations (3.7) and (3.8)) [15].

$$\alpha_L + \alpha_G = 1 \tag{3.7}$$

$$S_{\alpha G} = -S_{\alpha L} \tag{3.8}$$

In FLUENT, PISO algorithm is applied for the pressure-velocity coupling [113]. For the momentum equation and the transport of the user-defined scalar, third- order MUSCL scheme is selected [114]. The volume fraction equation is solved using the Geo-reconstruct method. [115]. The aforementioned model is implemented on the experimental system to estimate the diffusion coefficients [107]. The view-cell that is mentioned in procedure part has a height of 32 cm and a cross sectional area of 5.55 cm^2. The initial diffusivities and equilibrium diffusivities of CO_2 in ionic liquid are calculated by trial and error calculations.. Various diffusivity values are tested with until the CO_2 mole fraction obtained from the matches the experimental data at different time points.

As two-dimensional simulations 2000×4 and 2000×8 have given the same diffusivity results with 2000 [107], it was decided to carry out whole calculations with grid number 2000 in this study. In all simulations, time step is kept constant at 1 s.

4. RESULTS AND DISCUSSION

In this part, first, diffussion coefficients of [bmim][PF_6]-CO_2 system at dilute concentration of CO_2, and at thermodynamic phase equilibrum are presented at different pressures (5 and 8 MPa) and temperatures (313.15 K and 323.15 K). Then, the results obtained from the thermodynamic modeling of the system are explained.

4.1. DIFFUSIVITES AT DILUTE CONCENTRATION

Initial diffusivities are calculated for a mole fraction of 0.03 for each temperature and pressure. The time corresponding to mole fraction of 0.03 is determined by interpolating from polynomials fit to the experimental data. Trial and error method is used to determine the initial diffusion coefficient using CFD.

To determine the accuracy of the diffusivity values, two sets of experimental data are analyzed at each temperature and pressure, and the errors are indicated in Table 4.5.

The polynomial models for two sets of experimental mole fractions at 313.15 K, 5.4 MPa are given in Figures 4.1 and 4.2. The times to reach the mole fraction of 0.03 and the diffusion coefficients for each experimental run are presented (see Table 4.1).

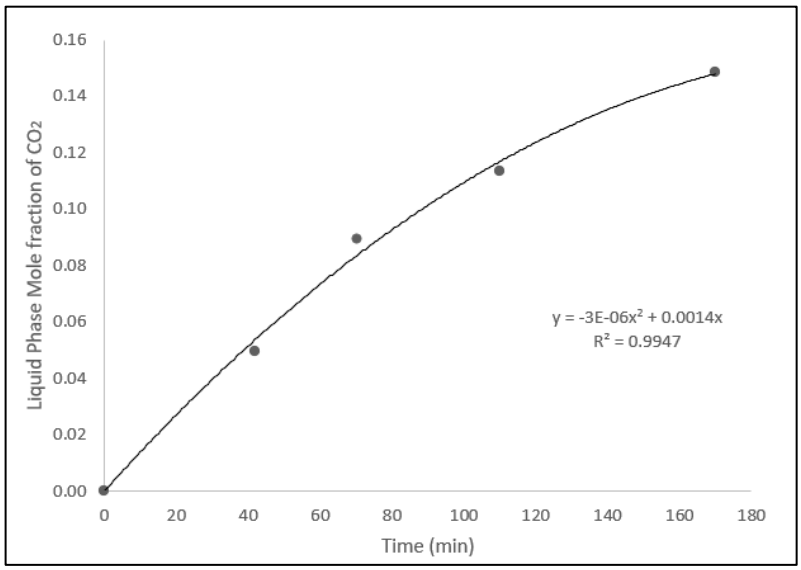

Figure 4.1. Mole fraction vs time for 5 data points for set 1 (313.15 K, 5.4 MPa)

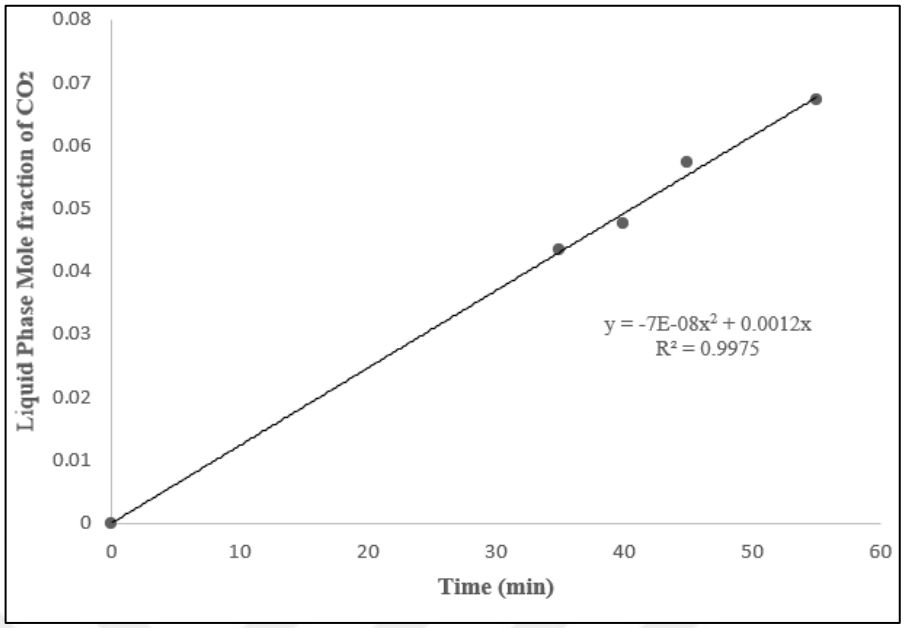

Figure 4.2. Mole fraction vs time for 5 data points for set 2 (313.15 K, 5.4 MPa)

Table 4.1. Diffusion coefficients of Carbon dioxide in [bmim][PF_6] at dilute concentration (313.15 K, 5.4 MPa)

	Temperature (K)	**Pressure (MPa)**	**Initial diffusion coefficient (10^{10} D/m^{2}s^{-1})**	**Time (sec)**
Set 1	313.15	5.4	1.15	1849
Set 2	313.15	5.4	1.20	1761

Figures 4.3 and 4.4 indicate the first five experimental data points collected at a temperature and pressure of 313.15 K and 8.3 MPa. The calculated diffusivities at the mole fraction of 0.03 are given in Table 4.2.

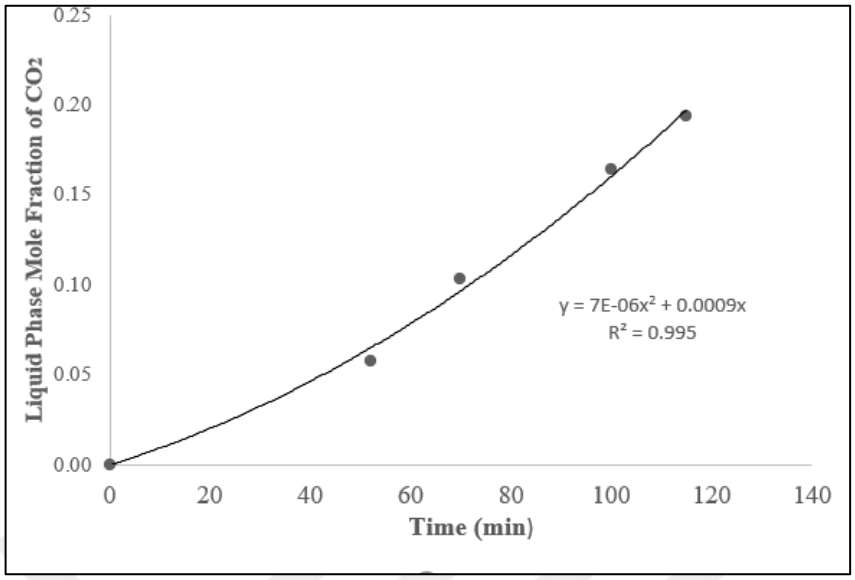

Figure 4.3. Mole fraction vs time for 5 data points for set 1 (313.15 K, 8.3 MPa)

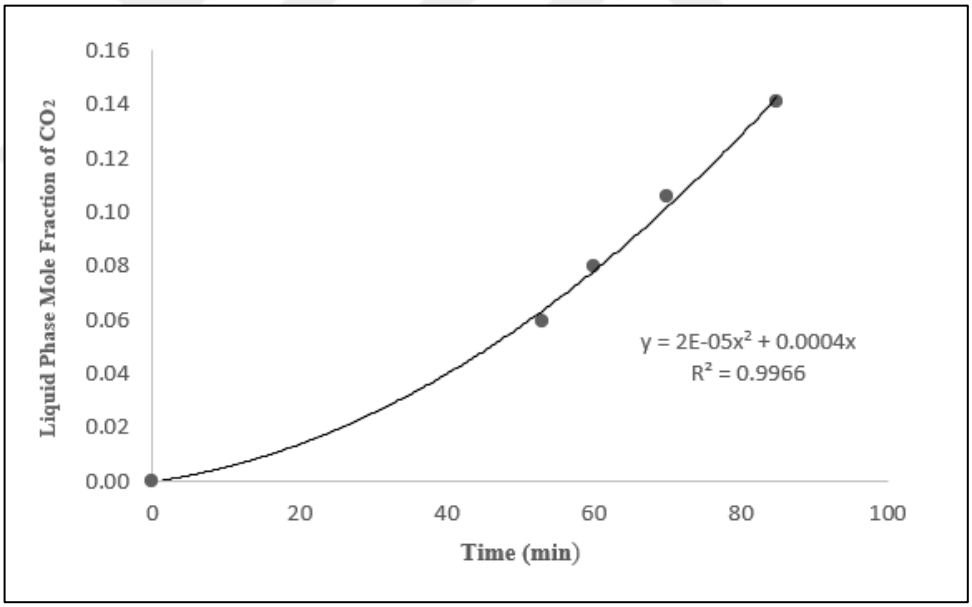

Figure 4.4. Mole fraction vs time for 5 data points for set 2 (313.15 K, 8.3 MPa)

Table 4.2. Diffusion coefficients of Carbon dioxide in [bmim][PF_6] at dilute concentration (313.15 K, 8.3 MPa)

	Temperature (K)	**Pressure (MPa)**	**Initial diffusion coefficient (10^{10} D/m^{2}s^{-1})**	**Time (sec)**
Set 1	313.15	8.3	1.20	1941
Set 2	313.15	8.3	1.18	1976

The polynomial fits to two sets of experimental mole fractions at a temperature and pressure of 323.15 K and 5.3 MPa respectively are given in Figures 4.5 and 4.6. Calculated times and the initial diffusion coefficients at the mole fraction 0.03 are shown in Table 4.3.

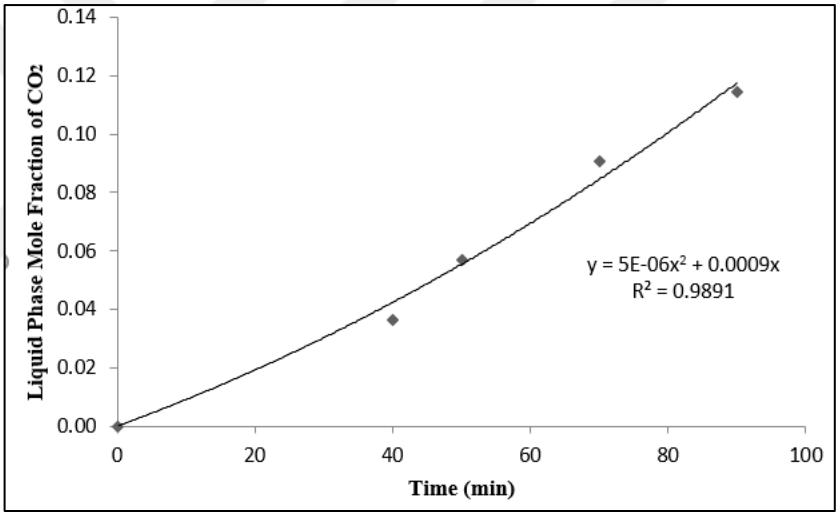

Figure 4.5. Mole fraction vs time for 5 data points for set 1 (323.15 K, 5.3 MPa)

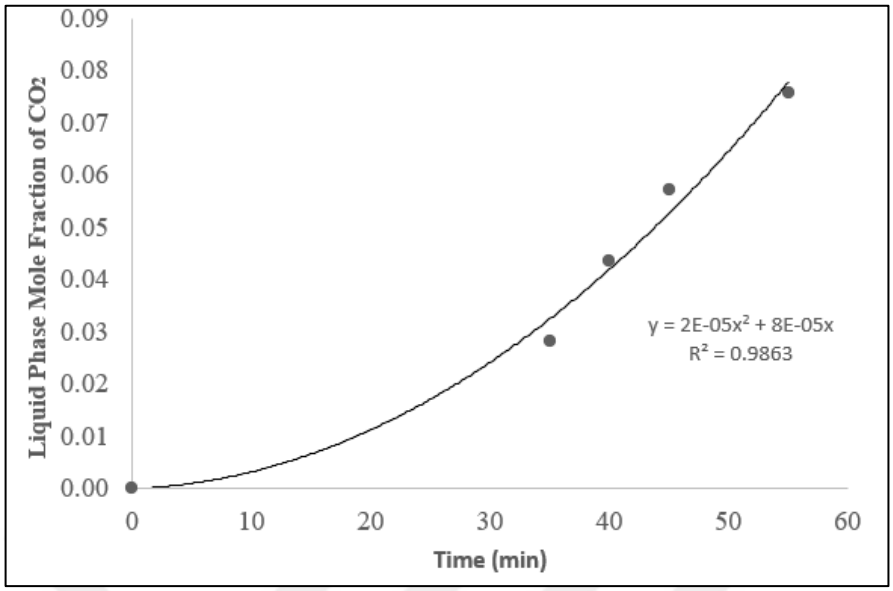

Figure 4.6. Mole fraction vs time for 5 data points for set 2 (323.15 K, 5.3 MPa)

Table 4.3 Diffusion coefficients of Carbon dioxide in [bmim][PF_6] at dilute concentration (323.15 K, 5.3 MPa)

	Temperature (K)	**Pressure (MPa)**	**Initial diffusion coefficient (10^{10} D/m^{2}s^{-1})**	**Time (sec)**
Set 1	323.15	5.3	1.30	2376
Set 2	323.15	5.3	1.28	2466

Figures 4.7 and 4.8 indicate the first five experimental data points collected at a temperature and pressure of 323.15 K and 8.1 MPa. The calculated diffusivities at the mole fraction of 0.03 are given in Table 4.4.

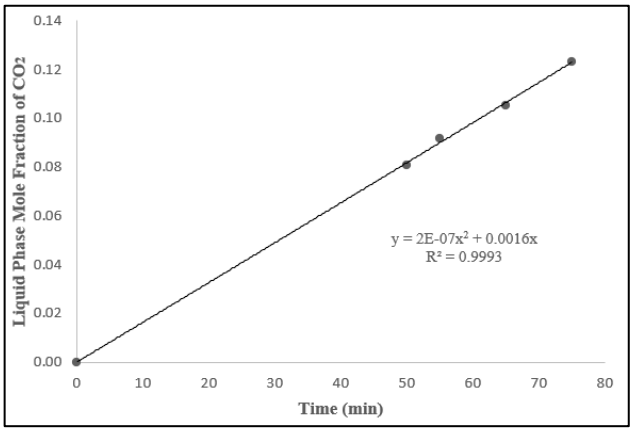

Figure 4.7. Mole fraction vs time for 5 data points for set 1 (323.15 K, 8.1 MPa)

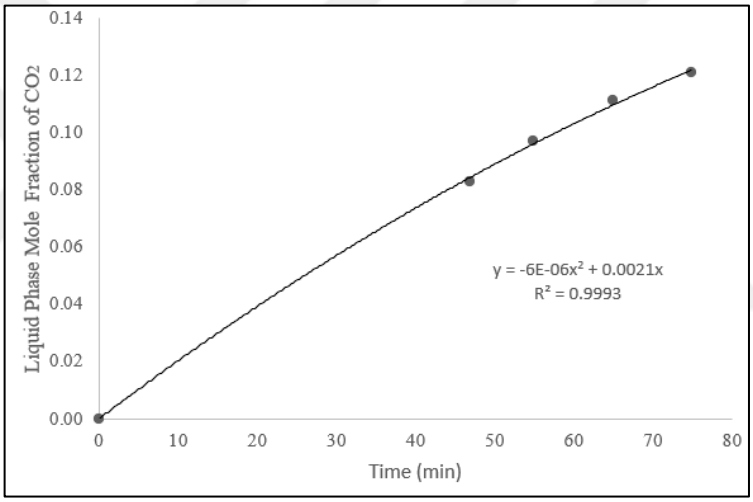

Figure 4.8. Mole fraction vs time for 5 data points for set 2 (323.15 K, 8.1 MPa)

Table 4.4. Diffusion coefficients of Carbon dioxide in [bmim][PF_6] at dilute concentration (323.15 K, 8.1 MPa)

	Temperature (K)	**Pressure (MPa)**	**Initial diffusion coefficient (10^{10} D/m^2s^{-1})**	**Time (sec)**
Set 1	323.15	8.1	1.30	1384
Set 2	323.15	8.1	1.35	1136

The diffusivities increase with temperature. However, increasing the pressure from 5 MPa to 8 MPa has not resulted in much difference. Table 4.5 presents the results.

Table 4.5. Initial diffusion coefficients of CO_2 in [bmim][PF_6]

T(K)	P (MPa)	Initial Diffusion Coefficient (10^{10} D/m^{2}s^{-1})
313.15	5.4	1.18 ± 0.03
313.15	8.3	1.19 ± 0.01
323.15	5.3	1.29 ± 0.01
323.15	8.1	1.32 ± 0.03

4.2. DIFFUSIVITIES AT PHASE EQUILIBRIUM

This part presents, the experimental mole fractions of CO_2 in the liquid phase that are accompanied by the corresponding modeling results. Additionally, the changes in liquid levels and molar volumes are analyzed. Finally, calculated diffusivities at phase equilibrium are presented. These investigations were carried out across different pressures (5 and 8 MPa) and temperatures (313.15 K and 323.15 K) specifically for the [bmim][PF_6]-CO_2 system.

4.2.1. [bmim][PF_6] – CO_2 System at 313.15 K and 794 PSIA (5.4 MPa)

At a pressure of 5.4 MPa and a temperature of 313.15 K, Figure 4.9 illustrates the determined equilibrium mole fraction of carbon dioxide in the liquid phase. The equilibrium mole fraction is 0.466. The process of determining the equilibrium mole fraction entailed considering the remaining volume of CO_2 in the syringe pump and the overall expansion of the liquid phase. Appendix A provides a detailed example for the equilibrium mole fraction calculation. Figure 4.10 presents the increase in the liquid level. The percent increase in volume is calculated using equation 4.1.

$$\text{Volume expansion (\%)} = \frac{A * h_{IL}}{V'_{IL}} * 100 \qquad (4.1)$$

The liquid volume has expanded 19 per cent through the experiment. Neglecting the expansion of the liquid phase gives a result of the equilibrium mole fraction as 0.430. Sample calculation is given in Appendix A. It is observed that the change in the liquid height has a significant effect on the equilibrium mole fraction. That is why the liquid height is monitored by a cathetometer.

During the diffusion process, carbon dioxide occupies the vacancies in the ionic liquid molecular network; ion displacements occur slightly [15,116]. Therefore, the molar volume decreases with time (see Figure 4.11).

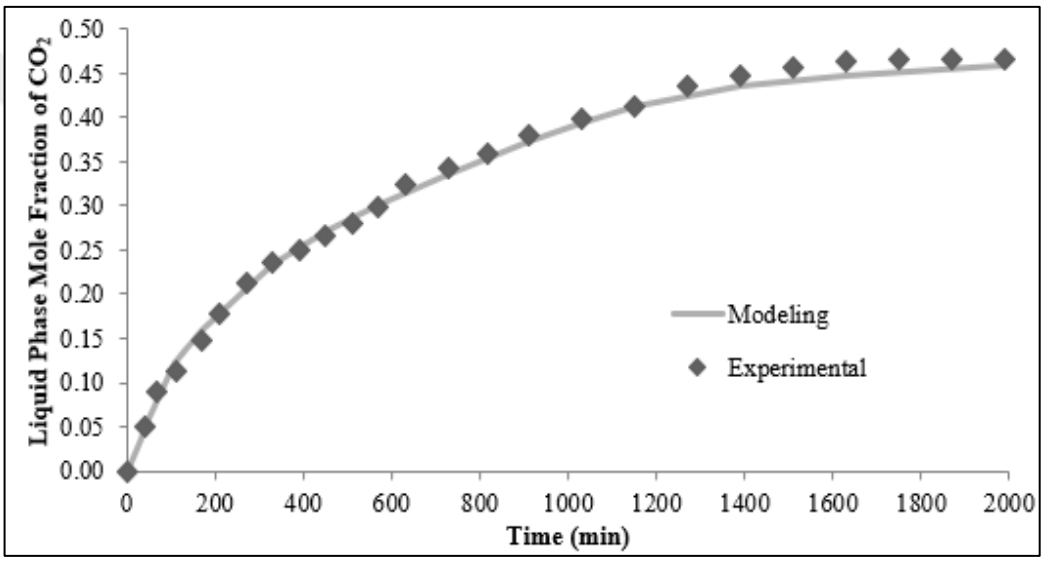

Figure 4.9. Time- dependent experimental solubilities and transport modeling results for (313.15 K, 5.4 MPa)

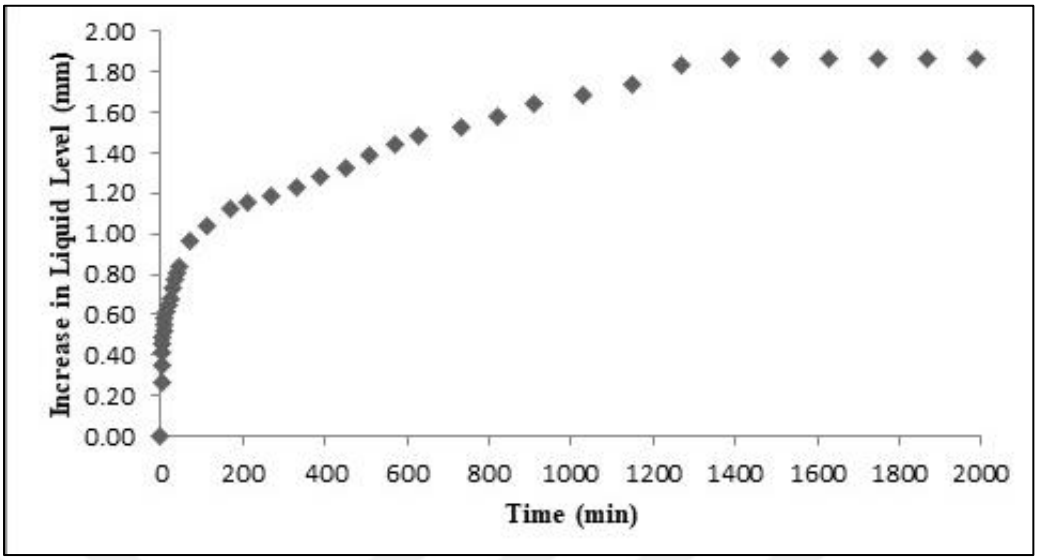

Figure 4.10. Change in the position of the liquid-vapor interface with time (313.15 K, 5.4 MPa)

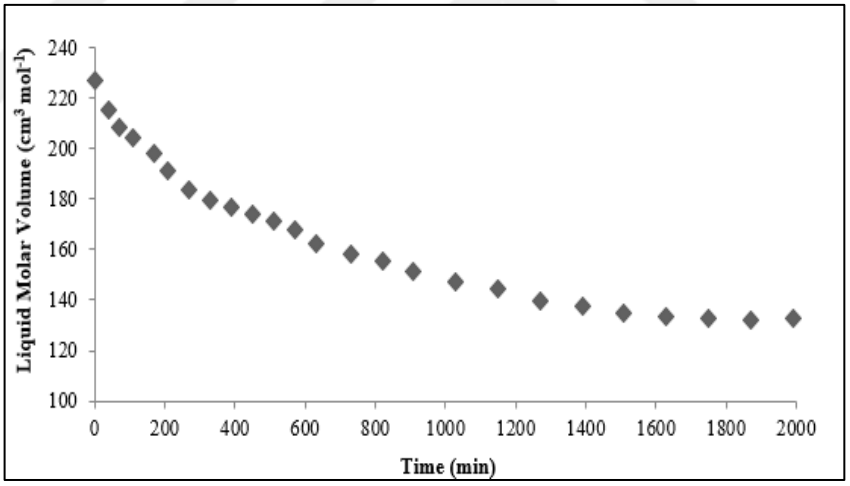

Figure 4.11. Change in the liquid molar volume with time (313.15 K, 5.4 MPa)

The % decrease in liquid molar volume in this system is calculated using Equation 4.2 [117].

$$\Delta V/\Delta V_0\,(\%) = \frac{V_m - V_{IL}}{V_{IL}} \times 100 \qquad (4.2)$$

Where V_m is the molar volume of the mixture, V_{IL} is the molar volume of ionic liquid. The equilibrium molar volume for this system is found as 42 % less than the initial value. As

shown in Figure 4.12, the molar volume obtained from the experiment change with liquid carbon dioxide mole fraction linearly. The transport model utilizes the equation of the line to calculate the molar volume applicable to each computational cell throughout the iterations.

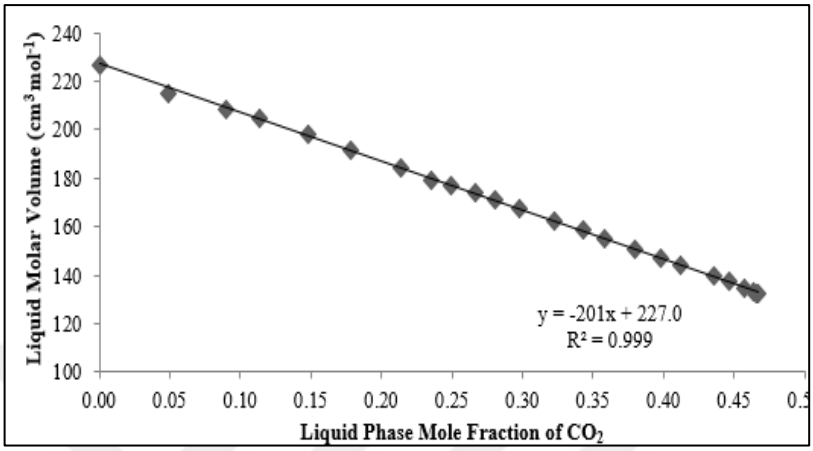

Figure 4.12. Change in the liquid molar volume with CO_2 mole fraction in liquid (313.15 K, 5.4 MPa)

The diffusivity at the phase equilibrium in this case is found as 18.5 $x10^{-10}$ m^2/s . Here, we have used a trial and error approach. Different values are tested until the average mole fraction of carbon dioxide obtained from the model matches with the experimental solubility at a time by using the CFD model [15]. The initial diffusivity value (1.18 ± 0.03 m^2/s) has increased more than one order of magnitude compared to the equilibrium diffusion coefficient.

4.2.2. [bmim][PF_6] – CO_2 System at 313.15 K and 1197 PSIA (8.3 MPa)

Figure 4.13 presents the increase in the mole fraction of CO_2 in the liquid phase with time. [bmim][PF_6]-CO_2 system finally reaches its equilibrium value [15]. The equilibrium mole fraction is found as 0.574. Comparing with the previous case, equilibrium mol fraction increases as pressure increases at the same temperature.

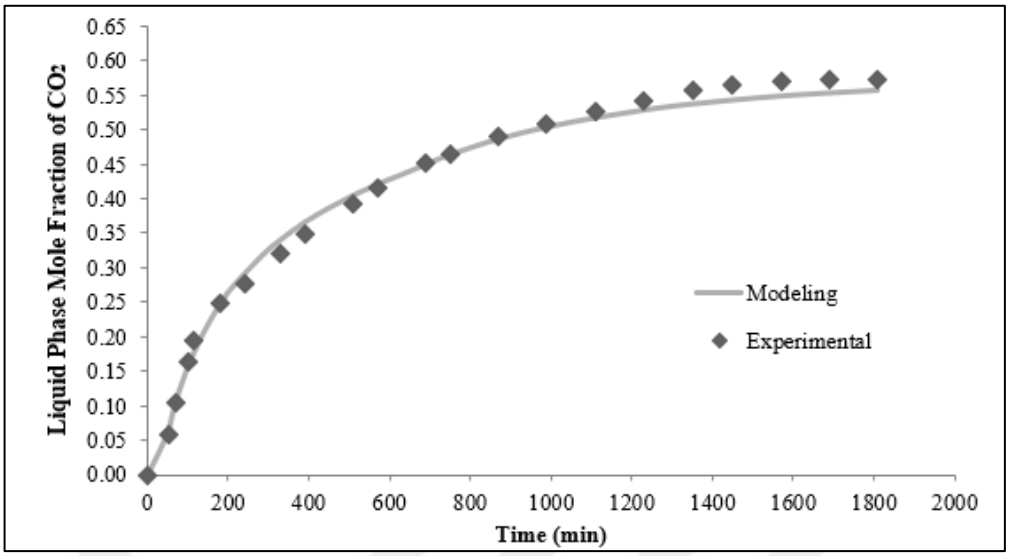

Figure 4.13. Time- dependent experimental solubilities and transport modeling results (313.15 K, 8.3 MPa)

Figure 4.14 illustrates the observed increase in the liquid level, with the liquid volume expanding by 18 percent. If the expansion of the liquid phase was not taken into account in the calculations, the resulting equilibrium mole fraction would be 0.519. In this case too, the molar volume decreases with time (see Figure 4.15).

The molar volume diminishe while the carbon dioxide mole fraction increases with time (see Figure 4.16). The molar volume has decreased to almost half of its initial value [15].

The final diffusivity value is found as 27.2 $x10^{-10}$ m^2/s [15]. The initial diffusivity value (1.19 ± 0.01 m^2/s) has increased more than one order of magnitude compared to the equilibrium diffusion coefficient.

Raising the pressure from 5 MPa to 8 MPa has led to an elevation in the equilibrium diffusivity due to higher CO_2 solubility at 8 MPa.

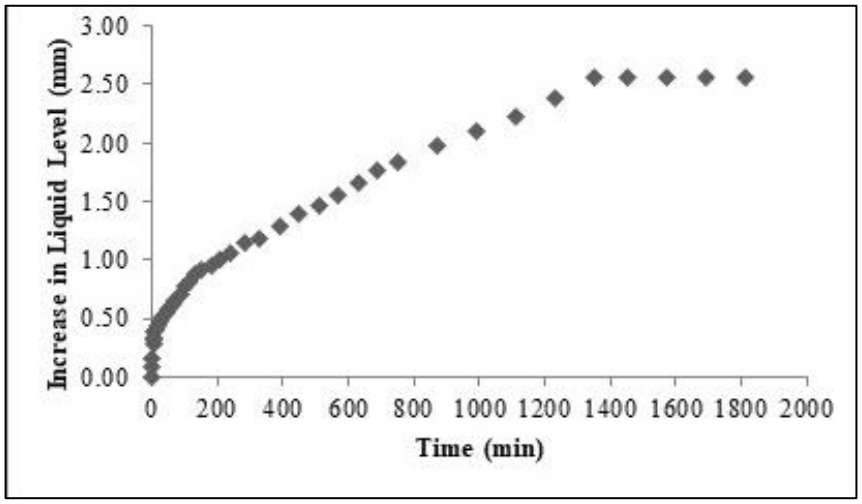

Figure 4.14. Change in the position of the liquid-vapor interface with time (313.15 K, 8.3 MPa)

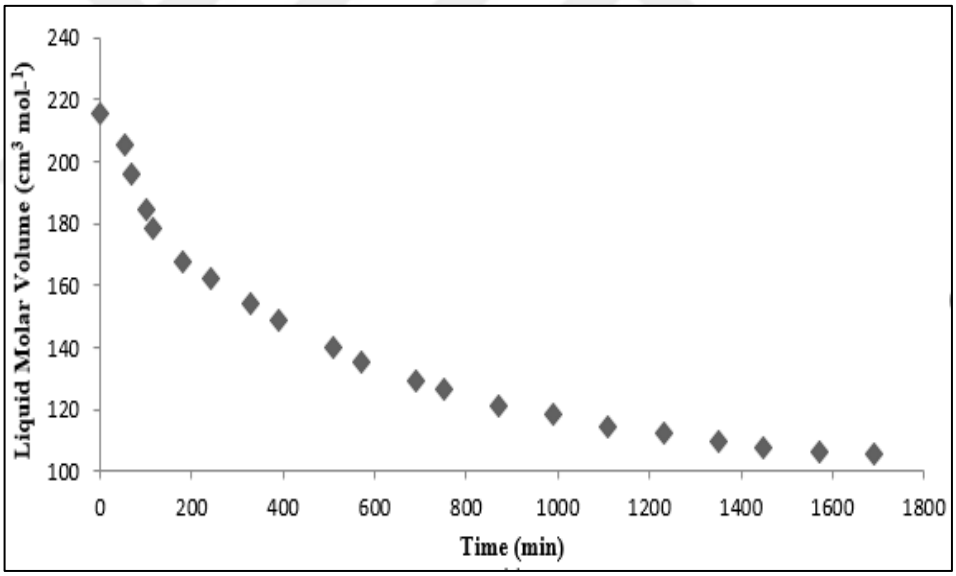

Figure 4.15. Change in the liquid molar volume with time (313.15 K, 8.3 MPa)

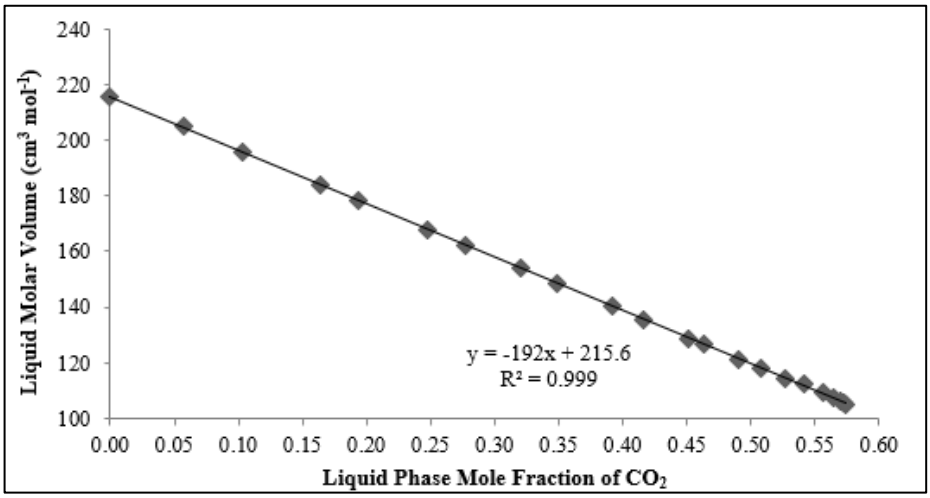

Figure 4.16. Change in the liquid molar volume with CO_2 mole fraction in a liquid (313.15 K, 8.3 MPa)

4.2.3. [bmim][PF_6] – CO_2 Mixture at 323.15 K and 771 PSIA (5.3 MPa)

The time-dependent data in Figure 4.17 shows that the mole fraction of carbon dioxide in the liquid phase increases with time. Eventually, the mole fraction reaches 0.426 which is the equilibrium value for CO_2 at this temperature and pressure [15]. Compared to the solubility result found for 313 K and 5.4 MPa, temperature increase has caused a decrease in the equilibrium mole fraction of CO_2.

Figure 4.18 illustrates the observed increase in the liquid level, with the liquid volume expanding by 21 percent. If the volume increase of the liquid phase was neglected in the calculations, the resulting equilibrium mole fraction would be 0.386. During the diffusion process, the molar volume decreases with time (see Figure 4.19). The molar volume diminishes with time while the carbon dioxide mole fraction increases in the liquid (see Figure 4.20) [15]. The equilibrium molar volume for this system is found to be 33 % less than the initial value.

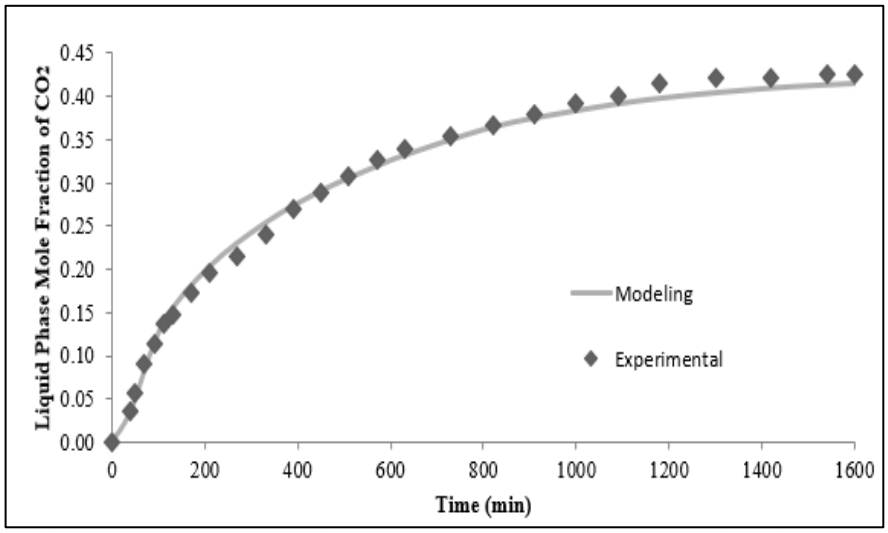

Figure 4.17. Time- dependent experimental solubilities and transport modeling results (323.15 K, 5.3 MPa)

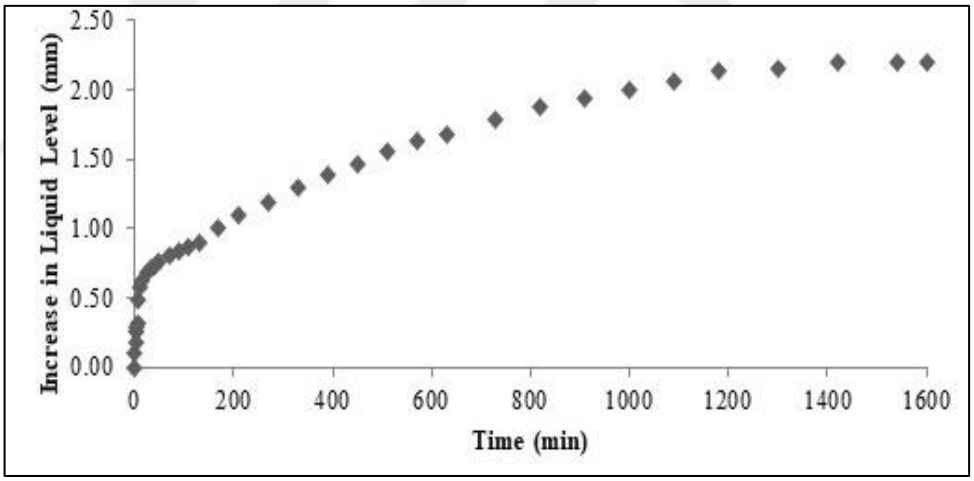

Figure 4.18. Change in the position of the liquid-vapor interface with time (323.15 K, 5.3 MPa)

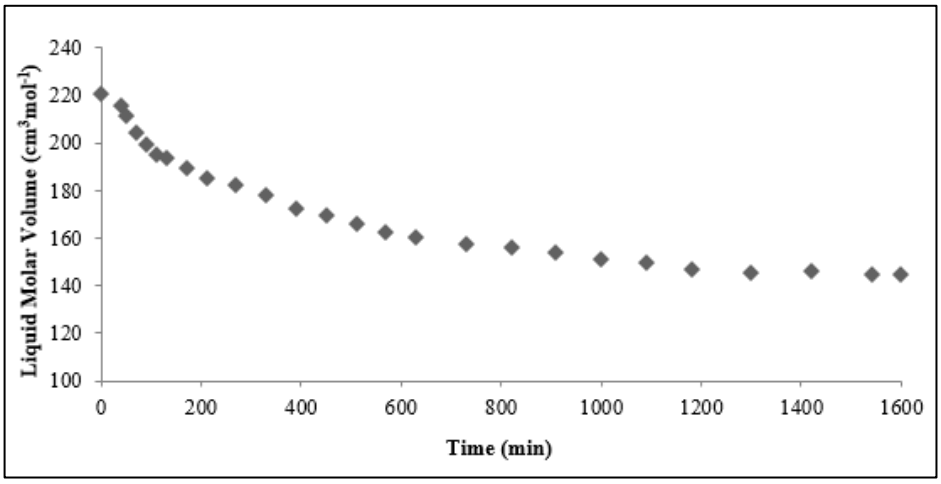

Figure 4.19. Change in the liquid molar volume with time (323.15 K, 5.3 MPa)

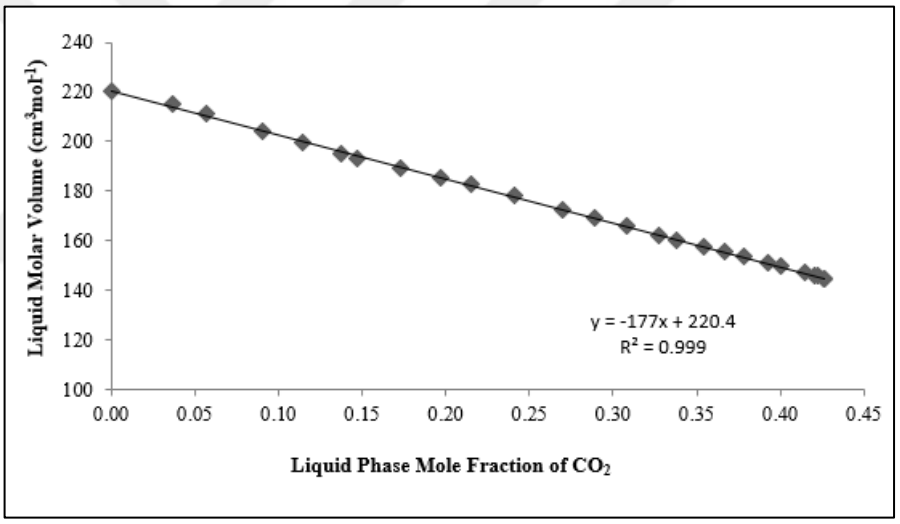

Figure 4.20. Change in the liquid molar volume with CO_2 in liquid (323.15 K, 5.3 MPa)

The diffusivity at the phase equilibrium in this case is found as 20.0 $x10^{-10}$ m^2/s [15]. The diffusivity value (1.29 ± 0.01 m^2/s) has increased fifteen times comparing its values at dilute condition and at phase equilibrium.

4.2.4. [bmim][PF_6] – CO_2 System at 323.15 K and 1175 PSIA (8.1 MPa)

For this case, too, the mole fraction of CO_2 in liquid increases steadily with time and reaches equilibrium as presented in Figure 4.21. The equilibrium mole fraction equals to 0.508.

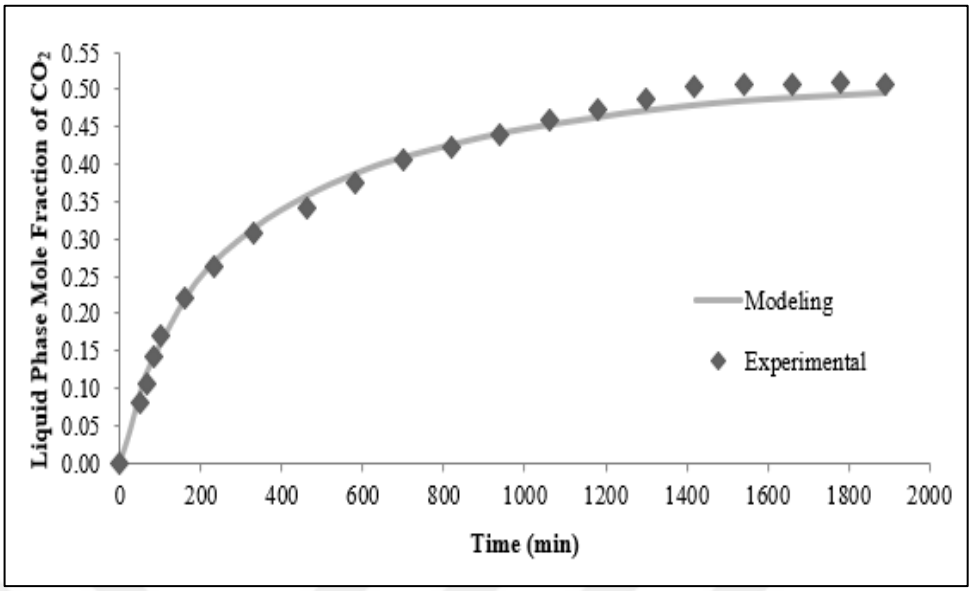

Figure 4.21. Time- dependent experimental solubilities and transport modeling results (323.15 K, 8.1 MPa)

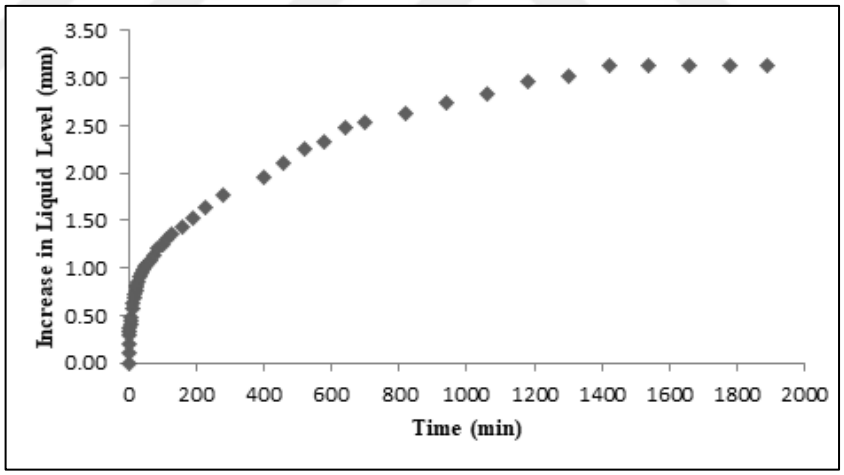

Figure 4.22. Change in the position of the liquid-vapor interface with time (323.15 K, 8.1 MPa)

Figure 4.22 illustrates the observed increase in the liquid level, with the liquid volume expanding by 26 percent. If the expansion of the liquid phase was not taken into account in the calculations, the resulting equilibrium mole fraction would be 0.427.

During the diffusion process, the molar volume again decreases with time (see Figure 4.23). The molar volume decreases while the carbon dioxide mole fraction increases in the liquid (see Figure 4.24). Percent decrease in molar volume in this case is 38 %.

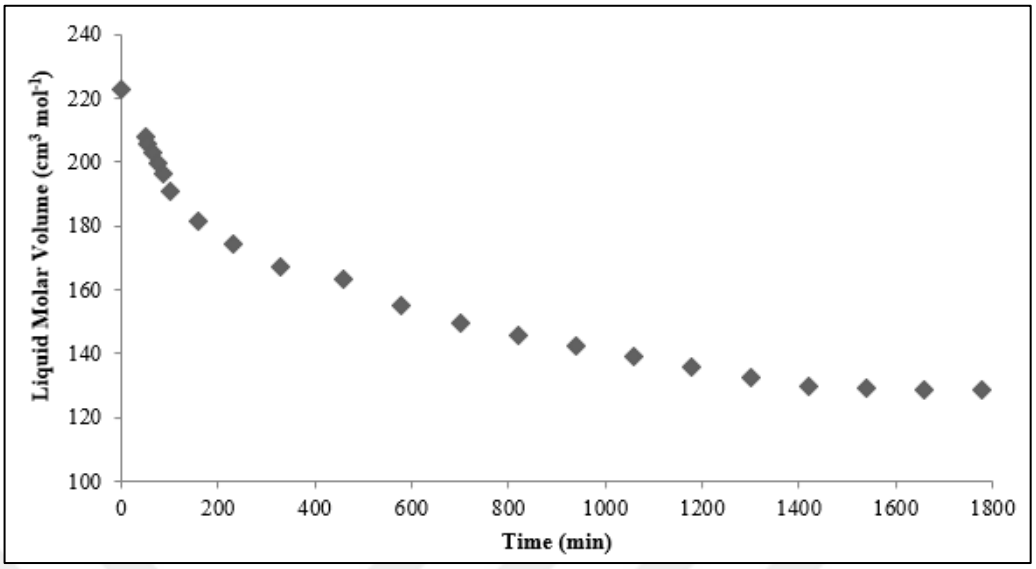

Figure 4.23. Change in the liquid molar volume with time (323.15 K, 8.1 MPa)

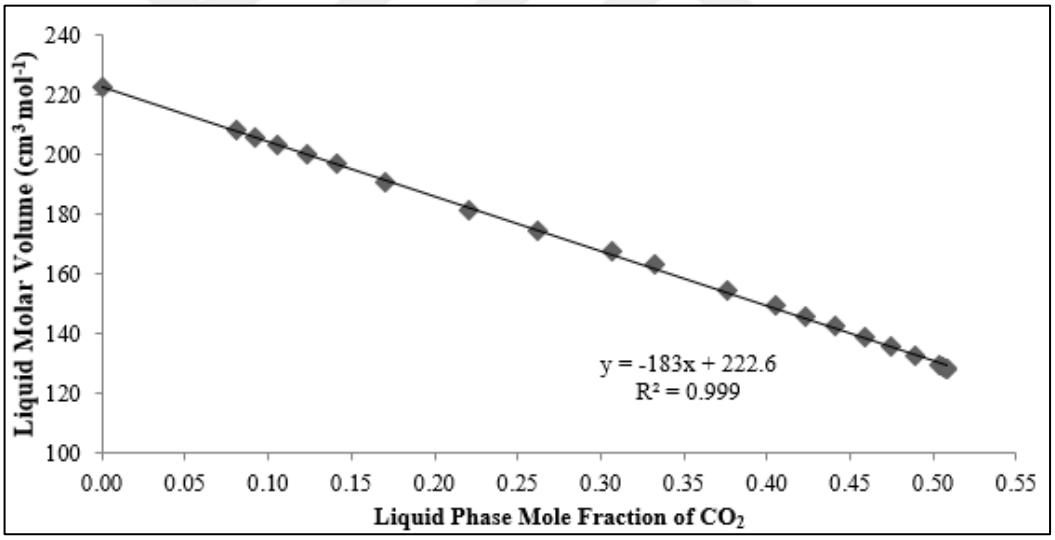

Figure 4.24. Change in the liquid molar volume with CO_2 mole fraction in a liquid (323.15 K, 8.1 MPa)

The final diffusivity value in this case is found as 24.2 $x10^{-10}$ m^2/s. There is again a huge increase in diffusivities (from 1.32 to 24.2 x $10^{-10}m^2/s$). Table 4.6 shows the diffusivities obtained at phase equilibria and R^2 values for the model fit to time-dependent solubility data at all temperatures and pressures. The mutual diffusivities increase when CO_2 dissolves in the [bmim][PF_6].

Table 4.6. Equilibrium mole fractions, diffusivities of CO_2- [bmim][PF_6] system and R^2 values for the model fit to time-dependent solubility data

Temperature (K)	Pressure (MPa)	Equilibrium diffusion coefficient (10^{10} D/m^{2}s^{-1})	Equilibrium mole fractions	R^2
313.15	5.4	18.5	0.466	0.999
313.15	8.3	27.2	0.574	0.997
323.15	5.3	20.0	0.426	0.999
323.15	8.1	24.2	0.508	0.995

4.3. PHASE EQUILIBRIUM MODELING

According to experimental data and the modeling results (Figures 4.9, 4.13, 4.17, 4.21 and Table 4.6) it can be concluded that the solubility of carbon dioxide in [bmim][PF_6] increases with pressure and decreases with temperature.

Figure 4.25 shows the solubility values at different pressures. The values other than those at 5 and 8 MPa have taken from the study conducted by Yıldız [118]. We observe that the solubilities are comparable to the values reported in the literature [15,22,96]. The figure also indicates thermodynamic modelling results obtained from Peng Robinson Equation of state with Stryjek-Vera (PRSV) modification and Wong-Sandler (WS) mixing rules where NRTL model is employed to determine the free energy term [15,119–121].

The critical constants of carbon dioxide used in the thermodynamic modeling are presented in Table 4.7 [122].

Due to the decomposition of ionic liquids at temperatures below the critical temperature, it is not possible to determine the critical constants using experimental methods For this reason, the critical constants are estimated [123–125].

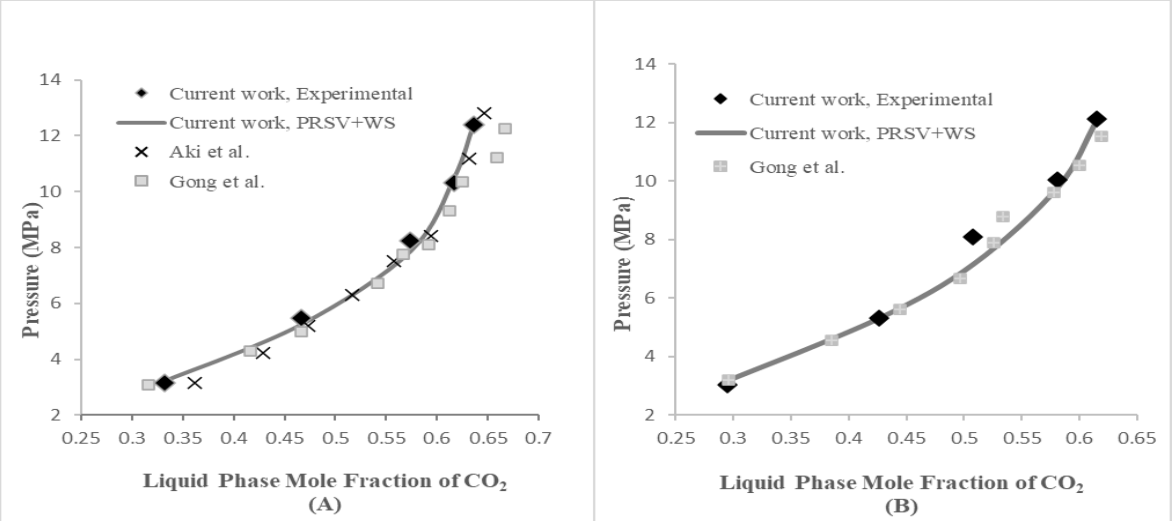

Figure 4.25. Experimental and calculated pressures for [bmim][PF_6] – carbon dioxide system for (A) 313.15 K (Gong et al. [96] and Aki et al. [22]) (B) 323.15 K (Gong et al. [96])

Table 4.7. Critical properties of CO_2 [122]

Tc (K)	**Pc (MPa)**	**ω**
304.21	7.382	0.225

In Table 4.8 different critical values which are reported for [bmim][PF_6] in the literature are presented [15,125–129]. The critical constants are obtained from Vetere's method [126], group contribution methods [125] and different equations of state [127,129]. Using van der Waals EoS, Morais and coworkers modeled the solubility of HFC-32 in [bmim][PF_6], testing different sets of critical parameters for the ionic liquid [128]. The objective function minimizing the sum of the squares of the difference between the experimental and calculated pressures did not depend on the parameter set when the critical pressure was taken greater than 0.5 MPa. Therefore, they set the T_c and P_c of the ionic liquid to 1000 K and 2.5 MPa respectively. These values are also included in Table 4.8. In some of these studies, the acentric factor, ω was not reported [126–128]. Therefore, we have carried out the parameter fit using the acentric factors reported with the other sets [15,125–129]. Also, for these sets ω is estimated using Equation 4.3 at a T_b/T_c ratio of 0.7709 which is the given value for [bmim][PF_6] in the study conducted by Valderrama et al. [15,125].

Table 4.8. Critical properties of [bmim][PF_6]

	T_c (K)	P_c (MPa)	ω	ω (T_b/T_c=0.7709)
Set 1 [146]	860.5	2.645	-	1.0575
Set 2 [145]	719.4	1.728	0.7917	-
Set 3 [147]	929.0	2.510	-	1.0233
Set 4 [147]	1074.9	3.026	-	1.1392
Set 5 [148]	1000	2.5	-	1.0198
Set 6 [149]	1121	3.55	1.5114	-

$$\omega=\frac{(T_b-43)\,(T_c-43)}{(T_c-T_{b)}(0.7T_c-43)}\log\left[\frac{P_c}{P_b}\right]-\frac{(T_c-43)}{(T_c-T_{b)}}\log\left[\frac{P_c}{P_b}\right]+\log\left[\frac{P_c}{P_b}\right]-1¤ \quad (4.3)$$

Tables 4.9 and 4.10 show the average absolute deviations in pressure and molar volume (see Equations 4.4 and 4.5) obtained using the critical parameters in Tables 4.7 and 4.8 at temperatures of 313.15 K and 323.15 K [15]. All the symbols are explained in the nomenclature part.

$$AAPD=\frac{1}{NP}\sum_{i=1}^{NP}\frac{\left|P_{i,cal}-P_{i,exp}\right|}{P_{i,exp}}\times 100 \quad (4.4)$$

$$AAV_MD=\frac{1}{NP}\sum_{i=1}^{NP}\frac{\left|V_{Mi,cal}-V_{Mi,exp}\right|}{P_{i,exp}}\times 100 \quad (4.5)$$

Tables 4.9 and 4.10 NC means that the program did not converge for the given critical values. We did not obtain converged results for Set 6 at any temperatures Therefore, this set is not included in the tables. For an ω of 0.7917, we observe that all the sets give comparable AAPDs. However, when the prediction of the molar volumes is taken into account, set 1 outperforms the rest. In general, taking the acentric factor as 0.7917 gives better predictions of molar volumes. Therefore, for the thermodynamic modeling of the experimental solubilities obtained in the current study, Set 1 and the acentric factor of 0.7917 are selected [15]. Figure 4.25 shows modeling results obtained using these values and the parameters of the model are presented in Table 4.11. Output Data of [bmim][PF_6]-CO_2 System for PRSV

equation of state and Wong-Sandler mixing rules at 313.15 and 323.15 K for each six set is presented in Appendix C.

Table 4.9. AAPD and AAVMD values calculated using different critical constants at a temperature of 313.15 K

		ω=0.7917	**ω (Tb/Tc=0.7709)**	**ω=1.5114**
Set 1	*AAPD*	2.467	2.551	2.329
	AAV_MD	3.008	4.290	8.690
Set 2	*AAPD*	2.126	-	-
	AAV_MD	20.33	-	-
Set 3	*AAPD*	2.951	2.505	5.390
	AAV_MD	10.24	12.02	19.49
Set 4	*AAPD*	2.135	11.02	NC
	AAV_MD	12.04	14.31	NC
Set 5	*AAPD*	2.729	2.174	NC
	AAV_MD	18.12	21.48	NC

Table 4.10. AAPD and AAV_MD values calculated using different critical constants at a temperature of 323.15 K

		ω=0.7917	**ω (Tb/Tc=0.7709)**	**ω=1.5114**
Set 1	*AAPD*	3.768	3.441	3.154
	AAV_MD	4.197	3.434	4.096
Set 2	*AAPD*	4.768	-	-
	AAV_MD	13.40	-	-
Set 3	*AAPD*	3.857	3.553	7.009
	AAV_MD	6.460	9.527	13.82
Set 4	*AAPD*	3.373	14.10	NC
	AAV_MD	8.435	10.58	NC
Set 5	*AAPD*	3.848	3.557	NC
	AAV_MD	14.86	18.27	NC

Table 4.11. Estimated parameters of the thermodynamic model

Temperature (K)	k_{12}	τ_{12}	τ_{21}
313.15	0.8683	-0.1374	0.1117
323.15	0.8637	1.0023	-0.8798

The thermodynamic nonideality factor, denoted as Γ, is established using the composition derivative of the fugacity coefficient [130].

$$\Gamma = 1.0 + x_{CO_2} \frac{\partial ln\Phi_{CO_2}}{\partial x_{CO_2}} \tag{4.6}$$

In order to find thermodynamic correction factor one needs the fugacity coefficients. They are determined by using PRSV Eos [119] and WS mixing rules [120]. Then a polynomial is fit to these values and differentiated at aforementioned temperatures and pressures are reported in Appendix D. The thermodynamic correction factor values are presented in Table 4.12. The fugacity coefficient values at different mole fractions were found by using Octave program [15].

Table 4.12. Thermodynamic correction factors

Temperature (K)	Pressure (MPa)	Thermodynamic Correction Factor (Γ)
313.15	5.4	1.109
313.15	8.3	1.129
323.15	5.3	1.097
323.15	8.1	1.115

The thermodynamic nonideality factor equals to 1 at infinite dilution. It is then decreases or increases depending on the mixture showing positive or negative deviation from ideality. As presented in Table 4.12, the thermodynamic factors calculated at the equilibrium composition are above 1 at all temperatures and pressures. They increase with the mole fraction of CO_2 in the ionic liquid [15]. This shows that the liquid phase exhibits a negative deviation from ideality which is the case observed for mixtures of small and large molecules [15,131,132].

Wong-Sandler mixing rules combine an activity coefficient model and an Eos to model low density and high density behavior of mixtures correctly. In the current study NRTL equation is used as the activity coefficient model in the Wong-Sandler mixing rules [15].

Figure 4.26 shows the change in the activity coefficients of carbon dioxide and [bmim][PF_6] with mole fraction. As CO_2 dissolves in the IL, the activity coefficient of ionic liquid starts from decreasing from 1. The activity coefficient of CO_2, on the other hand, approaches 1 as its liquid phase mole fraction increases in the liquid. This behavior again points to negative deviation from ideality [15].

Diffusivity values, at the equilibrium mole fraction of carbon dioxide, are compared with theoretical values using correlations proposed by Vignes, He-Yu and Shi-Lu [16,133,134].

By using Vignes equation, Fick diffusivities at any composition by using infinite dilution diffusivity and thermodynamic correction factor can be estimated. [15]. The Vignes equation is as follows [16]:

$$D_{BA}=(D^{0}_{BA})^{x_{IL}}(D^{0}_{AB})^{x_{CO_2}}\Gamma \qquad (4.7)$$

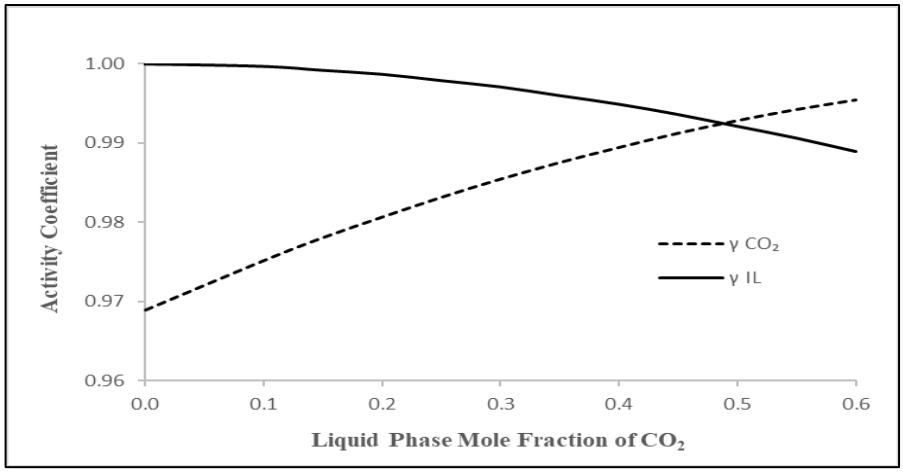

Figure 4.26. Change in the activity coefficients with CO_2 mole fraction in liquid at 313.15 K

Where D_{BA} is diffusion coefficient of carbon dioxide in [bmim][PF_6] (cm^2/s), D^{0}_{BA} and D^{0}_{AB} are the infinite dilution diffusion coefficient of carbon dioxide in [bmim][PF_6] and [bmim][PF_6] in carbon dioxide (cm^2/s), Γ which is thermodynamic correction factor, x_{IL} and

x_{CO_2} are the mole fractions of ionic liquid and carbon dioxide at thermodynamic equilibrium [15].

We have used the initial diffusion coefficient calculated in this study for the infinite dilution diffusion coefficient of carbon dioxide in [bmim][PF_6] in Vignes equation [15]. The infinite dilution diffusion coefficient of [bmim][PF_6] in carbon dioxide can be estimated using He-Yu correlation expressed as follows [133];

$$D_{AB}^{0} = \alpha \times 10^{-5} \left(\frac{T}{M_A}\right)^{1/2} \exp\left(-\frac{0.3887}{V_{rB} - 0.23}\right) \tag{4.8}$$

$$\alpha = 14.882 + 0.005908 \frac{T_{cB} V_{cB}}{M_B} + 2.0821 \times 10^{-6} \left(\frac{T_{cB} V_{cB}}{M_B}\right)^2 \tag{4.9}$$

Where D_{AB}^{0} is the infinite-dilution diffusion coefficient of solute A in supercritical solvent B in cm^2/s. V_{cB} stands for the critical molar volume of the solvent B in cm^3/mol, and V_{rB} is the solvent reduced molar volume. T_{cB} is the critical temperature of the solvent in K. M is the molar mass in g/mol.

Another correlation proposed by Shi and Lu is taking into account the solute density [135]:

$$10^5 D_{AB}^{0} = \rho_{A,\,298K} \left(2.79 + \rho_{A,\,298K}^{-9/4} + 10^{-3} T_{cB} \rho_{cB}^{-1}\right)^{9/4} \left[0.4336 + 0.2955 \exp(-2.342 \rho_{rB})\right] \times \exp\left(-\frac{0.547\, \rho_{A,\,298K}^{-1/10} - 0.247}{\rho_{rB}^{-1} - 0.247}\right) \frac{T^{0.52}}{M_A^{0.48}} \tag{4.10}$$

Where ρ_{cB} and ρ_{rB} stand for critical and reduced density of solvent B respectively and T_{cB} is the critical temperature of solvent B. The comparison of equilibrium diffusion coefficients of CO_2-[bmim][PF_6] systems with correlations are given in below: He-Yu and Shi-Lu correlations are used to find infinite dilution diffusivities in supercritical solvents. The limits of the reduced solvent densities for He-Yu and Shi-Lu correlations are $0.22<\rho_r<2.62$ and $0.21<\rho_r<2.34$ respectively. At 5 MPa and 323.15 K, the reduced density of carbon dioxide is 0.23. Therefore, in the current study, these equations are used at these conditions as well [15].

Table 4.13. Comparison of equilibrium diffusion coefficients of CO_2-[bmim][PF_6] system with correlations

Temperature (K)	Pressure (MPa)	He-Yu (10^{10} D/m^{2}s^{-1})	Shi-Lu (10^{10} D/m^{2}s^{-1})	Current study (10^{10} D/m^{2}s^{-1})
313.15	5.4	13.7	14.7	18.5
313.15	8.3	18.5	22.0	27.2
323.15	5.3	11.9	12.7	20.0
323.15	8.1	17.3	17.9	24.2

Table 4.13 indicates the diffusivities obtained using these correlations. The difference between the results obtained from the transport modeling of the time dependent CO_2 solubility data and those obtained from the correlations varies from 26 to 41 % (He-Yu) and from 19 to 36 % (Shi-Lu) [15,84,92].

.

5. CONCLUSION AND FUTURE WORK

In this study, experimental time-dependent solubilities and a transport model are used to find the diffusivities of the CO_2-[bmim][PF_6] system at dilute concentration of CO_2, and also at phase equilibrium. The operating temperatures and pressures are 313.15, 323.15 K, and 5, 8 MPa respectively. The following conclusions are drawn from the study.

For the diffusion coeffients at dilute condition, temperature is an increasing factor while we have not observed a dependence on pressure.

The equlibrium solubilities of CO_2 in [bmim][PF_6] increase with pressure, and decrease with temperature. The values obtained compare well with the results reported by the researchers. As the solubilities increase, the mutual diffusion coefficients of the system have increased. It is found more than one order of magnitude difference between the diffusivities at dilute concentration and those found at the thermodynamic liquid-vapor equilibrium.

The Vignes equation is employed to determine the diffusivities at phase equilibrium where both He-Yu and Shi-Lu correlations are tested for the infine dilution diffusivity of the ionic liquid in carbon dioxide. Vignes Equation with Shi-Lu correlation has resulted in closer values to those determined from the time-dependent solubilities and transport model.

The thermodynamic model of PRSV equation of state and Wong-Sandler mixing rules has matched the experimental data including the liquid molar volumes well. The activity coefficients determined at the aforementioned temperatures have pointed to the negative deviation from ideality in the carbon dioxide-[bmim][PF_6] system.

In future research endeavors, one can explore the diffusivities of CO_2 in ILs with varying molecular weights. Furthermore, the investigation of mutual diffusion coefficients in CO_2-ionic liquid mixtures, as well as CO_2-PEG and IL mixtures, can be approached as multicomponent diffusion. This approach is particularly relevant due to the emergence of various applications involving these systems.

REFERENCES

1. Ghandi K. A Review of Ionic Liquids, Their Limits and Applications. *Green and Sustainable Chemistry*. 2014;04(01):44–53.

2. Keskin S, Kayrak-Talay D, Akman U, Hortaçsu Ö. A review of ionic liquids towards supercritical fluid applications. *Journal of Supercritical Fluids*. 2007 Nov;43(1):150–80.

3. Cabeza LF, de Gracia A, Fernández AI, Farid MM. Supercritical CO_2 as heat transfer fluid: A review. *Applied Thermal Engineering*. 2017;125:799–810.

4. Nalawade SP, Picchioni F, Janssen LPBM. Supercritical carbon dioxide as a green solvent for processing polymer melts: Processing aspects and applications. *Progress in Polymer Science (Oxford)*. 2006;31(1):19–43.

5. Raventós M, Duarte S, Alarcón R. Application and Possibilities of Supercritical CO_2 Extraction in Food Processing Industry: An Overview. *Food Science and Technology International*. 2002 Oct;8(5):269–84.

6. Akien GR, Poliakoff M. A critical look at reactions in class I and II gas-expanded liquids using CO_2 and other gases. *Green Chemistry*. 2009 Aug 3;11(8):1083–100.

7. Jessop PG, Subramaniam B. Gas-expanded liquids. *Chemical Reviews*. 2007 Jun;107(6):2666–94.

8. Wei Ren by, Scurto AM, VCamarda K, Weatherley LR, Tsau J-S, Laird BB. High-Pressure Phase Equilibria of Ionic Liquids and Compressed Gases for Applications in Reactions and Absorption Refrigeration. 2009.

9. Stepnowski P, Storoniak P. Lipophilicity and metabolic route prediction of imidazolium ionic liquids. *Environmental Science and Pollution Research*. 2005 Jul;12(4):199–204.

10. Bennet V, Abidemi SA, Dikio ED. Effect of 1-Butyl-3-methylimidazolium hexafluorophosphate [bmim][PF_6] on N,N-dimethylformamide: Conductivity

Measurement at T (293.15 – 333.15) K. *Research Journal of Pure Science and Technology*. 2019;2(1):2579–0536.

11. Sutradhar M, Ribeiro APC, Guedes da Silva MFC, Palavra AMF, Pombeiro AJL. Application of molybdenum complexes for the oxidation of cyclohexane in acetonitrile, ionic liquid and supercritical CO_2 media, a comparative study. *Molecular Catalysis*. 2020 Feb 1;482:100356.

12. Ribeiro APC, Martins LMDRS, Alegria ECBA, Matias IAS, Duarte TAG, Pombeiro AJL. Catalytic performance of Fe(II)-scorpionate complexes towards cyclohexane oxidation in organic, ionic liquid and/or supercritical CO_2 media: A comparative study. *Catalysts*. 2017 Aug 2;7(8).

13. Ivanova M, Kareth S, Petermann M. Supercritical carbon dioxide and imidazolium based ionic liquids applied during the sol–gel process as suitable candidates for the replacement of classical organic solvents. *The Journal of Supercritical Fluids*. 2018 Feb 1;132:76–82.

14. Long NVD, Kim GS, Tran NN, Lee DY, Fulcheri L, Song Z, et al. Biogas upgrading using ionic liquid [bmim][PF_6] followed by thermal-plasma-assisted renewable hydrogen and solid carbon production. *International Journal of Hydrogen Energy*. 2022 Dec 30;47(100):42075–83.

15. Sekerci-Cetin M, Emek OB, Yildiz EE, Unlusu B. Diffusion coefficients and phase equilibria of carbon dioxide–ionic liquid, 1-butyl-3-methylimidazolium hexafluorophosphate ([bmim][PF_6]) system. *The Canadian Journal of Chemical Engineering*. 2023;1–11.

16. Vignes A. Diffusion in Binary Solutions Variation of Diffusion Coefficient with Composition. *Industrial and Engineering Chemistry Fundamentals*. 1966;5:189–99.

17. Krigmont H V, Lumley TL. Computational Fluid Dynamics Modeling Applicatons For Engineering Solutions. USA: *Allied Environment Technologies Inc.*; 2007.

18. Marsh KN, Boxall JA, Lichtenthaler R. Room temperature ionic liquids and their mixtures - A review. *Fluid Phase Equilibria*. 2004 May 10;219(1):93–8.

19. Nasirpour N, Mohammadpourfard M, Zeinali Heris S. Ionic liquids: Promising compounds for sustainable chemical processes and applications. *Chemical Engineering Research and Design*. 2020 Aug 1;160:264–300.

20. Ohno H. Graduate School of Engineering, 2-24 Nakacho [Internet]. Technology. *Japan Functional Organic Liquids*; 2019. Available from: http://quill.qub.ac

21. Welton T. Ionic liquids: a brief history. *Biophysical Reviews*. 2018 Jun 1;10(3):691–706.

22. Aki SNVK, Mellein BR, Saurer EM, Brennecke JF. High-Pressure Phase Behavior of Carbon Dioxide with Imidazolium-Based Ionic Liquids. *Journal of Physical Chemistry*. 2004;108:20355–65.

23. Emel'Yanenko VN, Boeck G, Verevkin SP, Ludwig R. Volatile times for the very first ionic liquid: Understanding the vapor pressures and enthalpies of vaporization of ethylammonium nitrate. *Chemistry - A European Journal*. 2014 Sep 8;20(37):11640–5.

24. Zech O. ethylammonium nitrate (CHEBI:63882) [Internet]. 2010 [cited 2023 Mar 23]. Available from: https://www.ebi.ac.uk/chebi/searchId.do?chebiId=CHEBI:63882

25. Wilkes JS, Levisky JA, Wilson RA, Hussey CL. Dialkylimidazolium Chloroaluminate melts: a new class of room temperature ionic liquids for electrochemistry, spectroscopy, and synthesis. *Inorganic Chemistry*. 1982;21:1263–4.

26. Wasserscheid P, Keim W. Ionic liquids - New "solutions" for transition metal catalysis. *Angewandte Chemie - International Edition*. 2000 Nov 3;39(21):3772–89.

27. Scheffler TB, Hussey CL, Seddon KR, Kear CM, Armitage PD. Molybdenum chloro complexes in room temperature chloroaluminate ionic liquids: stabilization of hexachloromolybdate(2-) and hexachloromolybdate (3-)). *Inorganic Chemistry*. 1983;22(15):2099–100.

28. Wilkes JS, Zaworotko MJ. Air and water stable 1-ethyl-3-methylimidazolium based ionic liquids. *Journal of the Chemical Society, Chemical Communications*. 1992;(13):965–7.

29. Vekariya RL. A review of ionic liquids: Applications towards catalytic organic transformations. *Journal of Molecular Liquids*. 2017 Feb 1;227:44.

30. Freemantle M, London C. Designer Solvents; Ionic liquids may boost clean technology development. *Chemical Engineering News*. 1998;76:32–7.

31. Siedlecka EM, Czerwicka M, Stolte S, Stepnowski P. Stability of Ionic Liquids in Application Conditions. *Current Organic Chemistry*. 2011;15.

32. Aparicio S, Atilhan M, Karadas F. Thermophysical properties of pure ionic liquids: Review of present situation. *Industrial and Engineering Chemistry Research*. 2010 Oct 20;49(20):9580–95.

33. Common Solvents Used in Organic Chemistry: Table of Properties [Internet]. 2005 [cited 2023 May 13]. Available from: https://organicchemistrydata.org/solvents/

34. Huddleston JG, Visser AE, Reichert WM, Willauer HD, Broker GA, Rogers RD. Characterization and comparison of hydrophilic and hydrophobic room temperature ionic liquids incorporating the imidazolium cation. *Green Chemistry*. 2001;3(4):156–64.

35. Ngo HL, Lecompte K, Hargens L, Mcewen AB. Thermal properties of imidazolium ionic liquids. 2000;97–102.

36. Villanueva M, Coronas A, García J, Salgado J. Thermal stability of ionic liquids for their application as new absorbents. *Industrial and Engineering Chemistry Research*. 2013 Nov 13;52(45):15718–27.

37. Endres F, Zein El Abedin S. Air and water stable ionic liquids in physical chemistry. *Physical Chemistry Chemical Physics*. 2006;8(18):2101–16.

38. Scurto AM, Newton E, Weikel RR, Draucker L, Hallett J, Liotta CL, et al. Melting point depression of ionic liquids with CO_2: Phase equilibria. *Industrial and Engineering Chemistry Research*. 2008 Feb 6;47(3):493–501.

39. Suarez P A Z, Einloft S, Dullius J E L, De Souza R F, Dupont J. Synthesis and physical-chemical properties of ionic liquids based on l-n-butyl-3-methylimidazolium cation. *J. Chim. Phys*. 1998;95:1626–39.

40. Fannin A A, Floreani D A, King L A, Landers J S, Piersma B J, Stech D J, et al. Properties of 1,3-dialkylimidazolium chloride-aluminum chloride ionic liquids. 2. Phase transitions, densities, electrical conductivities, and viscosities. *Journal of Physical Chemistry*. 1984;88:2614–21.

41. Bonhôte P, Dias A-P, Papageorgiou N, Kalyanasundaram K, Gra M. Hydrophobic, Highly Conductive Ambient-Temperature Molten Salts †. *Inorganic Chemistry*. 1996;35:1168–78.

42. Rebelo LPN, Lopes JNC, Esperança JMSS, Filipe E. On the critical temperature, normal boiling point, and vapor pressure of ionic liquids. *Journal of Physical Chemistry B*. 2005 Apr 7;109(13):6040–3.

43. Aschenbrenner O, Supasitmongkol S, Taylor M, Styring P. Measurement of vapour pressures of ionic liquids and other low vapour pressure solvents. *Green Chemistry*. 2009 Aug 3;11(8):1217–21.

44. Rooney D, Jacquemin J, Gardas R. Thermophysical properties of ionic liquids. *Topics in Current Chemistry*. 2009;290:185–212.

45. Valkenburg MEV, Vaughn RL, Williams M, Wilkes JS. Thermochemistry of ionic liquid heat-transfer fluids. *Thermochimica Acta*. 2005 Jan 20;425(1–2):181–8.

46. Olivier-Bourbigou H, Magna L. Ionic liquids: perspectives for organic and catalytic reactions. *Journal of Molecular Catalysis A: Chemical*. 2002 May 31;182–183:419–37.

47. Fredlake CP, Crosthwaite JM, Hert DG, Aki SNVK, Brennecke JF. Thermophysical properties of imidazolium-based ionic liquids. *Journal of Chemical and Engineering Data*. 2004 Jul;49(4):954–64.

48. Seddon KR, Stark A, Torres M-J. Influence of chloride, water, and organic solvents on the physical properties of ionic liquids*. *Pure Appl. Chem*. 2000;72(12):2275–87.

49. Heintz A, Ludwig R, Schmidt E. Limiting diffusion coefficients of ionic liquids in water and methanol: A combined experimental and molecular dynamics study. *Physical Chemistry Chemical Physics*. 2011 Feb 28;13(8):3268–73.

50. Wang X, Chi Y, Mu T. A review on the transport properties of ionic liquids. *Journal of Molecular Liquids*. 2014;193:262–6.

51. Umecky T, Kanakubo M, Ikushima Y. Self-diffusion coefficients of 1-butyl-3-methylimidazolium hexafluorophosphate with pulsed-field gradient spin-echo NMR technique. *Fluid Phase Equilibria*. 2005 Feb;228–229:329–33.

52. Tomida D. Thermal Conductivity of Ionic Liquids. In: Impact of Thermal Conductivity on Energy Technologies. *InTech*; 2018.

53. Ge R, Hardacre C, Nancarrow P, Rooney DW. Thermal conductivities of ionic liquids over the temperature range from 293 K to 353 K. *Journal of Chemical and Engineering Data*. 2007 Sep;52(5):1819–23.

54. De A, Dewan M, Mozumdar S. Ionic Liquids. In: Advanced Sensor and Detection Materials. 2014.

55. Sheldon RA. The: E factor 25 years on: The rise of green chemistry and sustainability. *Green Chemistry*. 2017;19(1):18–43.

56. Huddleston JG, Willauer HD, Swatloski RP, Visser AE, Rogers RD. Room temperature ionic liquids as novel media for "clean" liquid-liquid extraction. *Chemical Communications*. 1998 Aug 21;(16):1765–6.

57. Chapeaux A, Simoni LD, Ronan TS, Stadtherr MA, Brennecke JF. Extraction of alcohols from water with 1-hexyl-3-methylimidazolium bis(Trifluoromethylsulfonyl)imide. *Green Chemistry*. 2008 Dec 1;10(12):1301–6.

58. Wishart JF. Energy applications of ionic liquids. *Energy and Environmental Science*. 2009;2(9):956–61.

59. Reza Vakili-Nezhaad G, Alaisaee AM, Aljabri MA, Albarwani SS, Aljahwari ZK. Density Calculation of Ionic Liquids. *Materials Physics and Mechanics*. 2017;32:8–13.

60. Moganty SS, Baltus RE. Diffusivity of carbon dioxide in room-temperature ionic liquids. *Industrial and Engineering Chemistry Research*. 2010 Oct 6;49(19):9370–6.

61. Anthony JL, Maginn EJ, Brennecke JF. Solubilities and thermodynamic properties of gases in the ionic liquid 1-n-butyl-3-methylimidazolium hexafluorophosphate. *Journal of Physical Chemistry B*. 2002 Jul 25;106(29):7315–20.

62. Camper D, Scovazzo P, Koval C, Noble R. Gas solubilities in room-temperature ionic liquids. *Industrial and Engineering Chemistry Research*. 2004 Jun 9;43(12):3049–54.

63. Dupont J, Fonseca GS, Umpierre AP, Fichtner PFP, Teixeira SR. Transition-metal nanoparticles in imidazolium ionic liquids: Recycable catalysts for biphasic hydrogenation reactions. *Journal of the American Chemical Society*. 2002 Apr 24;124(16):4228–9.

64. Zhao H, Xia S, Ma P. Use of ionic liquids as "green" solvents for extractions. *Journal of Chemical Technology and Biotechnology*. 2005 Oct;80(10):1089–96.

65. Fan W, Zhou Q, Sun J, Zhang S. Density, excess molar volume, and viscosity for the methyl methacrylate + 1-butyl-3-methylimidazolium hexafluorophosphate ionic liquid binary system at atmospheric pressure. *Journal of Chemical and Engineering Data*. 2009 Aug 13;54(8):2307–11.

66. Palacio M, Bhushan B. A review of ionic liquids for green molecular lubrication in nanotechnology. *Tribology Letters*. 2010 Nov;40(2):247–68.

67. Knez, Markočič E, Leitgeb M, Primožič M, Knez Hrnčič M, Škerget M. Industrial applications of supercritical fluids: A review. *Energy*. 2014 Dec 1;77:235–43.

68. Kerton F. Alternative Solvents for Green Chemistry (RSC Green Chemistry Series). *The Royal Society of Chemistry* . 2009 Mar;170–80.

69. Sihvonen M, Järvenpää E, Hietaniemi V, Huopalahti R. Advances in supercritical carbon dioxide technologies. *Trends in Food Science & Technology*. 1999 Jun 1;10(6–7):217–22.

70. Cem G. Mathematical Modeling of Binary Interphase Diffusion in Gas-Expanded Liquid. *Yeditepe University*; 2011.

71. Jessop P G., Leitner W. Chemical Synthesis using Supercritical Fluids. New York: *Wiley-VCH*; 2008.

72. Thi L, Ihm H, Shim J. Equilibrium of Supercritical Fluid-Ionic Liquid-Organic Compound Ternary Phases. In: 11th European Meeting on Supercritical Fluids. 2008.

73. Kohli R. Applications of supercritical carbon dioxide for removal of surface contaminants. In: Developments in Surface Contamination and Cleaning: Applications of Cleaning Techniques Volume 11. *Elsevier*; 2018.

74. Jessop PG, Leitner W. Supercritical Fluids as Media for Chemical Reactions. In: Chemical Synthesis Using Supercritical Fluids. Germany: *Wiley-VCH Verlag GmbH*; 1999.

75. Palmer M V., Ting SST. Applications for supercritical fluid technology in food processing. *Food Chemistry*. 1995 Jan 1;52(4):345–52.

76. De Marco I, Riemma S, Iannone R. Supercritical carbon dioxide decaffeination process: A Life Cycle Assessment study. *Chemical Engineering Transactions*. 2017;57:1699–704.

77. Gaber MAFM, Tujillo FJ, Mansour MP, Juliano P. Improving Oil Extraction from Canola Seeds by Conventional and Advanced Methods. *Food Engineering Reviews*. 2018 Dec 1;10(4):198–210.

78. Zheng H, Yu T, Qu C, Li W, Wang Y. Basic Characteristics and Application Progress of Supercritical Water. In: IOP Conference Series: Earth and Environmental Science. *IOP Publishing Ltd*; 2020.

79. Pinkard BR, Gorman DJ, Tiwari K, Rasmussen EG, Kramlich JC, Reinhall G, et al. Supercritical water gasification: practical design strategies and operational challenges for lab-scale, continuous flow reactors. *Heliyon*. 2019;5:e01269. Available from: https://doi.org/10.1016/j.heliyon.2019.e01269

80. Supercritical Water Oxidation in Waste Water Treatment [Internet]. [cited 2023 Jul 18]. Available from: https://watermanaustralia.com/water-treatment-plants-manufacturer/

81. Scurto AM, Hutchenson K, Subramaniam B. Gas-expanded liquids: Fundamentals and applications. *Americam Chemical Society*. 2009 Jan 6;1006:3–37.

82. Sih R, Dehghani F, Foster NR. Viscosity measurements on gas expanded liquid systems—Methanol and carbon dioxide. *The Journal of Supercritical Fluids*. 2007 May 1;41(1):148–57.

83. Eckert CA, Liotta CL, Bush D, Brown JS, Hallett JP. Sustainable reactions in tunable solvents. *Journal of Physical Chemistry B*. 2004 Nov 25;108(47):18108–18.

84. Ahosseini A, Ren W, Scurto AM. Hydrogenation in biphasic ionic liquid-carbon dioxide systems. *American Chemical Society*. 2009 Jan 6;1006:218–34.

85. Shiflett MB, Maginn EJ. The solubility of gases in ionic liquids. *AIChE Journal*. 2017 Nov 1;63(11):4722–37.

86. Mellein BR, Scurto AM, Shiflett MB. Gas solubility in ionic liquids. *Current Opinion in Green and Sustainable Chemistry*. 2021 Apr 1;28:100425.

87. Blanchard LA, Gu Z, Brennecke JF. High-pressure phase behavior of ionic liquid/CO2 systems. *Journal of Physical Chemistry B*. 2001 Mar 29;105(12):2437–44.

88. Kim YS, Choi WY, Jang JH, Yoo KP, Lee CS. Solubility measurement and prediction of carbon dioxide in ionic liquids. *Fluid Phase Equilibria*. 2005 Feb 1;228–229:439–45.

89. Kamps ÁPS, Tuma D, Xia J, Maurer G. Solubility of CO_2 in the ionic liquid [bmim][PF_6]. *Journal of Chemical and Engineering Data*. 2003 May;48(3):746–9.

90. Rumpf B, Maurer G. An Experimental and Theoretical Investigation on the Solubility of Carbon Dioxide in Aqueous Solutions of Strong Electrolytes. *Berichte der Bunsengesellschaft für physikalische Chemie*. 1993;85–97.

91. Kumełan J, Pérez-Salado Kamps Á, Tuma D, Maurer G. Solubility of H_2 in the Ionic Liquid [bmim][PF_6]. *Journal of Chemical and Engineering Data*. 2006 Jan;51(1):11–4.

92. Liu Z, Wu W, Han B, Dong Z, Zhao G, Wang J, et al. Study on the phase behaviors, viscosities, and thermodynamic properties of CO_2/[C_4mim][PF_6]/methanol system at elevated pressures. *Chemistry - A European Journal*. 2003 Aug 18;9(16):3897–903.

93. Lim BH, Choe WH, Shim JJ, Ra CS, Tuma D, Lee H, et al. High-pressure solubility of carbon dioxide in imidazolium-based ionic liquids with anions [PF_6] and [BF_4]. *Korean Journal of Chemical Engineering*. 2009;26(4):1130–6.

94. Shiflett MB, Yokozeki A. Solubilities and diffusivities of carbon dioxide in ionic liquids: [bmim][PF_6] and [bmim][BF_4]. *Industrial and Engineering Chemistry Research*. 2005 Jun 8;44(12):4453–64.

95. Gonzalez-Miquel M, Bedia J, Abrusci C, Palomar J, Rodriguez F. Anion effects on kinetics and thermodynamics of CO_2 absorption in ionic liquids. *Journal of Physical Chemistry B*. 2013 Mar 28;117(12):3398–406.

96. Gong Y, Wang H, Chen Y, Hu X, Ibrahim AR, Tanyi AR, et al. A high-pressure quartz spring method for measuring solubility and diffusivity of CO_2 in ionic liquids. *Industrial and Engineering Chemistry Research*. 2013 Mar 13;52(10):3926–32.

97. Moya C, Palomar J, Gonzalez-Miquel M, Bedia J, Rodriguez F. Diffusion Coefficients of CO_2 in Ionic Liquids Estimated by Gravimetry. *Industrial and Engineering Chemistry Research*. 2014 Sep 3;53(35):13782–9.

98. Barghi SH, Tsotsis TT, Sahimi M. Solubility and diffusivity of H_2 and CO_2 in the ionic liquid [bmim][PF_6]. *International Journal of Hydrogen Energy*. 2015 Jul 27;40(28):8713–20.

99. Lomax H, Pulliam TH, Zingg DW. Fundamentals of Computational Fluid Dynamics. Toronto: *Springer*; 2001.

100. Kuzmin D. Introduction to Computational Fluid Dynamics [Internet]. 2017 [cited 2023 Mar 25]. Available from: https://www.mathematik.tu-dortmund.de/sites/cfdintro

101. Cebeci T, Shao J P, Kafyeke F., Laurendeau E. Computational Fluid Dynamics for Engineers. USA: *Horizon Publishing Inc.*; 2005.

102. Glatzel T, Litterst C, Cupelli C, Lindemann T, Moosmann C, Niekrawietz R, et al. Computational fluid dynamics (CFD) software tools for microfluidic applications - A case study. *Computers and Fluids*. 2008 Mar;37(3):218–35.

103. Ouyang Z, Bao D, Zhang X, Dong H, Yan R, Zhang X, et al. Numerical simulation of CO_2-ionic liquid flow in a stirred tank. *Science China Chemistry*. 2015 Dec 1;58(12):1918–28.

104. Wang P, Cilliers JJ, Neethling SJ, Brito-Parada PR. Effect of Particle Size on the Rising Behavior of Particle-Laden Bubbles. *Langmuir*. 2019 Mar 12;35(10):3680–7.

105. Wang X, Dong H, Zhang X, Xu Y, Zhang S. Numerical simulation of absorbing CO_2 with ionic liquids. *Chemical Engineering and Technology*. 2010 Oct;33(10):1615–24.

106. Meikandan M, Ganesh Kumar P, Sundarraj M, Yogaraj D. Numerical analysis on heat transfer characteristics of ionic liquids in a tubular heat exchanger. *International Journal of Ambient Energy*. 2020 Jul 2;41(8):911–7.

107. Sekerci-Cetin M, Emek OB, Yildiz EE, Unlusu B. Numerical study of the dissolution of carbon dioxide in an ionic liquid. *Chemical Engineering Science*. 2016 Jun 22;147:173–9.

108. Fu D, Sun X, Pu J, Zhao S. Effect of water content on the solubility of CO_2 in the ionic liquid [bmim][PF_6]. *Journal of Chemical and Engineering Data*. 2006 Mar;51(2):371–5.

109. Tyrrell HJV, Harris KR. Diffusion in Liquids. UK: *Butterworths &Co*; 1984.

110. Banerjee R. A numerical study of combined heat and mass transfer in an inclined channel using the VOF multiphase model. *Numerical Heat Transfer; Part A: Applications*. 2007 Jan;52(2):163–83.

111. Banerjee R. Turbulent conjugate heat and mass transfer from the surface of a binary mixture of ethanol/iso-octane in a countercurrent stratified two-phase flow system. *International Journal of Heat and Mass Transfer*. 2008 Dec;51(25–26):5958–74.

112. Hirt CW, Nichols BD. Volume of Fluid (VOF) Method for the Dynamics of Free Boundaries*. *Journal of Computational Physics*. 1981;39:201–25.

113. Issa RI. Solution of the Implicitly Discretised Fluid Flow Equations by Operator-Splitting. *Journal of Computational Physics*. 1985;62.

114. Van Leer B. Towards the Ultimate Conservative Difference Scheme. V. A Second-Order Sequel to Godunov's Method. *Journal of Computational Physics*. 1979;32:101–36.

115. Youngs DL. Time- Dependent Multi- Material Flow with Large Fluid Distortion. In: Numerical Methods in Fluid Dynamics. *Academic Press*; 1982.

116. Klähn M, Seduraman A. What Determines CO_2 Solubility in Ionic Liquids? A Molecular Simulation Study. *The Journal of Physical Chemistry*. 2015;119(31):10066–78.

117. Shiflett MB, Yokozeki A. Solubilities and diffusivities of carbon dioxide in ionic liquids: [bmim][PF_6] and [bmim][BF_4]. *Industrial and Engineering Chemistry Research*. 2005 Jun 8;44(12):4453–64.

118. Yildiz EE. Solubility of Carbon Dioxide in the Ionic Liquids [bmim][BF_4] and [bmim][PF_6] at high pressure. [Turkey]: *Yeditepe University*; 2014.

119. Stryjek R, Vera J H. PRSV: An Improved Peng-Robinson Equation of State for Pure Compounds and Mixtures. *The Canadian Journal of Chemical Engineering*. 1986;64:323–33.

120. Shan D, Wong H. A Theoretically Correct Equations Mixing Rule for Cubic of State. *AIChE Journal*. 1992;38(5):671–80.

121. Renon H, Prausnitz JM. Local compositions in thermodynamic excess functions for liquid mixtures. *AIChE Journal*. 1968;14(1):135–44.

122. Orbey H, Sandler Stanley I. Modeling vapor-liquid equilibria : cubic equations of state and their mixing rules. New York: *Cambridge University Press*; 1998.

123. Hamedi N, Rahimpour MR, Keshavarz P. Methane solubility in ionic liquids: Comparison of cubic-plus-association and modified Sanchez-Lacombe equation of states. *Chemical Physics Letters*. 2020 Jan 1;738:136903.

124. Jalili AH, Mehdizadeh A, Ahmadi AN, Zoghi AT, Shokouhi M. Solubility behavior of CO_2 and H_2S in 1-benzyl-3-methylimidazolium bis(trifluoromethylsulfonyl)imide ionic liquid. *The Journal of Chemical Thermodynamics*. 2022 Apr 1;167:106721.

125. Valderrama JO, Cardona LF, Rojas RE. A Simple Computer Tool for Simultaneously Estimating Critical, Transport, Physicochemical, and Phase Change Properties of Ionic Liquids. *Industrial and Engineering Chemistry Research*. 2021 Nov 10;60(44):16143–51.

126. Yokozeki A, Shiflett MB. Global phase behaviors of trifluoromethane in ionic liquid [bmim][PF_6]. *AIChE Journal*. 2006 Nov;52(11):3952–7.

127. Polishuk I, Chiko A, Cea-Klapp E, Matías Garrido J. Electronic Supporting Information Implementation of CP-PC-SAFT and CS-SAFT-VR-Mie for predicting thermodynamic properties of C1-C3 halocarbon systems. II. Inter-relation between solubilities in ionic liquids, their PVT and critical constants. *Industrial Chemical Engineering*. 2021;60:13084–94.

128. Morais ARC, Harders AN, Baca KR, Olsen GM, Befort BJ, Dowling AW, et al. Phase Equilibria, Diffusivities, and Equation of State Modeling of HFC-32 and HFC-125 in Imidazolium-Based Ionic Liquids for the Separation of R-410A. *Industrial and Engineering Chemistry Research*. 2020 Oct 7;59(40):18222–35.

129. Plakia A, Koulocheris V, Louli V, Voutsas E. Vapor-liquid equilibrium of acid gases with imidazolium-based ionic liquids using the UMR-PRU model. *Chemical Thermodynamics and Thermal Analysis*. 2022 Dec 1;8:100097.

130. Arce PF, Robles PA, Graber TA, Aznar M. Modeling of high-pressure vapor–liquid equilibrium in ionic liquids + gas systems using the PRSV equation of state. *Fluid Phase Equilibria*. 2010 Aug 15;295(1):9–16.

131. Poling B E, Prausnitz J M, O'connel J P. The Properties of Gases and Liquids . New York: *Mc Graw Hill*; 2004.

132. Zabala D, Nieto-Draghi C, De Hemptinne JC, De López Ramos AL. Diffusion coefficient in CO_2/n-binary liquid mixture by molecular simulation. *Journal of Physical Chemistry B*. 2008 Dec 25;112(51):16610–8.

133. He C, Yu Y. New Equation for Infinite-Dilution Diffusion Coefficients in Supercritical and High-Temperature Liquid Solvents. *Industrial & Engineering Chemistry Research*. 1998;37:3793–8.

134. Shi Y, Lu J. Correlation of infinite-dilution diffusion coefficients in supercritical fluids. *Industrial and Engineering Chemistry Research*. 2010 Oct 6;49(19):9542–7.

135. Shi Y, Lu J. Correlation of infinite-dilution diffusion coefficients in supercritical fluids. *Industrial and Engineering Chemistry Research*. 2010 Oct 6;49(19):9542–7.

136. NIST Chemistry Webbook [Internet]. [cited 2023 Mar 25] . Available from: http://webbook.nist.gov/chemistry/

APPENDIX A: EXPERIMENTAL DATA

A.1. Experimental data of [bmim][PF_6] – CO_2 System at 313.15 K AND 794 PSIA (5.4 MPa)

Table A.1. The experimental data for 313.15 K and 794 psia

Mass of the IL (g)	7.4659
Volume of CO_2 loaded to the system (ml)	149.36
Initial volume of CO_2 in syringe pump (ml)	253.75
Final volume of CO_2 in syringe pump (ml)	97.62
Pressure of the system during the experiment	794±2 psia (5.4 MPa)
Temperature of the system during the experiment (°C)	40.0 ±0.1

Below is the detailed calculation for equilibrium mole fraction.

The number of CO_2 in liquid is calculated by using equation below:

$$n_{i,isco} = n_{CO_2} + n_{f,isco} + n_{f,jer} \quad (A.1)$$

The volume of carbon dioxide remaining in the view cell after expansion is obtained by subtracting the expanded liquid volume from the initial volume of carbon dioxide in the view cell.

A (view cell) =5.55 cm^2

$V_{f,CO_{2(g)}} = 149.36 - (5.55 \times 0.187) = 148.32\ ml$

$V_{CO_{2(dissolvedintheIL)}} = 253.75 - 97.62 - 148.32 = 7.81\ ml$

$n_{CO_{2(in\ the\ liquid)}} = 7.81/340.79 = 0.022917\ mole$

$n_{IL} = 7.4659/284.18 = 0.02627$

$x_{CO_{2\ (in\ the\ IL)}} = 0.02292/(0.02292 + 0.02627) = 0.466$

$V_{m_{CO_2}}$=340.79 (cm^3/mol) [136] at 313.15 K and 794 psia.

$MW_{IL} = 284.18\ g/mole$ [136]

So, x_{CO_2} =0.466.

If the expansion is neglected:

$V_{f,CO_{2(g)}} = 149.36 - (5.55 \times 0.0) = 149.36\, ml$

$V_{CO_{2(dissolvedintheIL)}} = 253.75 - 97.62 - 149.36 = 6.77\, ml$

$n_{CO_{2(in\ the\ liquid)}} = 6.77/340.79 = 0.019865\, mole$

$n_{IL} = 7.4659/284.18 = 0.02627$

$x_{CO_{2\ (in\ the\ IL)}} = 0.019865/(0.019865 + 0.02627) = 0.430$

A.2. Experimental Data of [bmim][PF_6] – CO_2 System at 313.15 K and 1197 PSIA (8.3 MPa)

Table A2. The experimental data for 313.15 K and 1197 psia

Mass of the IL (g)	10.6247
Volume of CO_2 loaded to the system (ml)	151.32
Initial volume of CO_2 in syringe pump (ml)	251.14
Final volume of CO_2 in syringe pump (ml)	94.11
Pressure of the system during the experiment	1197±2 psia (8.3 MPa)
Temperature of the system during the experiment (°C)	40.0 ±0.1

A.3. Experimental Data of [bmim][PF_6] – CO_2 System at 323.15 K and 771 PSIA (5.3 MPa)

Table A3. The experimental data for 323.15 K and 771 psia

Mass of the IL (g)	7.8849
Volume of CO_2 loaded to the system (ml)	147.86
Initial volume of CO_2 in syringe pump (ml)	237.46
Final volume of CO_2 in syringe pump (ml)	82.83
Pressure of the system during the experiment	771±2 psia
Temperature of the system during the experiment (°C)	50±0.1

A.4. Experimental Data of [[bmim][PF_6] – CO_2 System at 323.15 K and 1175 PSIA (8.1 MPa)

Table A3. The experimental data for 323.15 K and 1175 psia

Mass of the IL (g)	9.3523
Volume of CO_2 loaded to the system (ml)	152.54
Initial volume of CO_2 in syringe pump (ml)	241.23
Final volume of CO_2 in syringe pump (ml)	83.77
Pressure of the system during the experiment	1175±2 psia (8.3 MPa)
Temperature of the system during the experiment (°C)	50.0 ±0.1

APPENDIX B: REPEAT EXPERIMENTS FOR [bmim][PF_6] – CO_2 SYSTEM

B.1. Repeat Experiment for [bmim][PF_6] – CO_2 System at 313.15 K and 5.4 MPa

In figure B.1. repeat experiment for [bmim][PF_6] at 313.15 K and 5.4 MPa is shown.

The repeat experiment fits the first experimental data.

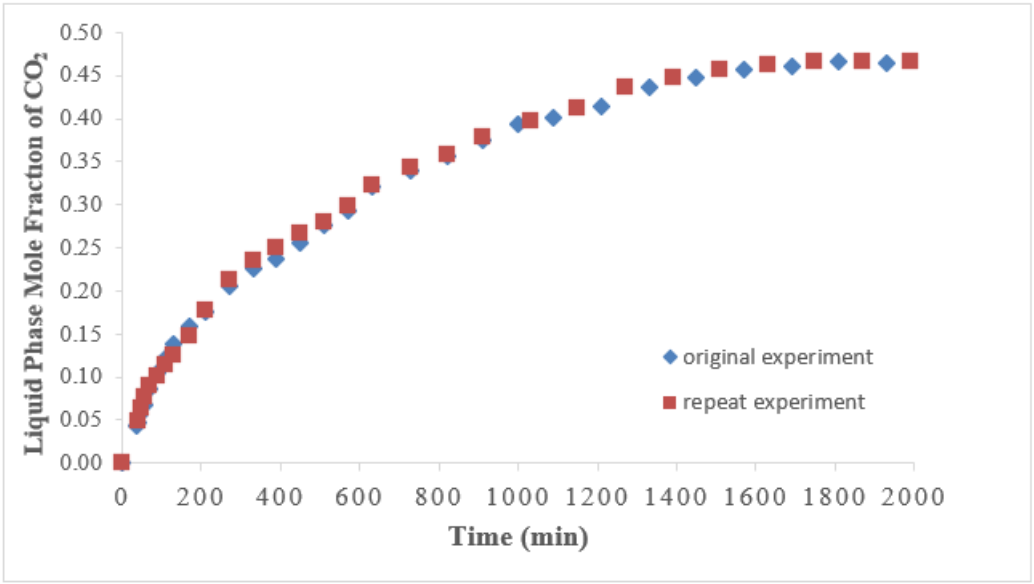

Figure B.1. Average carbon dioxide mole fractions in the liquid phase for both original and repeat experiments (313.15 K, 5.4 MPa)

Table B.1. Mass, pressure, temperature values of both experiments(313.15 K, 5.4 MPa)

	Original Experiment	**Repeat Experiment**
Mass of IL (g)	7.4314	7.4659
Pressure (psi)	792±2	794±2
Temperature (ºC)	40±0.1	40±0.1

B.2. Repeat Experiment for [bmim][PF_6] – CO_2 System at 313.15 K and 8.3 MPa

In figure B.2. repeat experiment for [bmim][PF_6] at 313.15 K and 8.3 MPa is shown. The repeat experiment fits the first experimental data.

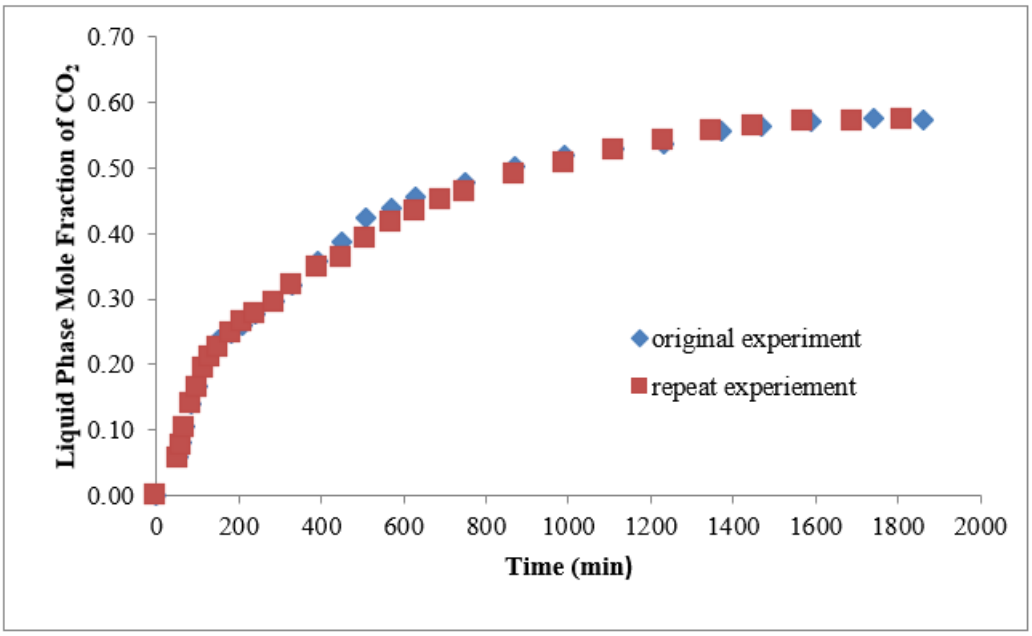

Figure B.2. Average Carbon dioxide mole fractions in the liquid phase for both original and repeat experiments (313.15 K, 8.3 MPa)

Table B.2. Mass, pressure, temperature values of both experiments (313.15 K, 8.3 MPa)

	Original Experiment	**Repeat Experiment**
Mass of IL (g)	10.5931	10.6247
Pressure (psia)	1201±2	1197±2
Temperature (ºC)	40±0.1	40±0.1

B.3: Repeat Experiment for [bmim][PF_6] – CO_2 System at 323.15 K and 5.3 MPa

In figure B.3. repeat experiment for [bmim][PF_6] at 323.15 K and 5.3 MPa is shown.

The repeat experiment fits the first experimental data.

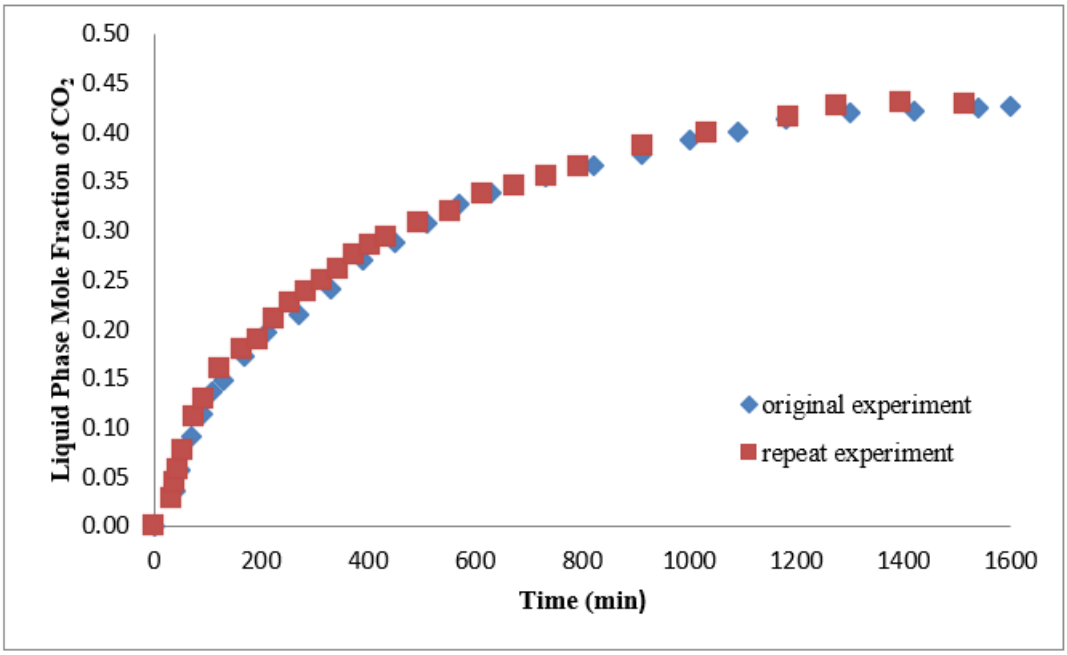

Figure B.3. Average carbon dioxide mole fractions in the liquid phase for both original and repeat experiments (323.15 K, 5.3 MPa)

Table B.3. Mass, pressure, temperature values of both experiments(323.15 K, 5.3 MPa)

	Original Experiment	**Repeat Experiment**
Mass of IL (g)	7.8849	7.5648
Pressure (psia)	771±2	749±2
Temperature (ºC)	50±0.1	50±0.1

B.4. Repeat Experiment for [bmim][PF_6] – CO_2 System at 323.15 K and 8.1 MPa

In figure B.4. repeat experiment for [bmim][PF_6] at 323.15 K and 8.1 MPa is shown. The repeat experiment fits the first experimental data.

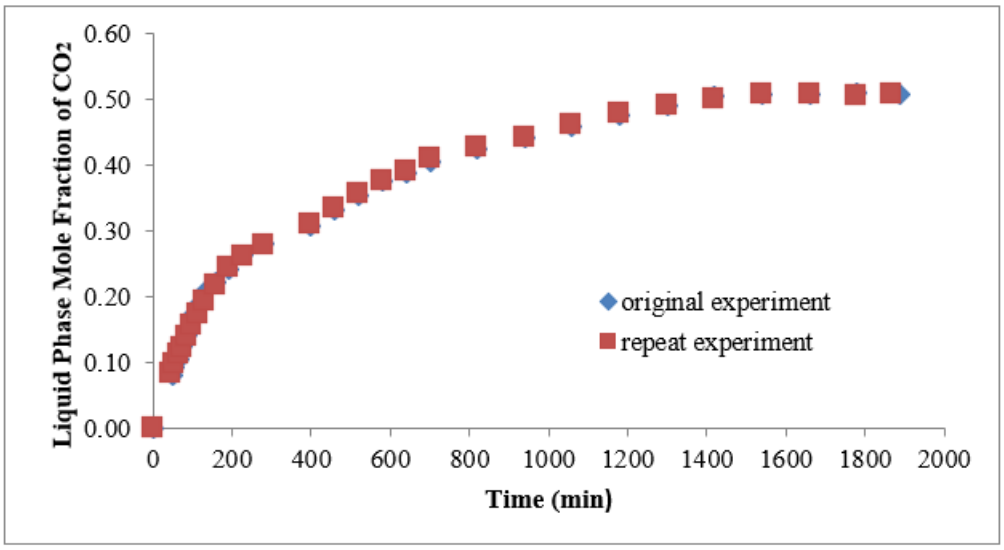

Figure B.4. Average carbon dioxide mole fractions in the liquid phase for both original and repeat experiments (323.15 K, 8.1 MPa)

Table B.4. Mass, pressure, temperature values of both experiments(323.15 K, 8.1 MPa)

	Original Experiment	**Repeat Experiment**
Mass of IL (g)	9.3523	9.3131
Pressure (psia)	1175±2	1195±2
Temperature (ºC)	50±0.1	50±0.1

APPENDIX C: OUTPUT DATA

Table C.1. Output Data of [bmim][PF_6]-CO_2 System for PRSV equation of state and Wong-Sandler mixing rules at 313.15 K for Set 1 (w= 0.7917)

WS: THE WONG-SANDLER MIXING RULE FOR BINARY VLE CALCULATIONS

EXCESS ENERGY MODEL= NRTL

ALPHA= .2000

K12= .8683

NRTL A12(CAL/MOL)= -85.5029

NRTL A21(CAL/MOL)= 69.5100

NRTL P12(=A12/RT) -.1374

NRTL P21(=A21/RT) .1117

pf6yoko2

bmimpf6

TEMPERATURE in K: 313.15

PHASE VOLUMES ARE IN CC/MOL, PRESSURE IS IN UNITS OF THE DATA.

X-EXP	P-EXP	P-CAL	Y-EXP	Y-CAL	VL-CAL	VV-CAL
.3320	31.578	32.052	1.00000	1.00000	153.41	679.9
.4660	54.470	52.311	1.00000	1.00000	126.10	355.5
.5740	82.530	78.725	1.00000	1.00001	104.41	161.8
.6170	103.145	105.150	1.00000	1.00000	95.84	73.1
.6360	123.968	124.361	1.00000	.99999	92.04	64.4

AAD-Y= .001

AAD-P= 2.467

AAD=SUM[ABS(EXP-CAL)/EXP]*100/(NO. OF DATA POINTS)

Table C.2. Output Data of [bmim][PF_6]-CO_2 System for PRSV equation of state and Wong-Sandler mixing rules at 313.15 K for Set 1 (w(Tb/Tc=0.7709))

WS: THE WONG-SANDLER MIXING RULE FOR BINARY VLE CALCULATIONS

EXCESS ENERGY MODEL= NRTL

ALPHA= .2000

K12= .8295

NRTL A12(CAL/MOL)= -28.3891

NRTL A21(CAL/MOL)= -7.1450

NRTL P12(=A12/RT) -.0456

NRTL P21(=A21/RT) -.0115

pf6yoko3

bmimpf6

TEMPERATURE in K: 313.15

PHASE VOLUMES ARE IN CC/MOL, PRESSURE IS IN UNITS OF THE DATA.

X-EXP	P-EXP	P-CAL	Y-EXP	Y-CAL	VL-CAL	VV-CAL
.3320	31.578	33.878	1.00000	1.00000	155.55	635.4
.4660	54.470	54.335	1.00000	1.00001	129.70	335.7
.5740	82.530	79.697	1.00000	1.00001	109.06	155.9
.6170	103.145	104.960	1.00000	1.00000	100.86	73.2
.6362	123.968	123.925	1.00000	.99999	97.19	64.5

AAD-Y= .001

AAD-P= 2.551

AAD=SUM[ABS(EXP-CAL)/EXP]*100/(NO. OF DATA POINTS)

Table C.3. Output Data of [bmim][PF_6]-CO_2 System for PRSV equation of state and Wong-Sandler mixing rules at 313.15 K for Set 1 (w=1.5114)

WS: THE WONG-SANDLER MIXING RULE FOR BINARY VLE CALCULATIONS

EXCESS ENERGY MODEL= NRTL

ALPHA= .2000

K12= .7664

NRTL A12(CAL/MOL)= -243.1536

NRTL A21(CAL/MOL)= 70.6530

NRTL P12(=A12/RT) -.3907

NRTL P21(=A21/RT) .1135

pf6yoko4

bmimpf6

TEMPERATURE in K: 313.15

PHASE VOLUMES ARE IN CC/MOL, PRESSURE IS IN UNITS OF THE DATA.

X-EXP	P-EXP	P-CAL	Y-EXP	Y-CAL	VL-CAL	VV-CAL
.3320	31.578	33.606	1.00000	1.00000	159.02	641.7
.4660	54.470	54.477	1.00000	1.00001	135.35	334.4
.5740	82.530	78.815	1.00000	1.00001	116.34	161.2
.6170	103.145	102.423	1.00000	.99999	108.76	75.2
.6362	123.968	123.980	1.00000	.99990	105.35	64.4

AAD-Y= .003

AAD-P= 2.329

AAD=SUM[ABS(EXP-CAL)/EXP]*100/(NO. OF DATA POINTS)

Table C.4. Output Data of [bmim][PF_6]-CO_2 System for PRSV equation of state and Wong-Sandler mixing rules at 313.15 K for Set 2 (w=0.7917)

WS: THE WONG-SANDLER MIXING RULE FOR BINARY VLE CALCULATIONS

EXCESS ENERGY MODEL= NRTL

ALPHA= .2000

K12= .9252

NRTL A12(CAL/MOL)= 2470.2903

NRTL A21(CAL/MOL)= -897.4106

NRTL P12(=A12/RT) 3.9697

NRTL P21(=A21/RT) -1.4421

pf6wald2

bmimpf6

TEMPERATURE in K: 313.15

PHASE VOLUMES ARE IN CC/MOL, PRESSURE IS IN UNITS OF THE DATA.

X-EXP	P-EXP	P-CAL	Y-EXP	Y-CAL	VL-CAL	VV-CAL
.3320	31.578	33.088	1.00000	1.00000	195.02	654.1
.4660	54.470	54.413	1.00000	1.00001	157.62	335.0
.5740	82.530	81.426	1.00000	1.00001	127.13	145.4
.6170	103.145	107.328	1.00000	.99999	115.22	71.7
.6362	123.968	123.982	1.00000	.99997	109.89	64.5

AAD-Y= .001

AAD-P= 2.126

AAD=SUM[ABS(EXP-CAL)/EXP]*100/(NO. OF DATA POINTS)

Table C.5. Output Data of [bmim][PF_6]-CO_2 System for PRSV equation of state and Wong-Sandler mixing rules at 313.15 K for Set 3 (w= 0.7917)

WS: THE WONG-SANDLER MIXING RULE FOR BINARY VLE CALCULATIONS

EXCESS ENERGY MODEL= NRTL

ALPHA= .2000

K12= .8813

NRTL A12(CAL/MOL)= 63.6614

NRTL A21(CAL/MOL)= 42.4154

NRTL P12(=A12/RT) .1023

NRTL P21(=A21/RT) .0682

pf6pol2

bmimpf6

TEMPERATURE in K: 313.15

PHASE VOLUMES ARE IN CC/MOL, PRESSURE IS IN UNITS OF THE DATA.

X-EXP	P-EXP	P-CAL	Y-EXP	Y-CAL	VL-CAL	VV-CAL
.3320	31.578	34.380	1.00000	1.00001	173.25	624.0
.4660	54.470	54.312	1.00000	1.00001	142.10	335.9
.5740	82.530	79.947	1.00000	1.00001	117.23	154.4
.6170	103.145	105.682	1.00000	1.00001	107.36	72.8
.6362	123.968	123.977	1.00000	1.00000	102.95	64.5

AAD-Y= .001

AAD-P= 2.951

AAD=SUM[ABS(EXP-CAL)/EXP]*100/(NO. OF DATA POINTS)

Table C.6. Output Data of [bmim][PF_6]-CO_2 System for PRSV equation of state and Wong-Sandler mixing rules at 313.15 K for Set 3 (w (Tb/Tc=0.7709))

WS: THE WONG-SANDLER MIXING RULE FOR BINARY VLE CALCULATIONS

EXCESS ENERGY MODEL= NRTL

ALPHA= .2000

K12= .8600

NRTL A12(CAL/MOL)= -174.7425

NRTL A21(CAL/MOL)= 36.5520

NRTL P12(=A12/RT) -.2808

NRTL P21(=A21/RT) .0587

pf6pol3

bmimpf6

TEMPERATURE in K: 313.15

PHASE VOLUMES ARE IN CC/MOL, PRESSURE IS IN UNITS OF THE DATA.

X-EXP	P-EXP	P-CAL	Y-EXP	Y-CAL	VL-CAL	VV-CAL
.3320	31.578	31.190	1.00000	1.00001	173.70	702.7
.4660	54.470	51.698	1.00000	1.00000	143.52	361.8
.5740	82.530	77.903	1.00000	1.00001	119.42	166.7
.6170	103.145	103.761	1.00000	1.00001	109.85	74.1
.6362	123.968	123.971	1.00000	1.00001	105.57	64.5

AAD-Y= .001

AAD-P= 2.505

AAD=SUM[ABS(EXP-CAL)/EXP]*100/(NO. OF DATA POINTS)

Table C.7. Output Data of [bmim][PF_6]-CO_2 System for PRSV equation of state and Wong-Sandler mixing rules at 313.15 K for Set 3 (w= 1.5114)

WS: THE WONG-SANDLER MIXING RULE FOR BINARY VLE CALCULATIONS

EXCESS ENERGY MODEL= NRTL

ALPHA= .2000

K12= .7840

NRTL A12(CAL/MOL)= -418.8376

NRTL A21(CAL/MOL)= 64.9163

NRTL P12(=A12/RT) -.6731

NRTL P21(=A21/RT) .1043

pf6pol4

bmimpf6

TEMPERATURE in K: 313.15

PHASE VOLUMES ARE IN CC/MOL, PRESSURE IS IN UNITS OF THE DATA.

X-EXP	P-EXP	P-CAL	Y-EXP	Y-CAL	VL-CAL	VV-CAL
.3320	31.578	28.970	1.00000	1.00001	178.63	767.5
.4660	54.470	50.650	1.00000	1.00001	151.37	372.8
.5740	82.530	76.512	1.00000	1.00001	127.98	175.1
.6170	103.145	102.126	1.00000	1.00001	119.15	75.5
.6362	123.968	128.177	1.00000	.99998	115.17	63.3

AAD-Y= .001

AAD-P= 5.390

AAD=SUM[ABS(EXP-CAL)/EXP]*100/(NO. OF DATA POINTS)

Table C.8. Output Data of [bmim][PF_6]-CO_2 System for PRSV equation of state and Wong-Sandler mixing rules at 313.15 K for Set 4 (w= 0.7917)

WS: THE WONG-SANDLER MIXING RULE FOR BINARY VLE CALCULATIONS

EXCESS ENERGY MODEL= NRTL

ALPHA= .2000

K12= .8200

NRTL A12(CAL/MOL)= -192.9104

NRTL A21(CAL/MOL)= 54.2173

NRTL P12(=A12/RT) -.3100

NRTL P21(=A21/RT) .0871

pf6ypol2

bmimpf6

TEMPERATURE in K: 313.15

PHASE VOLUMES ARE IN CC/MOL, PRESSURE IS IN UNITS OF THE DATA.

X-EXP	P-EXP	P-CAL	Y-EXP	Y-CAL	VL-CAL	VV-CAL
.3320	31.578	32.684	1.00000	1.00000	169.64	664.0
.4660	54.470	53.354	1.00000	1.00001	142.05	345.2
.5740	82.530	78.615	1.00000	1.00001	119.96	162.4
.6170	103.145	103.521	1.00000	1.00001	111.17	74.3
.6362	123.968	123.952	1.00000	1.00000	107.23	64.5

AAD-Y= .001

AAD-P= 2.135

AAD=SUM[ABS(EXP-CAL)/EXP]*100/(NO. OF DATA POINTS)

Table C.9. Output Data of [bmim][PF_6]-CO_2 System for PRSV equation of state and Wong-Sandler mixing rules at 313.15 K for Set 4 (w (Tb/Tc=0.7709))

WS: THE WONG-SANDLER MIXING RULE FOR BINARY VLE CALCULATIONS

EXCESS ENERGY MODEL= NRTL

ALPHA= .2000

K12= .7664

NRTL A12(CAL/MOL)= -572.5720

NRTL A21(CAL/MOL)= 89.4828

NRTL P12(=A12/RT) -.9201

NRTL P21(=A21/RT) .1438

pf6ypol3

bmimpf6

TEMPERATURE in K: 313.15

PHASE VOLUMES ARE IN CC/MOL, PRESSURE IS IN UNITS OF THE DATA.

X-EXP	P-EXP	P-CAL	Y-EXP	Y-CAL	VL-CAL	VV-CAL
.3320	31.578	27.321	1.00000	1.00000	172.41	822.3
.4660	54.470	43.752	1.00000	1.00001	146.82	457.6
.5740	82.530	72.304	1.00000	1.00001	121.61	200.8
.6170	103.145	99.686	1.00000	1.00001	113.20	77.8
.6362	123.968	131.630	1.00000	1.00000	109.41	62.4

AAD-Y= .001

AAD-P= 11.016

AAD=SUM[ABS(EXP-CAL)/EXP]*100/(NO. OF DATA POINTS)

Table C.10. Output Data of [bmim][PF_6]-CO_2 System for PRSV equation of state and Wong-Sandler mixing rules at 313.15 K for Set 5 (w= 0.7917)

WS: THE WONG-SANDLER MIXING RULE FOR BINARY VLE CALCULATIONS

EXCESS ENERGY MODEL= NRTL

ALPHA= .2000

K12= .8870

NRTL A12(CAL/MOL)= 95.1861

NRTL A21(CAL/MOL)= -49.5817

NRTL P12(=A12/RT) .1530

NRTL P21(=A21/RT) -.0797

pf6ahf2

bmimpf6

TEMPERATURE in K: 313.15

PHASE VOLUMES ARE IN CC/MOL, PRESSURE IS IN UNITS OF THE DATA.

X-EXP	P-EXP	P-CAL	Y-EXP	Y-CAL	VL-CAL	VV-CAL
.3320	31.578	33.535	1.00000	1.00001	186.01	643.4
.4660	54.470	53.595	1.00000	1.00000	152.42	342.8
.5740	82.530	79.407	1.00000	1.00001	125.57	157.6
.6170	103.145	105.228	1.00000	1.00001	114.91	73.1
.6362	123.968	123.922	1.00000	1.00001	110.14	64.5

AAD-Y= .001

AAD-P= 2.729

AAD=SUM[ABS(EXP-CAL)/EXP]*100/(NO. OF DATA POINTS)

Table C.11. Output Data of [bmim][PF_6]-CO_2 System for PRSV equation of state and Wong-Sandler mixing rules at 313.15 K for Set 5 (w (Tb/Tc=0.7709))

WS: THE WONG-SANDLER MIXING RULE FOR BINARY VLE CALCULATIONS

EXCESS ENERGY MODEL= NRTL

ALPHA= .2000

K12= .8569

NRTL A12(CAL/MOL)= -150.6101

NRTL A21(CAL/MOL)= 35.3735

NRTL P12(=A12/RT) -.2420

NRTL P21(=A21/RT) .0568

pf6shf3

bmimpf6

TEMPERATURE in K: 313.15

PHASE VOLUMES ARE IN CC/MOL, PRESSURE IS IN UNITS OF THE DATA.

X-EXP	P-EXP	P-CAL	Y-EXP	Y-CAL	VL-CAL	VV-CAL
.3320	31.578	32.112	1.00000	1.00001	187.68	678.4
.4660	54.470	52.592	1.00000	1.00001	155.43	352.7
.5740	82.530	78.305	1.00000	1.00001	129.61	164.3
.6170	103.145	103.777	1.00000	1.00001	119.34	74.1
.6362	123.968	123.967	1.00000	1.00001	114.74	64.5

AAD-Y= .001

AAD-P= 2.174

AAD=SUM[ABS(EXP-CAL)/EXP]*100/(NO. OF DATA POINTS)

Table C.12. Output Data of [bmim][PF_6]-CO_2 System for PRSV equation of state and Wong-Sandler mixing rules at 323.15 K for Set 1 (w= 0.7917)

WS: THE WONG-SANDLER MIXING RULE FOR BINARY VLE CALCULATIONS

EXCESS ENERGY MODEL= NRTL

ALPHA= .2000

K12= .8637

NRTL A12(CAL/MOL)= 643.6374

NRTL A21(CAL/MOL)= -564.9946

NRTL P12(=A12/RT) 1.0023

NRTL P21(=A21/RT) -.8798

pf6yoko2

bmimpf6

TEMPERATURE in K: 323.15

PHASE VOLUMES ARE IN CC/MOL, PRESSURE IS IN UNITS OF THE DATA.

X-EXP	P-EXP	P-CAL	Y-EXP	Y-CAL	VL-CAL	VV-CAL
.2950	30.300	31.833	1.00000	1.00000	161.98	722.2
.4260	53.100	53.105	1.00000	1.00000	135.34	377.5
.5080	81.000	71.711	1.00000	1.00001	118.83	238.2
.5810	100.300	97.996	1.00000	1.00001	104.27	122.0
.6150	121.100	121.110	1.00000	1.00000	97.51	80.6

AAD-Y= .000

AAD-P= 3.768

AAD=SUM[ABS(EXP-CAL)/EXP]*100/(NO. OF DATA POINTS)

Table C.13. Output Data of [bmim][PF_6]-CO_2 System for PRSV equation of state and Wong-Sandler mixing rules at 323.15 K for Set 1 (w (Tb/Tc=0.7709))

WS: THE WONG-SANDLER MIXING RULE FOR BINARY VLE CALCULATIONS

EXCESS ENERGY MODEL= NRTL

ALPHA= .2000

K12= .8302

NRTL A12(CAL/MOL)= -197.5218

NRTL A21(CAL/MOL)= 48.1179

NRTL P12(=A12/RT) -.3076

NRTL P21(=A21/RT) .0749

pf6yoko3

bmimpf6

TEMPERATURE in K: 323.15

PHASE VOLUMES ARE IN CC/MOL, PRESSURE IS IN UNITS OF THE DATA.

X-EXP	P-EXP	P-CAL	Y-EXP	Y-CAL	VL-CAL	VV-CAL
.2950	30.300	31.381	1.00000	1.00000	162.98	734.5
.4260	53.100	53.098	1.00000	1.00001	137.61	377.6
.5080	81.000	71.885	1.00000	1.00001	121.85	237.2
.5810	100.300	97.971	1.00000	1.00001	107.92	122.1
.6150	121.100	121.172	1.00000	1.00000	101.44	80.6

AAD-Y= .001

AAD-P= 3.441

AAD=SUM[ABS(EXP-CAL)/EXP]*100/(NO. OF DATA POINTS)

Table C.14. Output Data of [bmim][PF_6]-CO_2 System for PRSV equation of state and Wong-Sandler mixing rules at 323.15 K for Set 1 (w= 1.5114)

WS: THE WONG-SANDLER MIXING RULE FOR BINARY VLE CALCULATIONS

EXCESS ENERGY MODEL= NRTL

ALPHA= .2000

K12= .7639

NRTL A12(CAL/MOL)= -390.3700

NRTL A21(CAL/MOL)= 109.9608

NRTL P12(=A12/RT) -.6079

NRTL P21(=A21/RT) .1712

pf6yoko4

bmimpf6

TEMPERATURE in K: 323.15

PHASE VOLUMES ARE IN CC/MOL, PRESSURE IS IN UNITS OF THE DATA.

X-EXP	P-EXP	P-CAL	Y-EXP	Y-CAL	VL-CAL	VV-CAL
.2950	30.300	30.814	1.00000	1.00001	165.97	750.4
.4260	53.100	53.117	1.00000	1.00001	142.84	377.4
.5080	81.000	72.014	1.00000	1.00001	128.43	236.5
.5810	100.300	97.450	1.00000	1.00001	115.64	123.8
.6150	121.100	121.230	1.00000	1.00000	109.66	80.5

AAD-Y= .001

AAD-P= 3.154

AAD=SUM[ABS(EXP-CAL)/EXP]*100/(NO. OF DATA POINTS)

Table C.15. Output Data of [bmim][PF_6]-CO_2 System for PRSV equation of state and Wong-Sandler mixing rules at 323.15 K for Set 2 (w= 0.7917)

WS: THE WONG-SANDLER MIXING RULE FOR BINARY VLE CALCULATIONS

EXCESS ENERGY MODEL= NRTL

ALPHA= .2000

K12= .8569

NRTL A12(CAL/MOL)= -150.6101

NRTL A21(CAL/MOL)= 35.3735

NRTL P12(=A12/RT) -.2420

NRTL P21(=A21/RT) .0568

pf6shf3

bmimpf6

TEMPERATURE in K: 313.15

PHASE VOLUMES ARE IN CC/MOL, PRESSURE IS IN UNITS OF THE DATA.

X-EXP	P-EXP	P-CAL	Y-EXP	Y-CAL	VL-CAL	VV-CAL
.3320	31.578	32.112	1.00000	1.00001	187.68	678.4
.4660	54.470	52.592	1.00000	1.00001	155.43	352.7
.5740	82.530	78.305	1.00000	1.00001	129.61	164.3
.6170	103.145	103.777	1.00000	1.00001	119.34	74.1
.6362	123.968	123.967	1.00000	1.00001	114.74	64.5

AAD-Y= .001

AAD-P= 2.174

AAD=SUM[ABS(EXP-CAL)/EXP]*100/(NO. OF DATA POINTS)

Table C.16. Output Data of [bmim][PF_6]-CO_2 System for PRSV equation of state and Wong-Sandler mixing rules at 323.15 K for Set 3 (w= 0.7917)

WS: THE WONG-SANDLER MIXING RULE FOR BINARY VLE CALCULATIONS

EXCESS ENERGY MODEL= NRTL

ALPHA= .2000

K12= .8873

NRTL A12(CAL/MOL)= -58.6852

NRTL A21(CAL/MOL)= 26.5678

NRTL P12(=A12/RT) -.0914

NRTL P21(=A21/RT) .0414

pf6pol2

bmimpf6

TEMPERATURE in K: 323.15

PHASE VOLUMES ARE IN CC/MOL, PRESSURE IS IN UNITS OF THE DATA.

X-EXP	P-EXP	P-CAL	Y-EXP	Y-CAL	VL-CAL	VV-CAL
.2950	30.300	31.822	1.00000	1.00000	181.76	722.5
.4260	53.100	53.118	1.00000	1.00000	151.02	377.4
.5080	81.000	71.929	1.00000	1.00001	131.93	236.9
.5810	100.300	99.076	1.00000	1.00001	115.07	118.6
.6150	121.100	123.289	1.00000	1.00001	107.23	78.9

AAD-Y= .001

AAD-P= 3.857

AAD=SUM[ABS(EXP-CAL)/EXP]*100/(NO. OF DATA POINTS)

Table C.17. Output Data of [bmim][PF_6]-CO_2 System for PRSV equation of state and Wong-Sandler mixing rules at 323.15 K for Set 3 (w (Tb/Tc=0.7709))

WS: THE WONG-SANDLER MIXING RULE FOR BINARY VLE CALCULATIONS

EXCESS ENERGY MODEL= NRTL

ALPHA= .2000

K12= .8518

NRTL A12(CAL/MOL)= -224.9370

NRTL A21(CAL/MOL)= 100.2496

NRTL P12(=A12/RT) -.3503

NRTL P21(=A21/RT) .1561

pf6pol3

bmimpf6

TEMPERATURE in K: 323.15

PHASE VOLUMES ARE IN CC/MOL, PRESSURE IS IN UNITS OF THE DATA.

X-EXP	P-EXP	P-CAL	Y-EXP	Y-CAL	VL-CAL	VV-CAL
.2950	30.300	31.465	1.00000	1.00000	183.33	732.2
.4260	53.100	53.076	1.00000	1.00001	154.03	377.8
.5080	81.000	71.805	1.00000	1.00001	135.81	237.7
.5810	100.300	97.962	1.00000	1.00001	119.68	122.1
.6150	121.100	121.334	1.00000	1.00001	112.17	80.4

AAD-Y= .001

AAD-P= 3.553

AAD=SUM[ABS(EXP-CAL)/EXP]*100/(NO. OF DATA POINTS)

Table C.18. Output Data of [bmim][PF_6]-CO_2 System for PRSV equation of state and Wong-Sandler mixing rules at 323.15 K for Set 3 (w= 1.5114)

WS: THE WONG-SANDLER MIXING RULE FOR BINARY VLE CALCULATIONS

EXCESS ENERGY MODEL= NRTL

ALPHA= .2000

K12= .7920

NRTL A12(CAL/MOL)= -461.1089

NRTL A21(CAL/MOL)= 77.0839

NRTL P12(=A12/RT) -.7181

NRTL P21(=A21/RT) .1200

pf6pol4

bmimpf6

TEMPERATURE in K: 323.15

PHASE VOLUMES ARE IN CC/MOL, PRESSURE IS IN UNITS OF THE DATA.

X-EXP	P-EXP	P-CAL	Y-EXP	Y-CAL	VL-CAL	VV-CAL
.2950	30.300	28.788	1.00000	1.00000	186.03	812.3
.4260	53.100	49.801	1.00000	1.00001	159.12	412.3
.5080	81.000	70.265	1.00000	1.00001	140.88	246.6
.5810	100.300	100.495	1.00000	1.00001	125.81	114.4
.6150	121.100	133.687	1.00000	1.00000	118.76	72.7

AAD-Y= .001

AAD-P= 7.009

AAD=SUM[ABS(EXP-CAL)/EXP]*100/(NO. OF DATA POINTS)

Table C.19. Output Data of [bmim][PF_6]-CO_2 System for PRSV equation of state and Wong-Sandler mixing rules at 323.15 K for Set 4 (w= 0.7917)

WS: THE WONG-SANDLER MIXING RULE FOR BINARY VLE CALCULATIONS

EXCESS ENERGY MODEL= NRTL

ALPHA= .2000

K12= .8140

NRTL A12(CAL/MOL)= -233.9080

NRTL A21(CAL/MOL)= 24.8269

NRTL P12(=A12/RT) -.3642

NRTL P21(=A21/RT) .0387

pf6ypol2

bmimpf6

TEMPERATURE in K: 323.15

PHASE VOLUMES ARE IN CC/MOL, PRESSURE IS IN UNITS OF THE DATA.

X-EXP	P-EXP	P-CAL	Y-EXP	Y-CAL	VL-CAL	VV-CAL
.2950	30.300	31.179	1.00000	1.00000	178.06	740.1
.4260	53.100	53.087	1.00000	1.00000	151.23	377.7
.5080	81.000	71.872	1.00000	1.00000	134.52	237.3
.5810	100.300	97.653	1.00000	1.00001	119.71	123.1
.6150	121.100	121.141	1.00000	1.00001	112.80	80.6

AAD-Y= .001

AAD-P= 3.373

AAD=SUM[ABS(EXP-CAL)/EXP]*100/(NO. OF DATA POINTS)

Table C.20. Output Data of [bmim][PF_6]-CO_2 System for PRSV equation of state and Wong-Sandler mixing rules at 323.15 K for Set 4 (w (Tb/Tc=0.7709))

WS: THE WONG-SANDLER MIXING RULE FOR BINARY VLE CALCULATIONS

EXCESS ENERGY MODEL= NRTL

ALPHA= .2000

K12= .7321

NRTL A12(CAL/MOL)= -210.7532

NRTL A21(CAL/MOL)= 66.7214

NRTL P12(=A12/RT) -.3282

NRTL P21(=A21/RT) .1039

pf6ypol3

bmimpf6

TEMPERATURE in K: 323.15

PHASE VOLUMES ARE IN CC/MOL, PRESSURE IS IN UNITS OF THE DATA.

X-EXP	P-EXP	P-CAL	Y-EXP	Y-CAL	VL-CAL	VV-CAL
.2950	30.300	36.214	1.00000	1.00001	183.14	618.9
.4260	53.100	44.488	1.00000	1.00000	159.28	478.4
.5080	81.000	66.227	1.00000	1.00001	134.85	271.9
.5810	100.300	99.583	1.00000	1.00001	120.54	117.1
.6150	121.100	140.263	1.00000	1.00001	113.85	69.9

AAD-Y= .001

AAD-P= 14.103

AAD=SUM[ABS(EXP-CAL)/EXP]*100/(NO. OF DATA POINTS)

Table C.21. Output Data of [bmim][PF_6]-CO_2 System for PRSV equation of state and Wong-Sandler mixing rules at 323.15 K for Set 5 (w= 0.7917)

WS: THE WONG-SANDLER MIXING RULE FOR BINARY VLE CALCULATIONS

EXCESS ENERGY MODEL= NRTL

ALPHA= .2000

K12= .8869

NRTL A12(CAL/MOL)= -66.5985

NRTL A21(CAL/MOL)= 22.8843

NRTL P12(=A12/RT) -.1037

NRTL P21(=A21/RT) .0356

pf6shf2

bmimpf6

TEMPERATURE in K: 323.10

PHASE VOLUMES ARE IN CC/MOL, PRESSURE IS IN UNITS OF THE DATA.

X-EXP	P-EXP	P-CAL	Y-EXP	Y-CAL	VL-CAL	VV-CAL
.2950	30.300	31.894	1.00000	1.00000	195.75	720.4
.4260	53.100	53.097	1.00000	1.00000	162.84	377.5
.5080	81.000	71.633	1.00000	1.00001	142.38	238.5
.5810	100.300	97.912	1.00000	1.00001	124.26	122.1
.6150	121.100	121.132	1.00000	1.00001	115.84	80.5

AAD-Y= .001

AAD-P= 3.848

AAD=SUM[ABS(EXP-CAL)/EXP]*100/(NO. OF DATA POINTS)

Table C.22. Output Data of [bmim][PF_6]-CO_2 System for RSV equation of state and Wong-Sandler mixing rulesat 323.15 K for Set 5 (w (Tb/Tc=0.7709))

WS: THE WONG-SANDLER MIXING RULE FOR BINARY VLE CALCULATIONS

EXCESS ENERGY MODEL= NRTL

ALPHA= .2000

K12= .8508

NRTL A12(CAL/MOL)= -218.5959

NRTL A21(CAL/MOL)= 68.4031

NRTL P12(=A12/RT) -.3404

NRTL P21(=A21/RT) .1065

pf6shf3

bmimpf6

TEMPERATURE in K: 323.15

PHASE VOLUMES ARE IN CC/MOL, PRESSURE IS IN UNITS OF THE DATA.

X-EXP	P-EXP	P-CAL	Y-EXP	Y-CAL	VL-CAL	VV-CAL
.2950	30.300	31.420	1.00000	1.00000	197.59	733.4
.4260	53.100	53.119	1.00000	1.00001	166.22	377.4
.5080	81.000	71.871	1.00000	1.00001	146.69	237.3
.5810	100.300	98.021	1.00000	1.00001	129.36	121.9
.6150	121.100	121.716	1.00000	1.00001	121.29	80.1

AAD-Y= .001

AAD-P= 3.557

AAD=SUM[ABS(EXP-CAL)/EXP]*100/(NO. OF DATA POINTS)

APPENDIX D: THERMODYNAMIC FACTOR CALCULATION

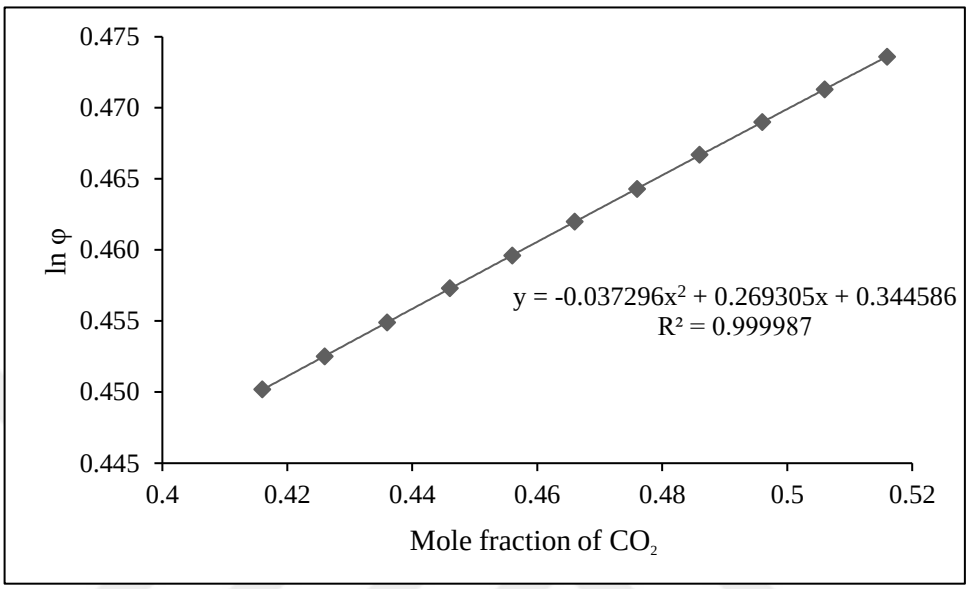

Figure D.1. ln ϕ versus carbon dioxide mole fractions to fit the polynomial for [bmim][PF_6]-CO_2 at 313.15 K, 5.4 MPa

As previously stated, the thermodynamic nonideality factor is determined by evaluating the composition derivatives of the fugacity coefficient, as depicted below.

$$\Gamma = 1.0 + x_{CO_2} \frac{\partial \ln \varphi_{CO_2}}{\partial x_{CO_2}} \qquad \text{(D.1)}$$

Taking the derivate of equation y= -0.037296x^2+0.269305x+0.344586 and inserting equilibrium mole fraction of 0.466 in x :

$$y = (-0.037296 \times 2 \times 0.466) + 0.269305 = 0.2346$$

So the thermodynamic correction factor is:

$$\Gamma = 1.0 + (0.466 \times 0.2346) = 1.109$$

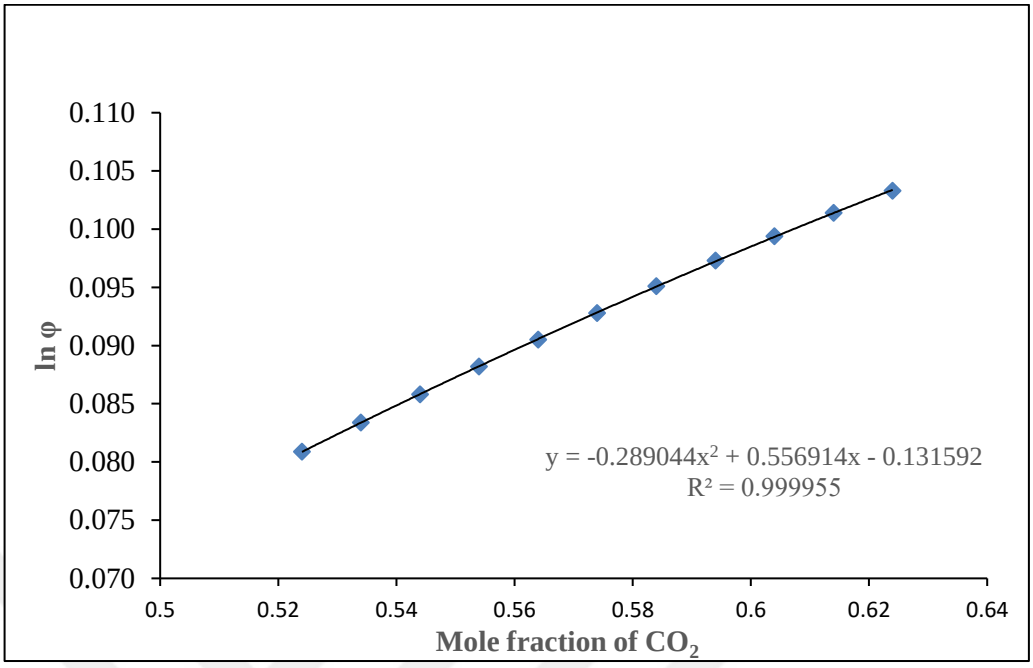

Figure D.2. ln ϕ versus carbon dioxide mole fractions to fit the polynomial for [bmim][PF_6]-CO_2 at 313.15 K, 8.3 MPa

Taking the derivate of equation y= -0.0289044x^2+0.556914x-0.131592 and inserting equilibrium mole fraction of 0.574 in x :

$$y = (-0.0289044 \times 2 \times 0.574) + 0.556914 = 0.2251$$

So the thermodynamic correction factor is:

$$\Gamma = 1.0 + (0.574 \times 0.2251) = 1.129$$

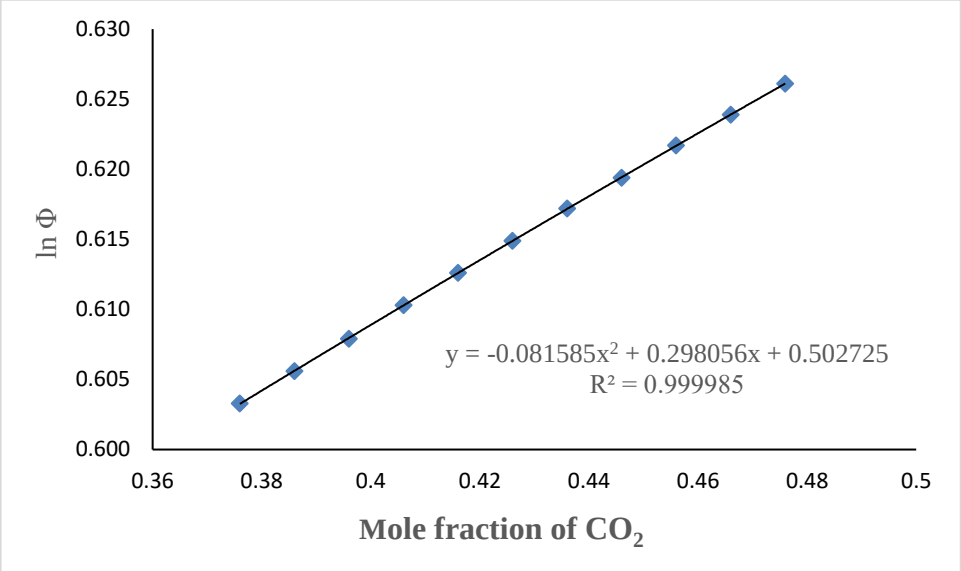

Figure D.3. ln ϕ versus carbon dioxide mole fractions to fit the polynomial for [bmim][PF_6]-CO_2 at 323.15 K, 5.3 MPa

Taking the derivate of equation y= -0.081585x^2+0.298056x+0.502725 and inserting equilibrium mole fraction of 0.426 in x :

$$y = (-0.081585 \times 2 \times 0.426) + 0.298056 = 0.2285$$

So the thermodynamic correction factor is:

$$\Gamma = 1.0 + (0.426 \times 0.2285) = 1.097$$

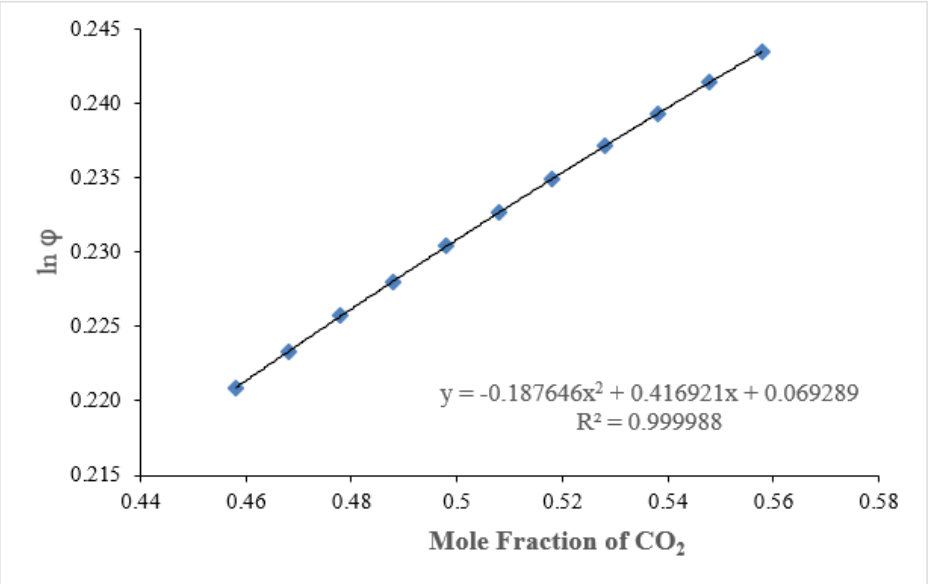

Figure D.4. ln ϕ versus carbon dioxide mole fractions to fit the polynomial for [bmim][PF_6]-CO_2 at 323.15 K, 8.1 MPa

Taking the derivate of equation y= -0.187646x^2+0.416921x+0.069289 and inserting equilibrium mole fraction of 0.508 in x :

$$y = (-0.187646 \times 2 \times 0.508) + 0.416921 = 0.2263$$

So the thermodynamic correction factor is:

$$\Gamma = 1.0 + (0.508 x 0.2263) = 1.115$$